Thermostatically Controllable Loads for Primary Frequency Control in Isolated Microgrids

by

William Francisco Mendieta

A thesis
presented to the University of Waterloo
in fulfilment of the
thesis requirement for the degree of
Master of Applied Science
in
Electrical and Computer Engineering

Waterloo, Ontario, Canada, 2019

Author's Declaration

I hereby declare that I am the sole author of this thesis. This is a true copy of the thesis, including any required final revisions, as accepted by my examiners.

I understand that my thesis may be made electronically available to the public.

Abstract

In the last few decades, governments, private investors, and nongovernmental organizations have gradually incentivized the integration of Renewable Energy Sources (RESs) and efficient Energy Storage System (ESS) technologies into remote microgrids, in good part because of commitments to counter the harmful effects of greenhouse gas emissions and to reduce dependence on fossil fuels. As a result, hybrid RESs-diesel systems are now being considered as an economic, attractive and reliable option to improve remote microgrids and to offset diesel consumption in isolated communities by displacing generation from conventional units; however, system security and stability is a challenge as the penetration of RESs increases. In this context, it is necessary to explore new mechanisms and control strategies for the provision of frequency support services in order to meet the increased ramp and capacity requirements to integrate RESs into the system effectively. From this standpoint, Demand Response (DR) can be used to increase grid flexibility, improve efficiency, and facilitate the penetration of RESs, by controlling loads in response to predefined control strategies, manipulating the demand profile to provide a service to the system. In particular, DR strategies are well-suited for northern remote communities, where the demand for electricity and heating is much higher than the Canadian residential average consumption due to the harsh climate and poor building energy efficiency. Thermostatically Controllable Loads (TCLs), i.e., Electric Water Heaters (EWHs), Air Conditioners (ACs), and Ground Source Heat Pumps (GSHPs), are ideal candidates to participate in a DR strategy, since they have a high thermal inertia, high-power consumption (among the appliances in a household), and are continuously operating over the day. Therefore, their power consumption can be shifted, or controlled by switching operations without significantly affecting consumer comfort. This is due to the thermal inertia of TCLs, which allow a smooth temperature variation that, in many cases, would be unnoticed by customers. Thus, TCLs provide energy storage capabilities, which are more significant with GSHP systems, and hence, a DR control strategy can use TCLs as thermal energy batteries with similar features than other ESS technologies. Therefore, the research presented in this thesis focus on developing a DR strategy for the provision of primary frequency control in hybrid isolated microgrids using TCLs, i.e., EWHs, ACs, and GSHPs.

A comprehensive review of the components, operation, and restrictions of these TCLs is performed in order to develop computationally efficient, simple, and accurate models, which are able to capture the relevant thermodynamic phenomena in dynamic studies. Based on the thermo-electrical characteristics of the developed models, a decentralized DR strategy is designed, which uses local frequency measurements to control the power consumption of the TCLs according to system frequency deviations while considering consumer comfort.

The control logic includes ON/OFF commands to modulate the duty cycle of the TCLs to provide primary frequency control and facilitate the integration of RESs.

The proposed DR strategy along with the developed thermo-electrical models of TCLs, i.e., EWHs, ACs, and GSHPs, are evaluated using a benchmark hybrid microgrid, which has a significant share of PV generation. In order to resemble realistic conditions, power and hot water consumption simulators are used to generate random demand profiles, while considering a droop control for the diesel genset and a solar PV with a Maximum Power Point Tracking (MPPT) control. Different study cases are conducted to analyze the system frequency response and determine the adequacy of the proposed DR strategy, demonstrating the effectiveness of the proposed TCL controls to provide primary frequency control, and thus facilitate higher penetration of RESs, while reducing costs and maximizing fuel savings.

Acknowledgements

I wish to express my sincere gratitude to all the people who helped me to complete my graduate studies. First and foremost, I would like to express my tremendous gratitude to my supervisor, Prof. Claudio Cañizares for the invaluable support and guidance through my MASc studies. I has been a privilege to learn and work under his supervision. I am grateful for his motivation, patience, and immense knowledge.

I am really thankfull to the professors who guided my studies by sharing their knowledge through outstanding lectures: Prof. Kankar Bhattacharya, Prof. Ramadan El-Shatshat, and Prof. Mehrdad Kazerani. I also sincrely aknowledge Prof. Kankar Bhattacharya and Prof. Mehrdad Prinia for serving as members of my committee, and for their insightful comments and feedback.

I offer my deepest gratitude to my friends of the EMSOL lab: Behnam, Carlos, Chioma, Dario, Emin, Enrique, Fabian, Ivan, Matheus, Mauricio, Mariano, Samuel and Sofia for all their help, support, and friendship during this journey. Thank you all for creating such a friendly environment and for the wonderful memories.

The hardest part of this thesis has been to find words to express the thanks to my parents, sister, niece, nephew, and my beloved wife and son. No amount of thanks will be enough for the unconditional support and love over these years.

Finally, I would like to specially acknowledge SENESCYT in Ecuador and NSERC in Canada for funding my Master's studies at the University of Waterloo.

Dedication

This is dedicated to the Blessed Virgin Mary and her son Jesus, thanks for everything in my life.

Table of Contents

List of Tables

List of Figures

List of Acronyms

AANDC	Aboriginal Affairs and Northern Development Canada
AC	Air Conditioner
ASHRAE	American Society of Heating, Refrigerating and Air-Conditioning Engineers
BESS	Battery Energy Storage System
DER	Distributed Energy Resource
DG	Distributed Generation
DR	Demand Response
ELD	Economic Load Dispatch
EMS	Energy Management System
EPA	Environmental Protection Agency
ESH	Electric Space Heater
ESS	Energy Storage System
EV	Electric Vehicle
EWH	Electric Water Heater
FCR	Fuel Consumption Rate
FEM	Finite Elements Model
GHX	Ground Heat Exchanger

GSHP	Ground Source Heat Pump
HPWH	Heat Pump Water Heater
HVAC	Heat Ventilation and Air Conditioning
HX	Heat Exchanger
LFC	Load Frequency Control
MPPT	Maximum Power Point Tracking
NRCan	Natural Resources Canada
PV	Photovoltaic
RES	Renewable Energy Source
RH	Relative Humidity
ROCOF	Rate of Change of Frequency
SoC	State of Charge
SRLS	Smart Residential Load Simulator
TCL	Thermostatically Controllable Load
UC	Unit Commitment
VSHP	Variable Speed Heat Pump

List of Nomenclature

Indices

i	Index for the time constants of the DEGOV_1 governor model, $i = 1, 2, ..., 6$
j	Index for the temperature nodes of the GHX model, $j = 1, 2$

Parameters

ΔT	Half dead band temperature [°C]
Δz	Height of each segment n of the borehole [m]
η_{EWH}	Efficiency of the EWH [%]
ρ_{fuel}	Fuel density [kg/m^3]
ρ_w	Density of the fluid inside the borehole [kg/m^3]
μ_w	Kinematic viscosity of the fluid inside the borehole [m^2/s]
τ_D	Engine firing time delay [s]
τ_i	Time constants of the DEGOV_1 governor model
ω_{ref}	Reference speed [p.u.]
A	Diode ideality factor
A_m	Area of a material [m^2]
C	Electrical capacitance [F]
C_{bj}	Thermal capacitance of the grout regions of the GHX model [J/°C]
C_f	Thermal capacitance of fluid inside each leg of the U-pipe [J/°C]
C_g	Thermal capacitance of the surrounding ground to the borehole [J/°C]
C_i	Thermal capacitance of the indoor air [J/°C]
C_m	Thermal capacitance of the concrete slab foundation (floor) [J/°C]
C_{th}	Thermal capacitance [J/°C]
CV_b	Grout volumetric thermal capacitance [kJ/m^3·°C]
CV_g	Ground volumetric thermal capacitance [kJ/m^3·°C]

C_w	Thermal capacitance of the building envelope (walls+ceiling) [J/°C]
C_{wt}	Thermal capacitance of water inside the tank [J/°C]
D	Droop characteristic [%]
EER_{ref}	Rated energy efficiency ratio of the HP
G	Electrical conductance [S]
G_s	Solar irradiation [W/m^2]
H	System inertia [p.u.]
I_{sc}	Short-circuit current [A]
K	Actuator gain of the DEGOV$_1$ governor model
K_i	Temperature coefficient of I_{sc} [%/°C]
K_v	Temperature coefficient of V_{oc} [%/°C]
L	Borehole depth [m]
L_m	Thickness of a material [m]
LHV_{fuel}	Lower heat value of fuel [MJ/kg]
N_s	Number of cells in series
$P_{AC,ref}$	Rated power of the AC [W]
P_{EWH}	Rated power of the EWH [W]
$Q_{AC,ref}$	Rated cooling capacity of the AC [W]
$Q_{c,ref}$	Rated cooling capacity of the HP [W]
$Q_{h,ref}$	Rated heating capacity of the HP [W]
R	Electrical resistance [Ω]
R_{bb}	Grout-to-grout thermal resistance [°C/W]
R_{bg}	Grout-to-ground thermal resistance [°C/W]
R_{bl}	Experimental mean borehole thermal resistance [°C/W]
R_c	Thermal resistance of the external glazed surfaces [°C/W]
R_h	Convective resistance of the GHX model [°C/W]
R_m	Thermal resistance of the concrete slab foundation (floor) [°C/W]
R_p	Shunt resistance [Ω]
R_{pp}	Pipe to pipe thermal resistance [°C/W]

R_s	Series resistance [Ω]
R_w	Half thermal resistance of the building envelope [℃/W]
S_h	Shank spacing [mm]
T_0	Thermostat setpoint temperature [℃]
T_{base}	Target temperature [℃]
T_c	Solar PV module temperature [℃]
T_{db}	Dead band temperature [℃]
$T_{EWH,max}$	Max hot water temperature [℃]
$T_{EWH,min}$	Min hot water temperature [℃]
T_{high}	Upper dead band limit [℃]
$T_{i,db}$	Thermostat dead band temperature for the household [℃]
$T_{i,max}$	Max indoor temperature [℃]
$T_{i,min}$	Min indoor temperature [℃]
T_{inlet}	Inlet cold water temperature [℃]
T_{lower}	Lower dead band limit [℃]
T_{MAX}	Upper torque limit [p.u.]
T_{MIN}	Lower torque limit [p.u.]
T_{ref}	temperature [℃]
UA_{EWH}	Thermal conductance of the tank shell [W/℃]
UA_{th}	Thermal conductance [W/℃]
$\dot{V}_{air,ref}$	Indoor air volumetric flow rate reference [m^3/s]
V_{oc}	Open-circuit voltage [V]
c	Specific fuel consumption [g/kWh]
c_p	Specific heat [J/kg ·℃]
c_{pw}	Specific heat capacity of water [J/kg ·℃]
c_w	Specific heat of the fluid inside the borehole [J/kg ·℃]
d_b	Borehole diameter [mm]
d_{eq}	Equivalent pipes diameter [mm]
d_g	Ground nodes position [mm]

d_{gp}	Ground radial penetration diameter [mm]
$d_{p,e}$	External U-pipe diameter [mm]
$d_{p,i}$	Internal U-pipe diameter [mm]
d_x	Grout node position [mm]
f_0	Target frequency [Hz]
f_{fl}	Full-load frequency of a diesel genset with a droop characteristic [Hz]
$f_{lim,max}$	Upper frequency limit [Hz]
$f_{lim,min}$	Lower frequency limit [Hz]
f_{low}	Lower intermediate frequency limit [Hz]
f_{nl}	No-load frequency of a diesel genset with a droop characteristic [Hz]
f_{up}	Upper intermediate frequency limit [Hz]
k	Boltzmann's constant [J/°C]
k_b	Grout thermal conductivity [W/m·°C]
k_f	Coefficient of temperature-frequency change [°C/Hz]
k_g	Ground thermal conductivity [W/m·°C]
k_{th}	Thermal conductivity [W/m·°C]
k_w	Thermal conductivity of the fluid inside the borehole [W/m·°C]
$\dot{m}_{W,ref}$	Mass flow rate reference [kg/s]
n	Number of nodes of the borehole discretization
q	Electron charge [C]
s_p	Slope factor [kW/Hz]
$t_{lockout}$	Lockout time [s]

Variables

ΔP_{ELEC}	Developed electrical power [p.u.]
ΔP_G	Active power supply deviation [p.u.]
ΔP_L	Active power demand deviation [p.u.]
ΔP_{MECH}	Driving mechanical power deviation [p.u.]
$\Delta\omega$	Rotor speed deviation [p.u.]

η_G	Diesel genset efficiency [%]
w	Velocity of the fluid inside the U-pipe [m^2/s]
COP	Coefficient of performance - GSHP (heating mode)
EER	Energy efficiency ratio - AC/GSHP (cooling mode)
FCR	Fuel consumption rate [l/h]
P_{AC}	Power consumed by the compressor of the AC [W]
P_c	Power consumed by the compressor of the HP [W]
P_G	Active power supplied to the system [W]
Q	Heat [W]
$Q_{absorbed}$	Heat absorbed from the ground [W]
Q_{AC}	Cooling capacity of the AC [W]
$Q_{AC/GSHP}$	Heat injected/extracted by the HVAC system [W]
Q_c	Cooling capacity of the HP [W]
Q_{EWH}	Heat injected into the tank [W]
Q_h	Heating capacity of the HP [W]
Q_{in}	Internal heat gains [W]
$Q_{rejected}$	Heat rejected to the ground [W]
Q_s	Solar irradiation on external walls [W]
RH	Relative humidity [%]
$ROCOF$	Rate of change of frequency [Hz/kW]
T	Temperature [°C]
T_j	Temperature of the fluid inside a leg of the U-pipe [°C]
T_{amb}	Outdoor temperature [°C]
T_{bj}	Temperature of the grout regions of the GHX model [°C]
T_{db}	Indoor air dry-bulb temperature for the GSHP model [°C]
$T_{db,ODC}$	Outdoor air dry-bulb temperature for the AC model [°C]
T_{EWH}	Temperatures of the hot water inside the tank [°C]
T_g	Temperature of the surrounding ground to the borehole [°C]
T_i	Indoor temperature [°C]

T_m	Temperature of the concrete slab foundation [°C]
T_t	Temperature monitored by a thermostat [°C]
T_w	Temperature on external walls [°C]
T_{wb}	Indoor air wet-bulb temperature [°C]
$T_{wb,IDC}$	Indoor air wet-bulb temperature [°C]
Tw_{in}	Inlet fluid temperature [°C]
Tw_{out}	outlet fluid temperature [°C]
$\dot{V}_{air}$	Indoor air volumetric flow rate [m^3/s]
f_{sys}	System frequency [Hz]
$\dot{m}_{EWH}$	Inlet water mass flow rate [kg/h]
$\dot{m}_W$	Mass flow rate of fluid through the GHX loop [kg/h]
m_{fuel}	Mass flow rate of the fuel [kg/h]

Chapter 1

Introduction

1.1 Motivation

The technological development of renewable energy-based generation, changes to emission-reduction policies, the growth of competition in the electricity industry, the increasing electricity demand, the liberalization of electricity markets, and others, are all driving the continuing evolution of power systems worldwide [1]. Among the many research areas related to these topics is the deployment of Renewable Energy Sources (RESs) into microgrids, which are localized clusters of Distributed Energy Resources (DERs) that may include renewable and non-renewable Distributed Generation (DG) units, Energy Storage Systems (ESSs), and controllable and uncontrollable loads, all of which can be operated as a self-sustained entity. Microgrids operate on both grid-connected and islanded/isolated mode, or may transit between these two modes [2], facilitating the integration of RESs, and have efficiently and reliably provided electricity to remote communities and islands worldwide [3].

A remote community is defined as a permanent or long-term settlement (five years or more) with a minimum of 10 dwellings that are not connected to an integrated electricity grid or the piped natural gas network [4]. These communities do not have an interconnection to the main electric grid due to technical and economic restrictions, and thus they must produce electricity locally through isolated microgrids, which rely on expensive fossil fuels, especially diesel, to generate electricity and help satisfy heating needs (space and water heating). For instance, as reported by the Aboriginal Affairs and Northern Development Canada (AANDC) approximately 200,000 people living in 280 remote communities across Canada have some of their energy demand currently served by their local isolated

microgrids. Collectively, they consume more than 90 million liters of diesel fuel every year for generating electricity, and an estimated two to three times more for heating [4].

In the last few decades, governments, private investors, and nongovernmental organizations have gradually incentivized the integration of RESs and efficient ESS technologies into remote microgrids, in good part because of commitments to counter the harmful effects of greenhouse gas emissions and to reduce dependence on fossil fuels [5]. As a result, hybrid RESs-diesel systems are now being considered as an economic, attractive and reliable option to improve remote microgrids and to offset diesel consumption in isolated communities [6], by displacing generation from conventional units; however, grid stability and security of supply must be carefully considering in RESs integration. Given the small size of an isolated microgrid when compared to a large-scale centralized grid, non-dispatchable RESs (e.g., solar photovoltaic (PV) or wind generation) can quickly reach medium-to-high penetration levels. Additionally, the daily load profile in remote communities is highly variable, with a peak load ranging from 5 to 10 times the average load, making it challenging for diesel gensets to supply electricity efficiently over the full range of load variation [5]. Thus, depending on the penetration level of RESs and the daily load variation, many technical challenges are presented for the stability of the frequency and voltage of hybrid RES-diesel microgrids, especially with reduced or non-existent ESS units [7].

In order to keep the frequency and voltage within their permitted limits and recover after disturbances while ensuring a continuous demand-supply balance, it is necessary to add flexibility to the system. In [8], flexibility is defined as the capacity of a power system to balance fluctuating generation with fluctuating demand, which requires novel mechanisms to increase it. Thus, a possibility for relieving the variability and uncertainty and providing frequency reserves is making strategic power demand adjustments whenever necessary, which is known as Demand Response (DR). By using controllable residential loads, through a DR strategy, many grid support services at normal operating conditions and for emergency services in case of large power imbalances can be provided [9].

Figure 1.1 shows a breakdown of electricity consumption according to the type of load in a typical household in Canada [10]. Residential thermal loads, i.e., electro-thermal and space-heating-cooling loads such as electric water heaters (EWHs) and heat-ventilation-and-air-conditioning (HVAC) systems, can represent up to 85% of the total electricity consumption in a household [9]. Therefore, the implementation of a DR control strategy for thermal loads has great potential to provide many grid support services by encouraging customers' participation [11]. In particular, a DR strategy is well-suited for remote communities, where according to [4], the demand for electricity and heating is much higher than the Canadian residential average consumption due to the harsh climate and poor

building energy efficiency.

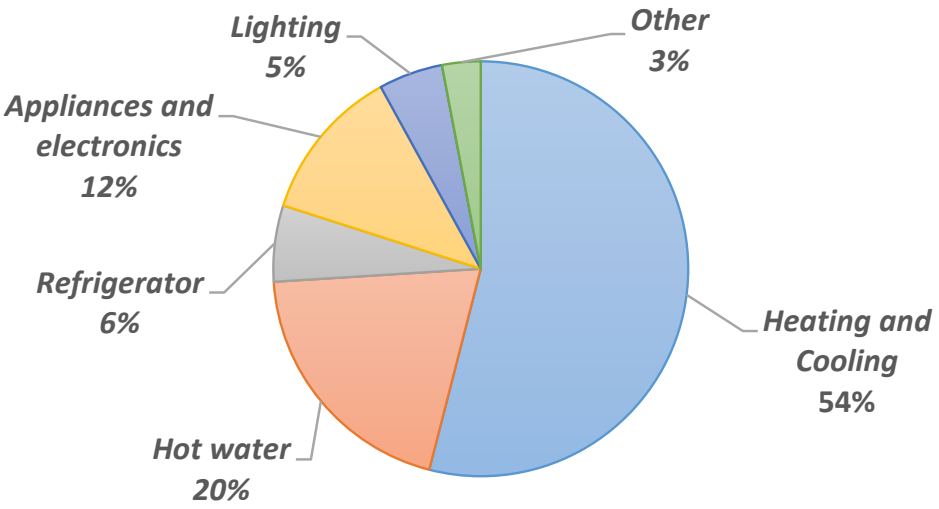

Figure 1.1: Typical breakdown of a household's electricity use in Canada [10].

According to Natural Resources Canada (NRCan), the most common type of residential HVAC system comprises a centralized forced-air system, with an air conditioner (AC) and a furnace to control the indoor temperature year-round [12]. Whereas AC is driven by electricity, the furnace consists of a fuel-burning system (propane, natural gas, oil) [13]. This combination is not only inefficient but also, due to the fuel combustion (for the furnace), yields emissions (e.g., carbon monoxide); furthermore, only with AC is possible to apply a DR strategy. Therefore, from an environmental and economic standpoint, a ground source heat pump (GSHP) system may replace the aforementioned HVAC system to provide year-round climate control, with reduced greenhouse emissions and with savings of up to 60% better than with conventional space conditioning systems [14]. A GSHP system, which can also be a thermal load driven by electricity, is a renewable heating and cooling technology more efficient than traditional climate control systems, and can be integrated into DR strategies.

As the power consumption of thermal loads is controlled by means of a thermostat, they are known as thermostatically controllable loads (TCLs). Control strategies for TCLs, especially GSHP-based ones, offer the potential to modify their regular duty cycles to provide frequency support services without affecting consumer comfort. This capacity exists because when a TCL is disconnected, its thermal inertia allows a smooth temperature

variation that, in many cases, will be unnoticed by customers [15], thus providing energy storage capabilities, which are more significant with GSHP systems. Therefore, a DR control strategy can adapt TCLs to emulate thermal energy batteries with similar features than other ESS technologies [16]. Hence, the focus of this thesis is on exploring the provision of primary frequency control in isolated microgrids by means of a DR strategy for residential TCLs equipped with GSHP systems.

1.2 Literature Review

This section presents an overview of some relevant research works for this thesis.

1.2.1 Demand Response for Frequency Regulation

A clean energy revolution is taking place worldwide, targeting increased RESs penetration in the near future. Reduction of polluting emissions, the promotion of energy mixes, increasing fuel prices and energy security are the major policy drivers for the expansion of RESs [17]. However, these inherently non-dispatchable energy sources may threaten the operation and control of power systems [18]. Numerous studies have been conducted to investigate the technical challenges of maintaining the instantaneous demand-supply balance in an isolated microgrid when there is a significant share of RESs [6], [9], [15], [19, 20]. These papers show that with significant penetration of renewables, RESs may jeopardize grid stability, degrade power quality, and impact power supply security.

Maintaining the instantaneous demand-supply balance in an isolated RESs-based microgrid is challenging. In addition to constant load variations, component unavailability, unpredictable disturbances and faults, the system is exposed to sudden power infeed fluctuations because of the uncertain and variable nature of RESs. As a result, the system operates under continuous power imbalances, which if not adequately compensated for, may lead to large frequency deviations [18]. Consequently, among the major challenges of integrating RESs, is a need for new frequency control mechanisms with higher ramp-rate responses and a larger magnitude of regulation for both long-term (hourly) and short-term (seconds-to-minutes) [19].

Recently, ESSs such as batteries and flywheels are being used to provide regulation services [21]. These systems have shown a superior response and accuracy to conventional generators. For instance, their ramp rates can be up to 600 times faster than that of a gas-fired plant, and a battery is able to provide its maximum power in less than one second [22].

Thus, new regulations have been issued (e.g., FERC order No. 755) in order to account for the speed and quality of the regulation service [21]. Even though some ESSs can provide very fast frequency regulation by performing repeated and high-speed charge-discharge cycles, some potential barriers could prevent a broader integration of these technologies; particularly, the high capital costs and the current market platforms with their regulatory structures hinder the deployment of ESSs [23]. Basically, in existing deregulated environments, storage systems are eligible to participate in only one market at a time, and in a vertically integrated system, they receive revenues from just one particular service. Additionally, the time-scales for different ancillary services overlap with the time-scales for various markets, making it difficult to properly assess revenues when ESSs are operating simultaneously in multiple markets and providing several services at a time. Therefore, some services that storage systems can provide are not being properly compensated [24]. In part, for these reasons, it is necessary to exploit additional resources to add flexibility to the system in order to properly deal with the challenges imposed by RESs.

Demand and generation can support system frequency [15]. However, in the past, demand has been underutilized, mostly for three reasons: (1) control architecture being designed to procure frequency services from a limited number of large power plants (conventional generators), rather than dealing with a large number of small controllable loads; (2) demand being considered as an inelastic resource that can be curtailed only in case of large frequency deviations; and (3) the absence of a specific frequency ancillary service market that incentivizes customers' participation. Technically, DR may provide the same frequency support services with improved performance characteristics that are not available from various conventional regulation providers (e.g., elasticity, time-scale response ranging from fractions of seconds to minutes, or even hours) [25]. Thus, if a DR strategy is adequately designed, it can contribute positively to improve power system operation and efficiency. As controllable loads are a fast-acting resource, a DR control of a cluster of loads can emulate synthetic mechanical inertia and also droop response from synchronous generators [15]. Moreover, depending on the strategy, controllable loads may respond to voltage and/or frequency control signals, market price signals, timer signals [26]. Therefore, from an environmental and cost-effective standpoint, DR is a pollution-free alternative that can help to reduce frequency service procurements and further reduce operating costs.

Because of the aforementioned advantages, considerable research has been conducted to improve current DR strategies or to develop new ones [27]. For instance, a wide variety of DR strategies has been designed to mitigate frequency deviation on a long-term basis, i.e., 24 hours [28]. A basic example is to shave peak demand by disconnecting loads during on-peak hours or load leveling by using low-price tariffs to encourage users to operate their loads during off-peak hours [29]. Furthermore, more-sophisticated approaches have been

developed for the same purpose. For example, in [30], a market price signal is proposed to shift demand from EWHs and heat pump-based EWHs to periods of low prices. The control logic consists of increasing the setpoint temperature to the maximum allowable value (60 ℃) when the price is low; once the temperature reaches the upper limit, the setpoint is switched to the minimum admissible value (49 ℃). As EWHs have high thermal inertia, the time for the hot water temperature to reach the lower limit is significant, and thus these thermal loads can readily shift their demand.

In terms of short-term frequency control, DR focuses on adjusting the power consumption of controllable loads as a function of frequency deviations, so as to mitigate power imbalances [18]. From a control perspective, these loads can be grouped into four categories [27, 28]: purely resistive loads (i.e., EWHs and electric space heaters (ESHs)), compressor-based loads (i.e., ACs and GSHPs), variable-speed heat pumps, and electric vehicles (EVs). The technical constraints and time responses are different among these loads; therefore, an understanding of each type of load is critical when designing the most-effective DR strategy. For example, in [28] electric vehicles (EVs) are considered as energy storage units with the technical capability to provide aggregated frequency regulation. When EVs are connected to a charging station, the control can dynamically modify the operating cycle and charge/discharge the EV in response to a frequency deviation signal and considering the state of charge (SoC) of the battery; however, since most remote communities do not have the conditions to harbor a significant population of EVs [4], this approach is not readily applicable to remote microgrids. Additionally, many researchers have focused on combining different types of controllable loads to improve frequency response. For instance, in [16], EVs and Heat Pumps Water Heaters (HPWHs) are used to reduce the capacity of complementary ESSs and mitigate the impacts of a large penetration of RESs. A Load Frequency Control (LFC) method is used in this case, in which a central load dispatching center sends a regulation signal to all the frequency-regulation providers (generators, controllable loads, and ESSs). The disadvantage of this study is the need for a two-way network to integrate all the frequency resources, which for remote microgrids presents a challenge due to the cost and reliability of communication channels.

1.2.2 Thermostatically Controllable Loads (TCLs)

A subcategory of controllable loads is made up of TCLs. These types of loads, i.e., EWHs, ACs, GSHPs, ESHs, refrigerators, and freezers, while providing thermal services, have the potential to be very responsive, because their thermal inertia allows instantaneous decoupling of the thermal load from their electricity consumption without compromising end-users' comfort. In other words, TCLs can emulate ESSs in terms of their capacity to

provide frequency regulation through switching actions (comparable to charge-discharge cycles), and energy management by adjusting their power consumption according to specific control logics [18]. Additionally, in the case of a surplus generation when there is significant penetration of RESs, TCLs can be used to store this extra energy instead of wasting it, in order to shift a portion of the cooling or heating needs, particularly in microgrids [31]. Due to these properties, in the literature, TCLs are also known as thermal batteries [32]; for example, in [33], it is shown that the response of some TCLs (i.e., refrigerators and ACs) is suitable to provide fast frequency reserves emulating the response of a Battery Energy Storage System (BESS).

EWHs and refrigerators are the most common types of TCLs available in houses worldwide. On the other hand, the climate determines the application of HVAC systems for cooling and/or heating. Regardless, all these loads represent the major component of the total residential electricity consumption everywhere. While EWH power consumption is constant throughout the year, the demand from an HVAC system has significant seasonal variation [18]. In Canada and the U.S., the typical arrangement for a residential HVAC consists of a central forced-air system along with an AC and a furnace [34]. However, according to the U.S. Environmental Protection Agency (EPA) [35], a GSHP is the most environment-friendly, efficient, and clean alternative for space climate conditioning that can be used almost any place, significantly reducing power consumption on a year-round basis by using geothermal energy as a source/sink of heat for climate control. Moreover, in [36], it is shown that the operational costs of a GSHP are lower than any other conventional HAVC system's, with a life expectancy of 20 to 25 years. The operating principle behind this technology is similar to that of conventional refrigerators or ACs, i.e., to pump heat to cool a space, but in addition, a GSHP is technically capable of providing both heating and cooling by pumping heat between a household and the ground or vice versa.

Mathematical models have been extensively developed to emulate the thermodynamic behavior of TCLs and obtain their power consumption as a function of time [9]. However, it is necessary to identify a proper model and consider a speed-accuracy trade-off when a TCL provides frequency regulation. As an example, the results in [9] show that for a 240-hour simulation of an EWH, a very detailed model can take up to 22 minutes, whereas for simpler models it can only take 15 seconds at the expense of losing just a few heating actions. Therefore, the thermal model choice must be computationally efficient, simple, and accurate enough to capture the required dynamics over the simulation time-horizon needed to design a suitable DR strategy [37]. In the specific case of ACs and GSHPs, fast dynamic simulations are highly complex due to the difficulty of linking the responses of their components in real-time to obtain a complete thermo-electrical picture of their behavior [14]. In this case, the models of the individual components require a large amount

of information and a high-level understanding of thermodynamics. For example, as shown in [14], the main component of a GSHP is the Ground Heat Exchanger (GHX), since heat is exchanged through it from/to the ground, with its thermal performance being affected by many factors that result in high computational costs [38]. In [39], a highly complex finite elements model (FEM) is presented, in which the borehole is discretized to build meshes to study three-dimensional heat transfer processes; this highly detailed model can be used as a reference for validating more simplified models. This thesis proposes simplified models for representing the dynamics associated with frequency regulation that capture the relevant thermodynamic phenomena at reasonable computational costs.

Many DR strategies have been proposed to study the performance of TCLs for frequency control. In effect, such strategies aim to control TCL switching actions in response to system frequency deviations, so the TCLs operate as fast frequency reserves [15]. For example, the authors in [40] study the feasibility of providing primary frequency control in a hybrid solar-diesel isolated microgrid using EWHs. However, some simplified assumptions are used, such as that all households have the same hourly averaged load and hot water usage profiles, irrespective of the number occupants or their patterns of active occupancy, which, as explained in [41], do not resemble reality, and thus the effectiveness of a DR strategy would be degraded if applied in practice. In [18], it is shown that a population of refrigerators can provide aggregated frequency reserves in an amount equivalent to their total average power consumption. Moreover, in [42], a dynamic DR strategy is presented for improving frequency stability by using refrigerators and freezers that are turned ON/OFF to counterbalance frequency deviations and maintain system frequency within a specified band, so that, when the frequency varies, the demand is dynamically adjusted. However, since the standard rated power of a refrigerator is just about 100 W and 200 W for a freezer, the aggregated frequency reserve might be insufficient to counter large frequency deviations in an isolated microgrid, which is the reason why this DR strategy is not considered in this research.

In [15], two methods are presented to correct frequency deviations by measuring frequency locally. The first method defines a frequency dead band located below the nominal system frequency, which establishes limits for disconnecting/reconnecting TCLs. If the frequency goes below the lower threshold, TCLs are disconnected until the frequency recovers and surpasses the upper limit. The second method uses a linear relationship between the temperature setpoint of TCLs and the frequency deviation (the same principle used in [40]), continuously adjusting the demand as a function of frequency deviations. Both methods have been applied to populations of EWHs and EHs in a large power system with promising results, and thus are used in the present work. Furthermore, the control logic from these methods can be modified and adapted for other types of TCLs such as

ACs and GSHPs for the provision of primary frequency control in an isolated microgrid, as demonstrated in this thesis.

1.2.3 DR Control Architecture for Frequency Control

In terms of control architecture, a DR strategy can be classified into centralized or decentralized in accordance with whether there is a communication platform or not [28]. In a centralized control architecture, a control center monitors the frequency and determines the total amount of regulation required to compensate for frequency deviations, and it then allocates the regulation required among all available frequency regulation providers, including controllable loads, sending a control signal to each one of them. The logic used by the control center aims to reduce frequency reserves at the generation side. However, some challenges arise in implementing such a control strategy. Thus, as stated in [15], to determine the power capacity required to compensate for frequency deviations, an aggregated model of the controllable loads is required; however, this aggregation may cause serious conflicts on individual loads, specifically in TCLs, because the control signal may force switching actions that could result in unacceptable temperature levels [43]. Furthermore, a dedicated two-way point-to-point communication channel is needed to transmit the regulation signal and monitor the current status of all controllable loads [44].

In a decentralized control architecture, each load controller measures the system frequency locally and follows a predefined logic to determine whether the load must be turned ON/OFF. In this manner, customers' participation can be incorporated into frequency control. In fact, conventional generators also use this type of architecture for primary frequency control, since their response is determined by a droop characteristic that uses a local frequency measurement as input [42]. In [15] and [28], it is shown that this architecture provides a faster and smoother frequency response since the logic decisions are taken in parallel between all controllable loads. Moreover, in [44], demand is found to react to frequency deviations in a similar way to that of conventional generators, even when there is no two-way communication channel. However, the aggregated load response may be inadequate, since there is no coordination between controllable loads, which may also result in over or sub-regulation [41]. Nevertheless, given the challenges of implementing a centralized control approach in remote microgrids [5], the decentralized control approach is adopted here.

1.3 Research Objectives and Expected Contributions

Based on the literature review and associated discussions presented in the previous section, the following are the main objectives and expected contributions of this research work for the provison of primary frequency regulation in isolated microgrids by using a decentralized DR strategy on autonomous controllers for residential TCLs:

- Implement suitable and novel models of residential TCLs, i.e., EWHs, ACs, and GSHPs, to represent their dynamic thermo-electrical response in real-time with good accuracy for frequency regulation applications.

- Improve the DR strategy presented in [15] and [40] for EWHs, and develop a new frequency-based DR strategy for ACs and GSHPs. The control strategy includes ON/OFF commands to modulate the duty cycle of these TCLs to provide primary frequency control and facilitate the integration of RESs.

- Test and compare the developed DR strategies for two types of configurations of TCLs, i.e., AC+EHW and GSHP+EHW, in a real isolated microgrid with a high RESs penetration, in order to test, demonstrate, and validate the effectiveness of the proposed strategies for practical applications.

1.4 Thesis Outline

The remaining of this thesis is structured as follows:

- Chapter 2 presents a background review of the main concepts used in this research work, including primary frequency regulation, hybrid isolated microgrids, and DR strategies for TCLs. It also describes the operating restrictions of EWHs, ACs, and GSHPs that must be considered when developing thermal models. Finally, a brief description of the simulators used to generate the load and hot water consumption profiles is presented here.

- Chapter 3 describes the models used in this thesis, starting with the electromechanical model of a diesel genset, followed by the modeling of a solar PV system with an MPPT control. Then, the developed thermal models of residential TCLs, are shown and discussed, followed by a detailed description of the proposed frequency control strategy for each type of TCL.

- Chapter 4 presents a description of the isolated microgrid used in the present studies. Load and hot water consumption profiles are generated to represent a realistic thermoelectrical behavior of each household participating in the DR strategy. Then, several case studies are defined in order to examine the performance of the proposed DR strategy for the provision of primary frequency control. Finally, a detailed comparison of the results for the different cases is presented and discussed.

- Chapter 5 summarizes the conclusions and main contributions of this research work and suggests potential pathways for future work.

Chapter 2

Background Review

This chapter reviews the background of the main concepts and analytical tools used in this research work. Thus, it first briefly describes the concepts of frequency regulation and ancillary services. Then, the main characteristics and existing challenges for the operation of hybrid RESs-diesel microgrids are presented. The common architectures and DR strategies to provide frequency control are summarized next, followed by a review of the fundamentals of the operation of TCLs and their mechanical and thermal constraints. Finally, the simulators used in this thesis are described.

2.1 Frequency Control in Isolated Microgrids

Grid-connected microgrids have one clearly identifiable point of connection to the main electricity grid, which is commonly known as the Point of Common Coupling (PCC) [2]. Therefore, when connected, frequency and voltage at the PCC are primarily determined by the host grid, with the microgrids providing pre-defined ancillary services. In contrast, in the case of isolated microgrids, voltage and frequency control are a major concern and must be performed by various DER units [2]. In principle, most DER technologies may provide voltage control, whereas frequency control is available and dependable on certain ESS technologies, microturbines/CHP, diesel gensets, and controllable loads.

Immediately after a deviation in the demand-supply balance, the kinetic energy stored in the rotating masses (e.g., rotors and turbines of synchronous generators) will try to compensate for this mismatch. This action, known as an inertial response, is an intrinsic and a crucial property of any system and reduces both the magnitude of the frequency

deviation and the rate-of-change-of-frequency ($ROCOF$). For a single-machine system, the $ROCOF$ is derived from the swing equation [45]:

$$ROCOF = \frac{f_0}{2H}(\Delta P_G - \Delta P_L) \tag{2.1}$$

where f_0 is the frequency before the disturbance, H is the system inertia, ΔP_G is the power supply, and ΔP_L is the power demand. Typically, the kinetic energy, which is proportional to H, can supply the full load for a few seconds. Hence, if a large frequency deviation occurs, frequency control mechanisms must operate quickly to adjust both the power supplied by generators and the controllable loads' power consumption to restore the demand-supply balance; otherwise, frequency deviations may lead to frequency oscillations, which in turn can yield generator tripping, load curtailment, and in the worst-case scenarios, equipment damage and/or system collapse. Therefore, the objective of frequency control consists on maintaining the demand-supply balance at all time. This task can be very challenging in isolated microgrids due to their low inertia, especially if the penetration of RESs is significant. Moreover, microgrids are also exposed to sudden small and large disturbances, such as load and RESs variations, as well as equipment trips.

In terms of control architecture, several controllers operate in parallel over different time frames and under a hierarchical arrangement to maintain the system frequency within acceptable limits during disturbances. This architecture presents three very distinct control levels: (a) primary control, (b) secondary control, and (c) tertiary control [2]. These control levels differ in their speed of response, operation time frame, and required infrastructure (e.g., communications requirements). Figure 2.1 depicts the architecture of the frequency control levels in an isolated microgrid, which can be described as follows [2]:

- Primary control is the first control level and provides an autonomous response in the first few seconds after an unexpected frequency change. This control is performed by different mechanisms such as governor action or load control. In the case of governor action, individual local controllers measure the frequency deviation and regulate the output power of their associated generators. In the case of load and ESSs control, a local controller adjusts the power consumption of its associated controllable equipment according to a regulation signal sent from a central controller or by using a control logic based on a local frequency measurement. The objective of this control level is to bring the frequency back to a temporary acceptable value. Thus, the frequency is stabilized at a slightly different value than the initial one.

- Secondary control, also called load frequency control, provides balancing functions to restore the system frequency to its nominal value (60 Hz in Canada). It is performed

by a central controller that determines and transmits the appropriate setpoints to local controllers of different DERs (e.g., generators and ESSs) and controllable loads. To transmit the setpoints a communication channel between all the available frequency control participants is necessary. The time response of this control level is in the order of minutes (or faster in some instances). In the case of microgrids, this is typically linked to the Energy Management System (EMS).

- Tertiary control, in large systems, involves unit commitment (UC) and economic load dispatch (ELD) problems, and is a task executed offline based on economic optimization. However, for microgrids, this level implies the optimal coordination of the system and its host grid.

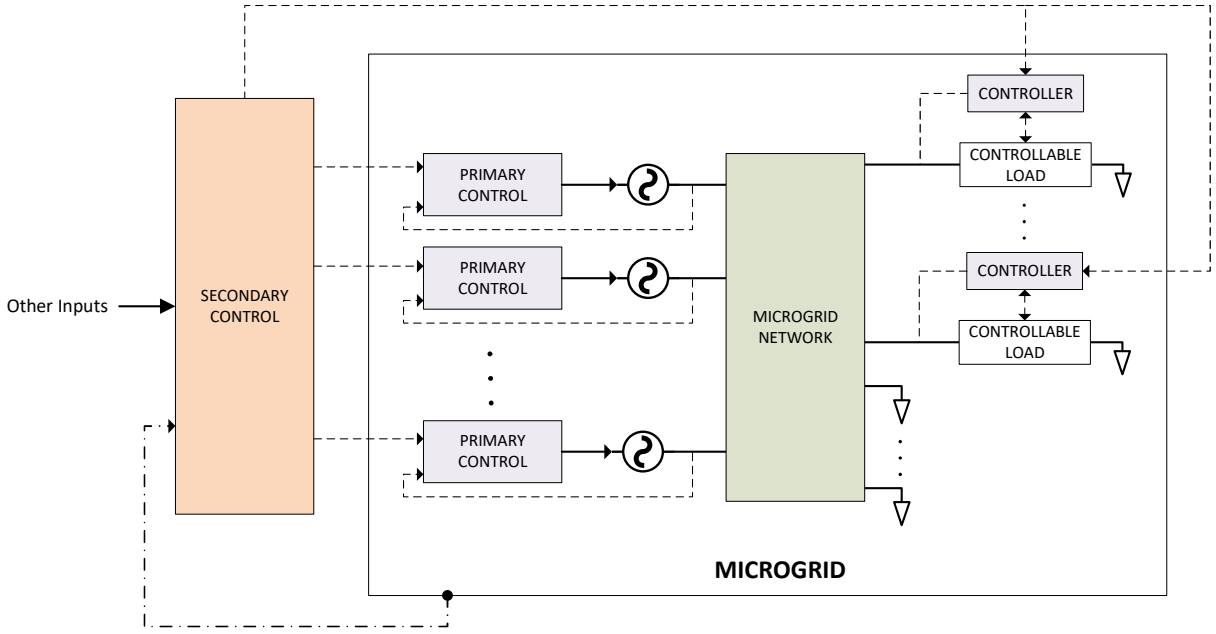

Figure 2.1: Frequency control architecture in an isolated microgrid [2].

Figure 2.2 illustrates the different frequency control levels and their time frame response after a disturbance.

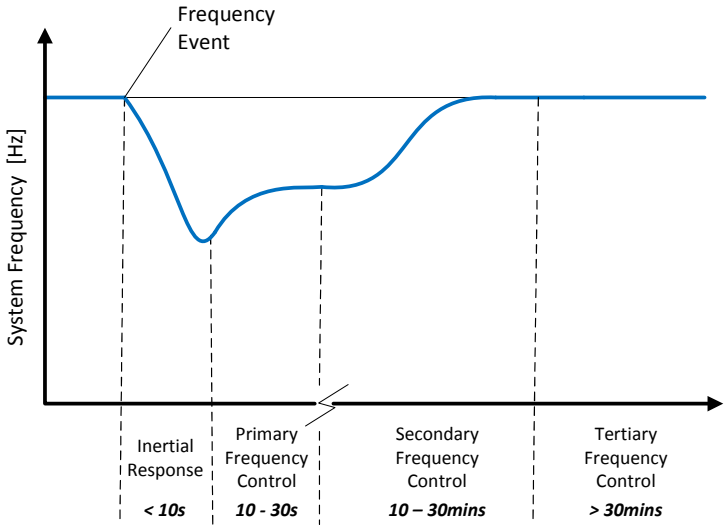

Figure 2.2: Time frame for frequency control levels after a frequency event in large systems [46]. For microgrids the time responses are typically shorter [19].

2.1.1 Grid Support Services

Grid support services refer to the provision of online and offline generation, and voltage control capability (reactive support) to respond to load variations during normal and contingency operating conditions [45]. The main purpose of these services is to track and compensate for the second-to-second imbalance between generation and demand, as well as maintain acceptable voltage levels on the grid. Traditionally, these services have been provided by more expensive reserves supplied by flexible generating units whose output is adjusted to compensate for the active power fluctuation between demand and supply. Such fluctuations may contain very fast and/or slow time components, ranging from fractions of seconds to hours, or even days. Depending on the time at which these fluctuations must be corrected, a specific service should be used. For instance, according to the U.S. Department of Energy, the following services are required over a typical time interval [47]:

- Voltage control: $\geq\sim$ 0.1 min.
- Regulation: $\geq\sim$ 1 to 10 mins.
- Load following/energy imbalance: $\geq\sim$ 10 mins.
- Frequency responsive spinning reserve: $\geq\sim$ 0.3 to 10 mins.

- Supplemental reserve: $\geq$10 to $\sim$ 60 mins.
- Replacement reserve: $\geq\sim$ 60 mins.

In general, similar services are required in microgrids, but at shorter time ranges [2], [19].

2.2 Hybrid RESs-Diesel Isolated Microgrids

Isolated microgrids, as defined in Chapter 1, have no tie to an interconnected system. As a result, they must supply their electricity demand locally. Worldwide, the preferred option for supplying electricity in remote communities is diesel gensets due to their scalability, mature technology, flexible operation, and competitive investment costs [48]. However, fuel costs are highly volatile and likely to increase. Moreover, as diesel-based generation is sized to supply peak load demand, gensets tend to run inefficiently at low loads during off-peak hours, thus reducing their lifetime and increasing their maintenance costs [49]. Furthermore, as some of these remote communities are accessible only by airplane, boat, or ice-roads in the winter, the price of electricity can be as much as ten times higher than the electricity generated on the main grid, as a result of the expensive transportation and storing costs [4, 5]. From an environmental standpoint, there is always a high risk of fuel spills during transportation and leaks during storing, plus diesel emissions are one of the major contributors to pollution problems, having a direct impact on people and animal health and global climate change.

To ameliorate the aforementioned problems with diesel-based microgrids, hybrid systems are cost-effective alternatives that combine conventional diesel generation with RESs. This energy supply mix provides a cleaner, sustainable, and reliable choice to increase energy security, reduce reliance on diesel-based generation, limit green house emissions, and lower the price of electricity [50]. Nowadays, various RES technologies are available; however, due to the vast resource availability and their continuously decreasing cost, solar PV panels and wind turbines are the fastest growing technologies. Thus, solar PV generation is 80% cheaper than ten years ago, whereas wind turbines have reduced their cost by half over a similar period [51]. Moreover, solar PV and wind generation are scalable, meaning that they can be used as concentrated sources, or they can be dispersed throughout the network. According to [6], the predominant configuration in emerging markets is a hybrid solar PV-diesel mixture, since solar PV generation has some advantages over wind generation, such as simpler installation, lower maintenance costs, and higher generating forecasting accuracy.

Based on the shared generation capacity from RESs and gensets, hybrid microgrids may have: (a) generation mainly based on RESs with gensets as standby backup, or (b) generation mainly based on gensets with RESs used for reducing diesel consumption. In both cases, gensets add reliability to the grid, since they are able to respond quickly when a load variation takes place, or when a sudden change in RES generation occurs. However, a RESs-diesel generation mix presents various technical challenges to the operation, monitoring, and control of these microgrids, such as the following:

- In terms of generation control, diesel gensets are fully dispatchable, while RESs are highly intermittent and can experience fast changes due to their dependence on meteorological factors; for example, solar PV generation can vary in the order of seconds to minutes and wind generation in the order of minutes [52]. Moreover, solar PV panels generate fluctuating power during sunlight hours, whereas wind turbines generate power according to wind conditions over the entire day. Consequently, this variability may force the gensets to operate with steep ramps and intense cycling, or to work beyond their safe and efficient operating ranges to adjust the demand-supply balance. The result is further performance degradation, a shorted lifetime due to excessive wear on mechanical components, and increased operational and maintenance costs. Additionally, as the share of RESs increases, there is a corresponding increase in the need for improved balancing services (e.g., frequency control, load following, etc.) to counteract the sudden infeed power fluctuations [53].

- In the case of high penetration of RESs, forecasting generation models are affected due to the intrinsic variability of renewables, which may significantly affect the dispatch decisions of conventional generation units [54]. Moreover, when DR is used, the payback effect of the control strategy will also affect the forecast, since after actions are taken on controllable loads for the provision of a frequency service, the load profile will be altered and may considerably differ from the forecasted one; as a result, uncertainty is introduced into the operation. Therefore, the number of variables and constraints that should be taken into account to operate the system substantially increases.

- In a diesel genset, the electromechanical coupling of the rotating masses enables the conversion of mechanical into electrical power. Moreover, as a result of the movement of these masses, rotational inertia is added to the system via the stored kinetic energy. On the other hand, most RES units require a static inverter interface to supply power to an AC grid. Therefore, as the penetration of RESs increases, the system inertia is reduced. This condition leads to larger frequency deviations and

faster $ROCOF$, which together have a serious impact on system frequency stability since the rotational inertia provides the immediate damping to counteract any power imbalance until the primary frequency control is activated (typically > 10 s) [19].

In view of the challenges mentioned above, isolated microgrids must be self-sufficient to maintain the demand-supply balance at any instant, independently of the RESs installed capacity. Therefore, the system requires new alternatives with higher flexibility to counter the stress caused by the integration of RESs, instead of forcing costly diesel gensets to respond quickly so as to maintain frequency stability. Thus, depending on the penetration level of RESs, ESSs may be employed as a buffer to provide flexibility to the system by helping gensets respond more smoothly under variable generation, storing and releasing power as needed, and providing some ancillary services (e.g., frequency and voltage control, load balancing, peak shaving, etc.). Over the past decade, extensive related research has been done, particularly on the use of BESSs and flywheels [21], [46].

Another important source of flexibility can be elasticity on the demand side. By controlling customers' appliances through a DR strategy, many grid-support services can be provided, either for normal operating conditions or emergencies (in the case of large power imbalances) [27]. DR offers a promising cost-effective way to support system frequency, since the aggregated power consumption of controllable loads may be readily manipulated in accordance with system requirements. For example, the power consumption of these loads can be removed or added, ramped up or down, or changed in step patterns, as frequently and rapidly as needed. Therefore, DR can be used to increase system reliability and efficiency, enable high penetration of RESs, reduce electricity costs, and maximize fuel savings [26]. However, the challenging task of controlling many dispersed small loads presents a major obstacle to implementing DR strategies [15].

Reliable, efficient, and coordinated integration of all resources in hybrid microgrids require an autonomous central controller to monitor, control, and optimize overall system operation. These tasks are highly complex due to the dynamics in the demand-supply balance, low inertia of the system, and the presence of RESs and ESSs. In addition, advanced control strategies, sophisticated computer software, and communications systems are needed to effectively integrate all resources. Figure 2.3 depicts a hybrid isolated microgrid representing active interaction between customers, power producers, regulation providers, and a central controller.

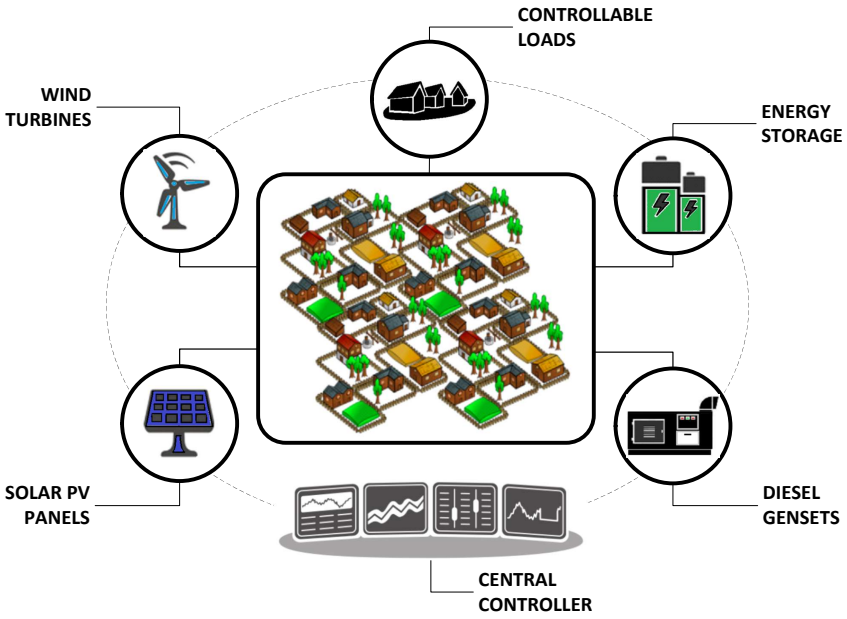

Figure 2.3: Schematic of a hybrid isolated microgrid.

2.3 Diesel Gensets

A packaged diesel engine-synchronous generator set, commonly known as a diesel genset, consists of three main components coupled through the same shaft: an internal combustion engine, a drive-train (mechanical coupling), and a synchronous generator. The governor of the diesel engine is responsible for controlling the rotating speed of the machine, i.e., frequency control, by regulating the fuel intake to the engine according to system frequency deviations. Meanwhile, the excitation system supplies and regulates the DC current to the field winding of the synchronous generator in order to control the voltage at its output terminals. Figure 2.4 schematically depicts the components of a diesel engine.

Gensets are equipped with both frequency and voltage controls. The voltage control acts much faster than the frequency control because of the order of their time constants. In fact, the larger constant in voltage control is that of the excitation field. This constant is smaller than the main constant from the frequency control, which is given by the engine and the genset's moment of inertia. Therefore, transients in the voltage control disappear faster and do not significantly affect the dynamics of the frequency control [45].

The recommended operating range of gensets is between 30 to 90% of their rated power capacity. Running them at lower levels ($< 30\%$) for extended periods leads to a pressure

drop inside the cylinders, preventing proper combustion and causing the accumulation of unburnt fuel around the piston rings, ultimately impeding adequate sealing. This condition leads to carbon buildup, glazing of the cylinder walls, and a loss in engine power. As these carbon particles are highly abrasive, they wear down the cylinder walls, which in turn reduces effective sealing. Thus, this continuous cycle leads to premature engine damage, shortening the life of the engine [48]. On the other hand, operating gensets over the recommended limit (> 90 %) restricts their capacity to bear sudden load increases without being overloaded.

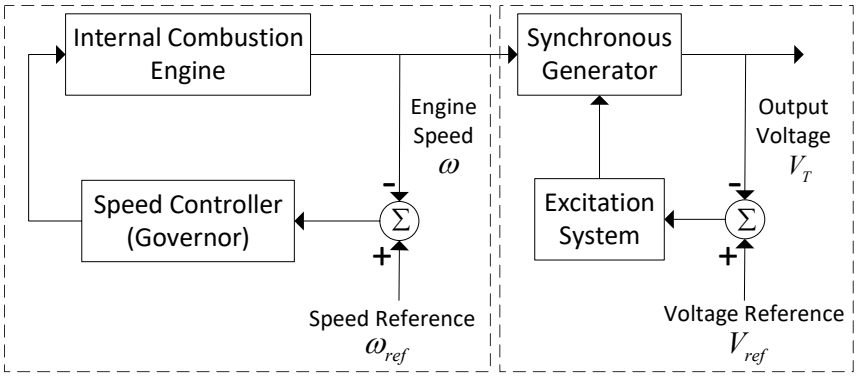

Figure 2.4: Block diagram of the main components of a diesel genset.

2.3.1 Frequency Control

Frequency is proportional to the rotation speed of the synchronous generators; therefore, the problem of frequency control can be viewed as a speed regulation control problem of the gensets. The governor regulates the fuel being injected into the engine to control its speed (or mechanical power) in order to respond rapidly to a deviation in the demand-supply balance, and provide primary frequency control [49]. To perform this action, the governor senses the speed deviation and adjusts the fuel flow according to a predefined power-frequency characteristic. Based on this characteristic, the governor's control mode is classified into isochronous control or droop control, as illustrated in Figure 2.5. In practice, these controls include a frequency dead band to avoid unnecessary adjustments during small frequency deviations, and a speed limiter to prevent the genset from surpassing its maximum speed [45].

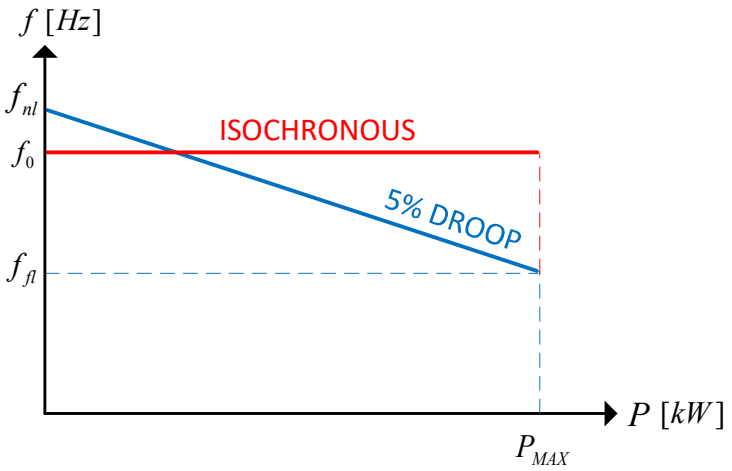

Figure 2.5: Power-frequency characteristic of a governor control.

2.3.1.1 Isochronous Control

An isochronous control keeps the same frequency setpoint regardless of the generator loading. It adjusts the fuel flow to bring the frequency back to the target frequency value. This control mode is implemented when there are a small number of gensets connected in parallel, and the frequency control (load variation) is shared proportionally to their power rating. When several units are equipped with this control, they may affect against each other, as each tries to regulate the frequency following its power-frequency characteristics independently of the actions of other units.

2.3.1.2 Droop Control

A droop control changes the steady-state frequency setpoint as a function of the generator loading, using a linear relationship, as follows (Figure 2.5):

$$P_G = s_p \left(f_{nl} - f_{sys} \right) \tag{2.2}$$

where f_{nl} is the no-load frequency, s_p is the slope factor in kW/Hz, f_{sys} is the system frequency, and P_G is the active power supplied to the system. This droop characteristic is fixed by the parameters s_p and f_{nl}, and gives all possible operating points (P_G, f_{sys}). Droop D is defined in practice as the percentage change in frequency needed for a governor

to drive the unit from zero to full-load condition (or vice-versa):

$$D = \frac{f_{nl} - f_{fl}}{f_{fl}} \, 100\% \tag{2.3}$$

where f_{fl} is the frequency at full-load. D is designed to reduce f_{nl} between 3 to 5% as the unit reaches its maximum load [55]. This control mode is necessary when many generating units are connected in parallel. Thus, every unit reacts according to its droop characteristic to control frequency deviations. Some units may respond faster, but all operate to counteract a disturbance. Typically, this control mode is implemented in small gensets due to their flexibility to modify their output power quickly [48].

2.3.2 Fuel Consumption Rate

The Fuel Consumption Rate (FCR) denotes the amount of fuel needed to generate a certain amount of electricity kW over one hour. A chart with the correlations between the specific fuel consumption at certain percentages of the generator output power P_G, i.e., 25%, 50%, 75%, 100%, is usually provided by the manufacturer. Using this chart, it is possible to calculate the FCR related to the same percentages of P_G as follows:

$$FCR = c \, P_G \, \frac{1}{\rho_{fuel}} \, \sigma \tag{2.4}$$

where c is the specific fuel consumption, ρ_{fuel} is the fuel density, and σ is a conversion factor used to transform m^3/h to L/h. In order to obtain the FCR at any point over the entire operating range of the diesel genset, the FCR data points previously calculated are used to build a second order function.

2.3.3 Efficiency

Efficiency η_G is a parameter used to evaluate the performance of the energy conversion in a genset. It is expressed as the combined efficiency from the diesel engine and the synchronous generator. Typically, for internal combustion engines, η_G varies between 30-55%, and it depends on several factors such as size, fuel type, technology, cooling systems, control systems, as well as the current loading condition. Efficiency can be directly calculated by expressing the ratio between the input chemical energy and the output electrical energy,

as a function of FCR and P_G, as follows:

$$m_{fuel} = \rho_{fuel} \left(\frac{FCR}{1000} \right) \tag{2.5}$$

$$\eta_G = \frac{3.6\, P_G}{m_{fuel}\, LHV_{fuel}} \, (\%) \tag{2.6}$$

where the constant 3.6 is a conversion factor, since 1 kWh = 3.6 MJ, m_{fuel} is the mass flow rate of the fuel, and LHV_{fuel} is the lower heat value of the fuel.

2.4 Demand Response

Maintaining system security and stability becomes challenging as the penetration of RESs increases. In this context, it is necessary to explore new mechanisms and control strategies for the provision of frequency support services in order to meet the increased ramp and capacity requirements to integrate renewables into the system effectively. From this standpoint, DR has the potential to become an essential contributor to grid modernization and as a key to extend grid flexibility, improve efficiency, and facilitate the penetration of RESs [26]. DR has shown equal or better performance and response characteristics than conventional generating units. In fact, theoretically, demand can contribute to frequency control in a similar fashion to that of conventional generation reserves [15].

Based on the available resources, i.e., communication channels and type of controllable loads, and the control strategy adopted, DR may provide various frequency support services on different time scales (e.g., regulation, ramping, spinning reserves). These services are indispensable in dealing with the critical demand-supply balance and mitigate the variability and uncertainty associated with significant renewable energy penetration. In general, the DR control strategies for the provision of frequency support services can be grouped into two categories [18]:

- Utility-side control: This control strategy focusses on the response of an aggregated cluster of loads for improving system security and stability. It requires a two-way communication channel to transmit a control signal to all controllable loads. In principle, it aims to reduce the generation-side frequency reserves and increase the response speed from the aggregated cluster of loads. Although this control precisely determines the total aggregated demand needed to provide a specific frequency support service, it may require that individual responses from controllable loads remain

unchanged for long periods, thus increasing their duty cycles and affecting customer comfort. The major challenge in implementing this control strategy is to coordinate the response of many dispersed controllable loads in real-time to provide frequency services [15].

- Customer-side control: This control strategy focusses on the individual response from controllable loads. Thus, each load has a controller that measures the system frequency locally and based on a predefined control logic, it adjusts the load power consumption. In general, the logic used to perform these operations is based on minimizing the effects on consumer comfort while responding to frequency deviations. Since there is no communication channel to allocate the capacity between generators and controllable loads and coordinate their operation, the aggregated load response may be insufficient to correct large frequency deviations [41].

In essence, DR controls customers' controllable loads in response to predefined logics, in order to manipulate the aggregated demand profile to provide a service to the system. Consequently, the individual load consumption from each type of controllable load must be adjusted according to its intrinsic characteristics. In this regard, residential controllable loads can be grouped into four types [27], [28]:

- Pure resistive loads: These loads can tolerate high-frequency operations since there is no lockout time after each switching action; therefore, they can be immediately connected/disconnected to provide fast frequency regulation. EWs and EHs are examples of this type.

- Compressor-based loads: The operating cycle of these loads is restricted by a lockout time after being turned OFF. Commonly, the lockout time is 5 minutes to avoid compressor stall. ACs and GSHPs are examples of this type.

- Variable Speed Heat Pumps (VSHPs): These loads differ from the two previous types because their power consumption can be dynamically adjusted as a function of the compressor rotor speed. In other words, VSHP's power consumption can be regulated to any point between zero and the full rated capacity by varying its compressor speed; therefore, fast frequency regulation can be provided by using a compressor variable-speed controller.

- Electric Vehicles (EVs): These loads are considered to be distributed ESSs. Their charge-discharge cycles can be dynamically adjusted to provide fast frequency regulation considering both the state-of-charge of the battery (SoC) and the system frequency deviation.

Elasticity from the aggregated load demand to track and compensate frequency deviations is reflected through different response levels, i.e., period, depth, and direction, which can be obtained by using a DR strategy [26]. Thus, depending on the adopted strategy, one or more of these levels can be combined to achieve a specific effect on system frequency at a particular time. Figure 2.6. shows a schematic of these response levels.

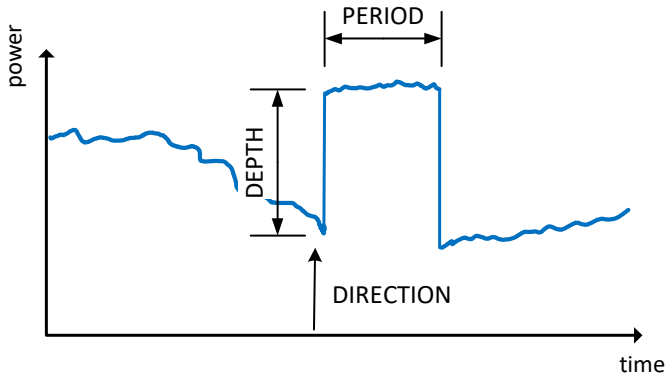

Figure 2.6: Response levels from an aggregated load profile.

DR strategies must be adequately designed to balance the system's response requirements and individual consumer comfort choices and usage patterns, since customer preferences differ. Moreover, wear and tear of appliances and the impacts on their lifespan must be addressed when designing a control strategy. Therefore, the success of DR depends on customers' satisfaction and awareness of the benefits obtained from implementing it. For example, in [33], it is shown that if the operation of frequency-responsive appliances has an unnoticeable pattern consumption change, most consumers will agree to participate in a DR program.

2.5 Residential Loads

The electric power consumption of single-family households depends on many factors such as the number of occupants and their patterns of active occupancy, socio-economic condition, geographic location, house archetype, the time of the day, season, etc. Moreover, daily load profiles vary not only between households with similar characteristics but also from one day to another. Thus, the frequency at which every appliance and electronic device is powered in a household is influenced by user habits and their attitude towards

energy use/energy savings [41]. Therefore, to design a DR strategy, it is necessary to consider the load consumption patterns (duty cycle) of individual loads and how they can be modified. In this regard, household loads can be classified into TCLs and non-TCLs. In the case of TCLs, since these loads provide thermal services (e.g., heating or cooling), they cycle throughout the whole day, with a periodicity determined by a thermostat setting and customer behavior. On the other hand, the power consumption pattern of non-TCLs depends exclusively on customer behavior. Figure 2.7 depicts a classification of the loads in a typical household.

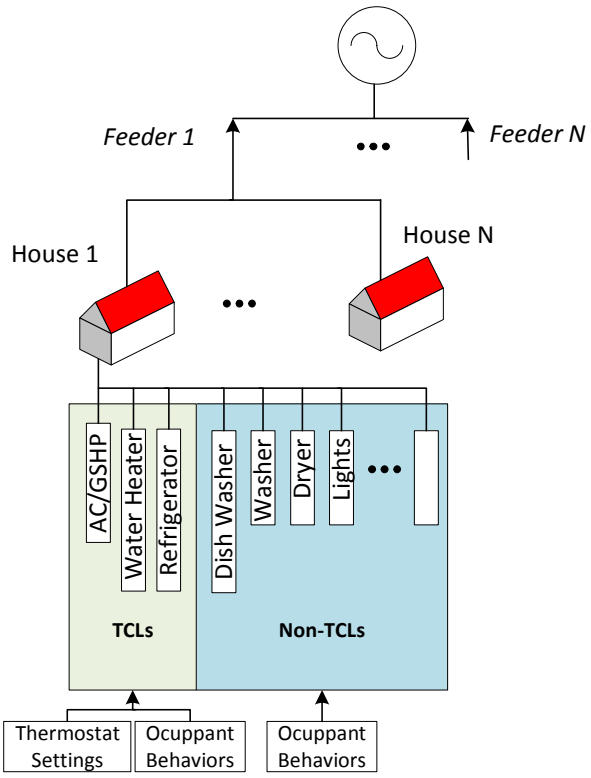

Figure 2.7: Loads in a typical household [56].

2.5.1 Thermostatically Controllable Loads

DR strategies for TCLs are presented as fast-acting and non-fuel-consuming alternatives for improving power quality, supporting RESs integration, and providing fast frequency regulation and load balancing services. Moreover, by virtue of their thermal inertia, TCLs

can be considered as thermal batteries [32]. Therefore, their power consumption can be shifted, or controlled by switching operations without affecting consumer comfort.

The duty cycle of a TCL is determined by the dynamics of the temperature T_t (e.g., hot water temperature, indoor air temperature, etc.) that is constantly monitored by a thermostat. The thermostat has a setpoint temperature T_0, and in order to prevent a sequence of rapid operations and excessive wear due to small temperature variations, a dead band temperature T_{db} is used during regular operation. If T_t hits the dead band limits, the thermostat sends commands to a controller to turn the TCL ON/OFF. If turned ON, the TCL consumes its rated power; otherwise, no power is consumed. Most TCLs only allow changing the T_0 setting, while the dead band is invariant. Figure 2.8 illustrates the duty cycle of a TCL under normal operation conditions, where the dead band temperature and its upper and lower threshold limits (T_{high} and T_{low}) are defined as follows:

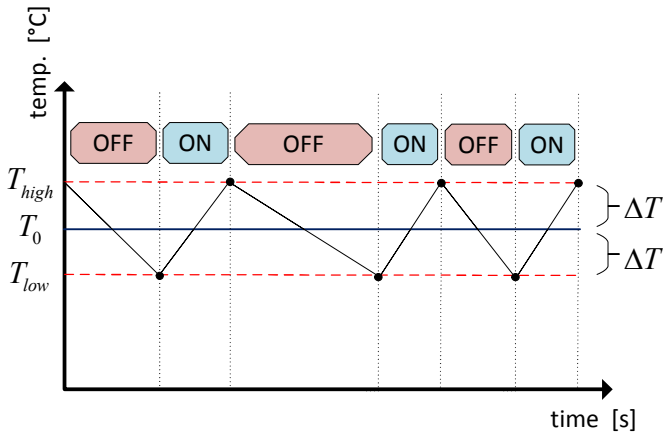

Figure 2.8: Duty cycle of a TCL.

$$T_{db} = 2\Delta T = \frac{T_{low} + T_{high}}{2} \tag{2.7}$$

$$T_{high} = T_0 + \Delta T \tag{2.8}$$

$$T_{low} = T_0 - \Delta T \tag{2.9}$$

For a TCL providing cooling (e.g., AC or GSHP (cooling mode)), the following equation determines the thermostat operating states (switch position):

$$state \begin{cases} ON & T_t > T_{high} \\ OFF & T_t < T_{low} \\ s_{n-1}(t) & T_{low} < T_t < T_{high} \end{cases} \tag{2.10}$$

Conversely, for a TCL providing heating (e.g., EWH or GSHP(heating mode)), the relationship of the ON/OFF states are inverted with respect to the limits of the dead band temperature. Equation (2.10) shows that the power consumption of a TCL can be modulated by controlling T_0. In this context, a DR strategy can control TCLs duty cycles to provide primary frequency control, while considering their thermal constraints and consumer comfort. Therefore, among TCLs, the ideal candidates to participate in a DR strategy should meet the following conditions [28], [32]: (a) high-thermal inertia to avoid affecting user comfort, while providing frequency support services; (b) high-power consumption to obtain a significant aggregated power compensation; and (c) continuous operation, since frequency support can be unexpectedly required. Thus, ACs, GSHPs, and EWHs have great potential to provide regulation services, since these loads not only have high-thermal inertia and a high-power rating, but also their power consumption represents a significant percentage (70 to 80%) of the daily load demand of a household. Moreover, these are frequently in operation, which is indispensable, as regulation is required all the time.

2.5.2 Thermal Load Modeling

Accurate modeling of the heat transfer processes and power consumption cycles of TCLs is essential in successfully designing a DR strategy. In this regard, the method called Thermal Equivalent Circuit (TEC) can be adopted to model the thermodynamic processes. This method uses the analogy between the thermal and electrical variables to represent heat transfer processes by means of an electrical circuit with few lumped parameters [57]. Then, by using common circuit solution techniques, i.e., network nodal analysis, the differential equations that describe the thermodynamic processes are formulated. Table 2.1 shows the analogy between thermal and electrical variables.

The thermal and mechanical properties used to describe the basics of heat transfer processes occurring through a homogeneous material are:

- Thermal conductivity k_{th} specifies the rate of heat transfer through a homogenous material.

- Specific heat c_p determines the amount of heat per unit mass needed to increase the temperature of a homogenous material by 1 ℃.
- Density ρ is a measure of mass per unit volume.

These properties, along with the geometric dimensions of the material (i.e., area A_m and thickness L_m), allow defining the lumped parameters as follows:

- Thermal capacitance represents the thermal inertia of a specific material, and qualitatively expresses the amount of heat the material can store:

$$C_{th} = c_p \, \rho \, A_m \, L_m \tag{2.11}$$

- Thermal Resistance is a measure of the capacity of a specific material to resist heat flow:

$$R_{th} = \frac{L_m}{k_{th} \, A_m} \tag{2.12}$$

Table 2.1: Thermal-electrical analogies.

Thermal Variable	**Symbol**	**Units**	**Electrical Variable**	**Symbol**	**Units**
Temperature	T	℃	Voltage	V	V
Heat	Q	W	Current	I	A
Conductance	UA_{th}	W/℃	Conductance	G	S
Resistance	R_{th}	℃/W	Resistance	R	Ω
Capacitance	C_{th}	J/℃	Capacitance	C	F

Commonly, the building envelope sections of a household (i.e., walls, roof, floor, and windows) are built of various layers of different materials. Consequently, C_{th} and R_{th} must be expressed as the equivalent of the individual lumped parameters of its layers:

$$R_{th} = R_{th1} + R_{th2} + ... + R_{thn} \tag{2.13}$$

$$C_{th} = C_{th1} + C_{th2} + ... + C_{thn} \tag{2.14}$$

The rate of heat transfer $\dot{Q}$ through a material with thermal resistance R_{th}, as depicted in Figure 2.9, is calculated as a function of a differential of temperature $\Delta T = T_1 - T_2$:

$$\dot{Q} = \frac{T_1 - T_2}{R_{th}} = UA_{th}\,(T_1 - T_2) \tag{2.15}$$

where UA_{th} is known as the heat transfer coefficient $(U - factor)$ and is the inverse of the thermal resistance R_{th}.

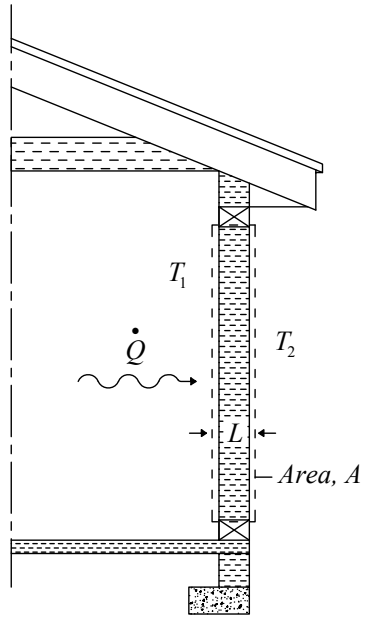

Figure 2.9: Heat transfer through a wall [58].

2.5.3 Air Conditioner

In [58], heat is defined as a form of energy that is always transferred when there is a temperature difference, and according to the second law of thermodynamics, heat always moves from a warmer to a cooler zone. From this standpoint, the main objective of a residential AC is to remove extra heat entering a household from the outside environment. In other words, an AC is used to maintain the household temperature below that of its surroundings by pumping heat from inside to outside [36].

A typical AC (Figure 2.10) consists of four main components: compressor, condenser, expansion valve (throttling device), and evaporator. The evaporator is connected to an internal open loop circuit, whereas the condenser is in contact with the outside environment. The internal circuit comprises the forced-air distribution system inside the household. To provide cooling for climate control, the AC removes heat from the indoor air by circulating a refrigerant through the four components, in accordance with a vapor-compression refrigeration cycle. The condenser and evaporator are known as heat exchangers (HXs), as they enable heat exchange between two fluids while preventing their contact [58]. Both HXs consist of tubing loops with fins to increase the surface area where the heat exchange takes place.

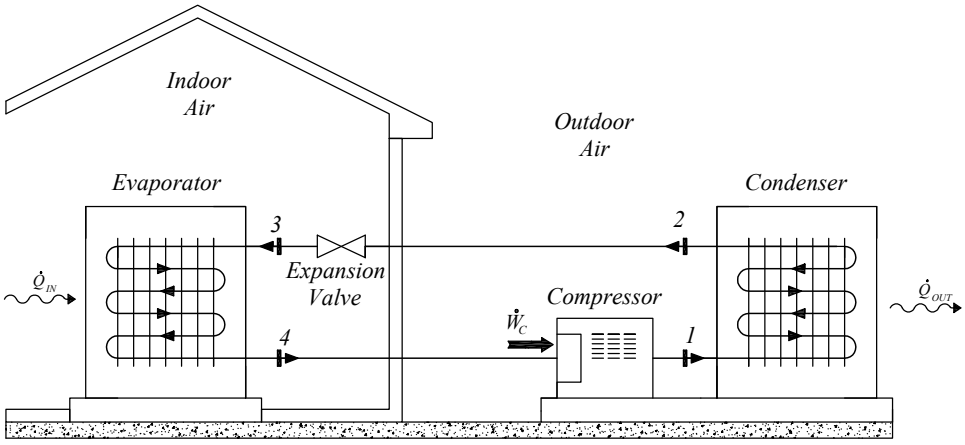

Figure 2.10: Basic configuration of a split AC [59].

Two types of residential AC systems are available on the market: (a) packaged AC systems, and (b) split AC systems; most consumers prefer a split AC system in their homes [60]. A packaged AC is a self-contained unit that combines all its components in a single cabinet, whereas the split AC has the compressor and condenser installed in an outdoor cabinet while, the expansion valve and the evaporator are installed in a cabinet inside the household. The operating principle for both configurations of ACs is similar and is explained next.

The refrigeration cycle is conducted in four stages:

1. The compressor unit compresses the low-pressure, low-temperature vapor refrigerant, transforming it into a high-pressure, high-temperature vapor refrigerant.

2. This vapor refrigerant passes through the condenser while outside air is blown over the condenser' finned tubes. Since this vapor has a temperature higher than of the outside air, heat is released to the environment. Therefore, the vapor reduces in temperature and is transformed into a high-pressure, high-temperature liquid.

3. The liquid refrigerant passes through the expansion valve, and becomes a low-pressure, low-temperature liquid.

4. The liquid refrigerant passes through the evaporator while the air in the internal loop is blown over the evaporator's finned tubes. At this stage, the liquid has a temperature lower than that of the indoor air; therefore, two sub-processes take place: (1) the liquid absorbs heat from the indoor air, thus increasing in temperature, resulting in the liquid being transformed into a low-pressure, low-temperature vapor; and (2) the air in the internal loop circuit reduces in temperature and is blown back to the household to provide cooling.

When the compressor is turned ON, a small electric pump circulates the refrigerant through the four components. Additionally, two fans blow the internal and external air over the evaporator and condenser coils, respectively.

To maintain an adequate indoor temperature, prevent health problems, and reduce electricity bills, the American Society of Heating, Refrigerating and Air-Conditioning Engineers (ASHRAE) recommends a thermostat setpoint within 23 to 25 ℃ during summer and 21 to 23 ℃ during winter [60]. Furthermore, with today's AC technology, cooling systems may provide additional functions such as relative humidity (RH) and air motion control [59]. High RH may cause structural damage to households and serious health problems [58]; thus according to health organizations such as the Lung Association of Ontario, the acceptable indoor RH range varies between 40 to 60%, with 50% being the most desirable level to reduce the growth of moulds and dust mites, and increase the rate mortality of certain harmful organisms. Figure 2.11 shows a chart with the optimal humidity range for human exposure. On the other hand, indoor air motion is a determining factor for thermal comfort, as in excess it may cause an undesired cold sensation; therefore, the indoor air velocity must be strong enough to unnoticeably replace the warm air generated around a body with fresh air [58]. The literature suggests an air velocity of less than 9 m/min in winter and 15 m/min in summer [59].

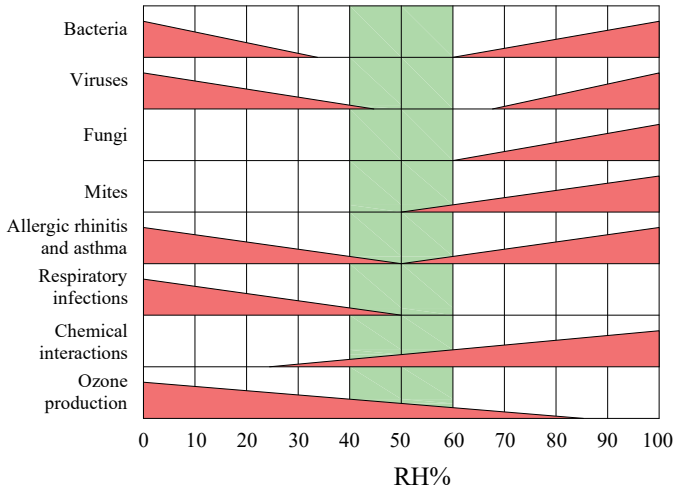

Figure 2.11: Sterling Chart. Recommended indoor RH% for optimal health benefits [61].

2.5.3.1 Coefficient of Performance

The heat transfer process from a cold space (household) to a warm space (outside environment) requires work (AC compressor) to pump heat in this direction, against its natural flow. Figure 2.12 depicts the heat flow balance performed by an AC in cooling a household. The efficiency of an AC is referred to as the Energy Efficient Ratio EER and relates the amount of heat removed from the household Q_c divided by the electric power required to move this heat W_c. Thus, EER is a measure of how many units of heat (cooling effect) are removed from the household for each unit of electrical energy consumed by the AC, as follows:

$$EER = \frac{\text{desired output}}{\text{required input}} = \frac{\text{cooling effect}}{\text{work input}} = \frac{Q_c}{W_c} \tag{2.16}$$

EER is affected by different factors such as the outdoor and the indoor air temperatures, the compressor, condenser, and evaporator efficiencies, the AC technology, the internal heat gains in the household, etc. Therefore, EER given in (2.16) is determined for a set of specific operating conditions. In general, for ENERGY STAR® certified ACs[1], EER ranges from 8 to 12. Commonly, the capacity of an HVAC system (i.e., AC or GSHP)

[1]The ENERGY STAR® symbol certifies that an appliance is among the most energy-efficient on the market.

is given in Tons or in British Thermal Units (BTU), and its typical capacity ranges from 9,000 to 60,000 BTU [34].

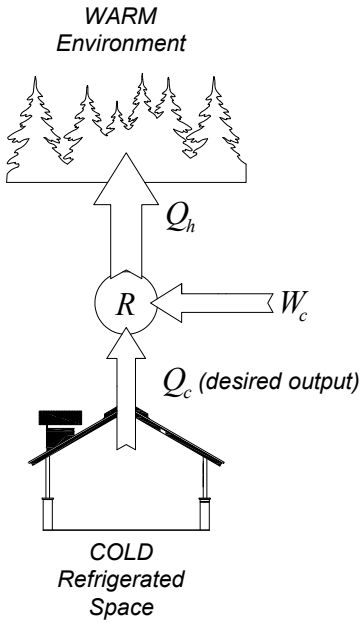

Figure 2.12: Sankey diagram of an AC.

2.5.3.2 Operating Cycling

According to the classification presented in Section 2.4, an AC corresponds to a compressor-based load. In this regard, its switching operations are restricted by a lockout time [18]. The AC compressor is powered via a PTC resistor; therefore, when the compressor is turned OFF, the PTC is still warm and requires recovery time to cool down, which commonly ranges from 3 to 5 minutes; otherwise, the PTC resistance value will be high enough to reduce the starting current to an insignificant value, and the compressor will stall. Consequently, a DR strategy has to consider this lockout time when controlling the duty cycle of the AC to provide frequency regulation.

2.5.4 Ground Source Heat Pump

A GSHP is an eco-friendly technology able to provide year-round climate control for residential households and commercial buildings [36]. This system uses the ground as a heat

sink in summer and as a heat source in winter. A few meters below the surface, the ground temperature remains relatively constant throughout the year, unlike the ambient air temperature, which suffers significant variations over the year. Thus, when the temperature of the ambient air is higher than that of the ground, the GSHP pumps heat to the ground so as to cool the household; otherwise, the GSHP absorbs heat from the ground and releases it into the household [14]. Two types of GSHP systems are available on the market, and their differences lie in the orientation of their ground heat exchanger (GHX): (a) GHX with pipes buried in horizontal trenches, and (b) GHX with pipes buried in vertical boreholes. However, according to [62], the system most commonly used in North America is the one with a vertical GHX, because of the minor land area required to drill the boreholes. Therefore, for the purposes of this thesis, only this type of GSHP system is studied.

A GSHP with a vertical GHX consists of a compact water-to-air heat pump (HP) with the capacity to reverse the flow of its refrigerant according to the cooling or heating operating mode. The HP is connected to an external closed loop circuit and an internal open loop circuit (Figure 2.13). The external circuit includes one or more boreholes drilled into the ground where heat is exchanged between the borehole (connected in series or parallel) and its surrounding ground. On the other hand, the internal circuit comprises the forced-air distribution system (ductwork) inside the household.

The HP has five main elements: (a) a refrigerant-to-air HX (connected to the internal circuit), (b) a water-to-refrigerant HX (connected to the external circuit), (c) a reversible valve, (d) a compressor, and (e) an expansion valve. Both HXs can switch their functions to operate either as a condenser or as an evaporator. According to the indoor temperature, which is monitored by a thermostat, the HP controller turns its compressor ON/OFF to control the heat transfer process between the household and the ground. The GHX consists of a circular borehole containing a high-density polyethylene U-pipe, across which a biodegradable and non-toxic fluid (e.g., water or a water-antifreeze solution) is circulated to absorb/reject heat from the ground. The rest of the borehole is filled with a high-thermal-conductivity material known as grout (e.g., sand, a cement-bentonite mix, etc.). The standard diameter of the borehole ranges from 20 to 40 cm, whereas the diameter of the legs of the U-pipe varies from 25 to 40 mm [62]. The GHX is designed according to the cooling/heating demand and the ground conditions, and commonly its depth ranges between 30 to 300 m.

2.5.4.1 Cooling Mode

In this operating mode, heat is pumped from the household to the ground. The heat transfer process is conducted by means of a refrigeration-cycle as follows:

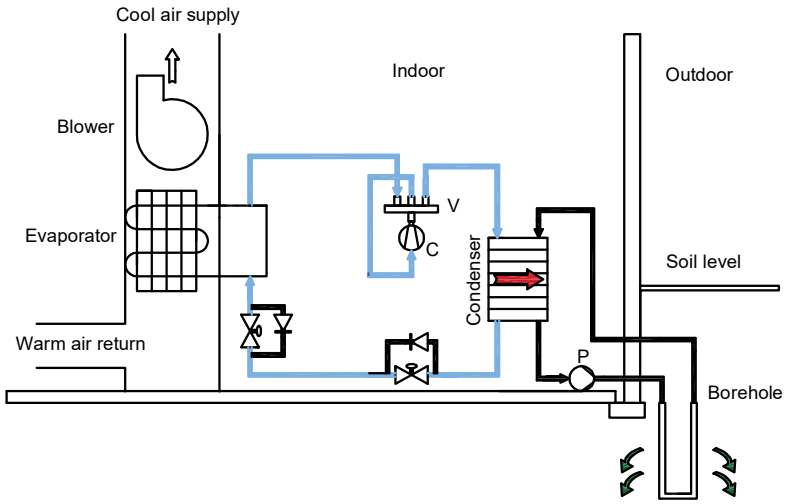

(a) Cooling mode

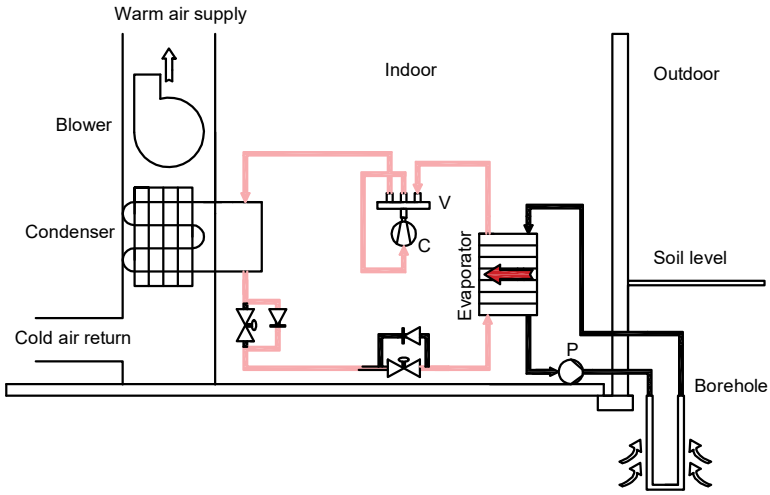

(b) Heating mode

Figure 2.13: Operating cycle of a GSHP [13].

1. The compressor unit compresses the low-pressure, low-temperature vapor refrigerant, transforming it into a high-pressure, high-temperature vapor refrigerant.

2. Both, the vapor refrigerant and the fluid coming from the GHX pass through the water-to-refrigerant HX (acting as a condenser). Since the vapor has a temperature higher than that of the fluid, two sub-processes take place: (1) the fluid absorbs

heat and increases in temperature (subsequently, this extra heat will be released to the ground, thus reducing the fluid temperature to start the process over); and (2) the vapor reduces in temperature and is transformed into a high-pressure, high-temperature liquid.

3. The liquid refrigerant passes through the expansion valve, transforming it into a low-pressure, low-temperature liquid.

4. This liquid refrigerant passes through the air-to-refrigerant HX (acting as an evaporator) while the air in the internal loop is blown over the HX tubing. In this stage, the liquid has a temperature lower than the indoor air's; therefore, two sub-processes take place: (1) the liquid absorbs heat from the indoor air and increases in temperature, transforming it into a low-pressure, low-temperature vapor; and (2) the air in the internal circuit reduces in temperature and is blown back to the household to provide cooling.

2.5.4.2 Heating Mode

In this operating mode, heat is absorbed from the ground and pumped into the household. The reversible valve is used to reverse the flow of the refrigerant, and both heat exchangers switch their functions. The heat transfer process is conducted by means of a heat-pump-cycle as follows:

1. The compressor unit compresses the low-pressure, low-temperature vapor refrigerant, transforming it into a high-pressure, high-temperature vapor refrigerant.

2. This vapor refrigerant passes through the air-to-refrigerant HX (acting as a condenser), while the air in the internal loop is blown over the HX tubing. This vapor has a temperature higher than that of the indoor air; therefore, two sub-processes occur: (1) the vapor reduces in temperature and is transformed into a high-pressure, high-temperature liquid, since it releases heat to the air in the internal loop; and (2) the air in the internal open loop increases in temperature and is blown back to the household to provide heating.

3. The liquid refrigerant passes through the expansion valve, and becomes a low-pressure, low-temperature liquid.

4. The liquid refrigerant passes through the water-to-refrigerant HX (acting as an evaporator) and the fluid coming from the GHX loop is also pumped through it. As the

liquid has a temperature lower than the fluid, two sub-processes occur: (1) the fluid by releasing heat to the liquid refrigerant reduces in temperature (subsequently, this fluid will flow across the GHX and so increase its temperature by absorbing heat from the ground to start the process over); and (2) the liquid increases in temperature and is transformed into a low-pressure, low-temperature vapor.

2.5.4.3 Coefficients of Performance

As previously discussed, when a GSHP is working in cooling mode, it performs a refrigeration-cycle. Otherwise, the refrigerant flow is reversed, and both heat exchangers switch their functions; thus, the GSHP performs a heat-pump-cycle. In principle, both cycles are conducted similarly; however, their roles differ. Whereas the purpose of a refrigeration-cycle is to remove heat from the household, the heat-pump-cycle supplies heat to the household. The thermal performance for both operating modes relates the heat removed/absorbed from/to the household divided by the electric power required to move this heat. For the cooling mode, the coefficient of performance is known as the EER (analog to that of an AC), whereas for the heating mode it is simply COP, as follows, based on Figure 2.14:

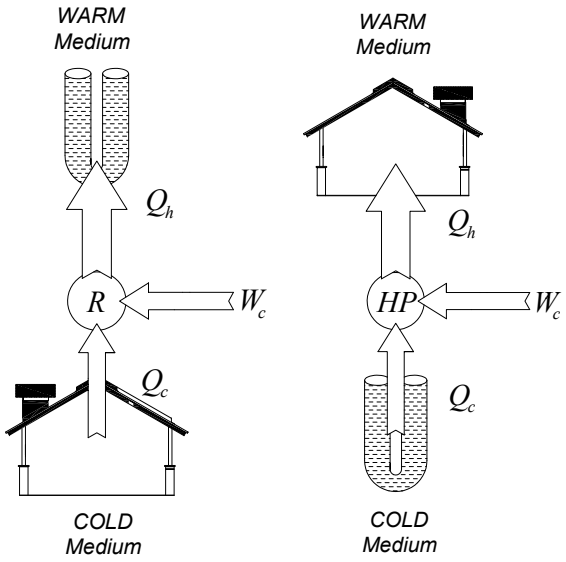

(a) Cooling mode (b) Heating mode

Figure 2.14: Sankey diagram of a residential GSHP.

$$EER = \frac{\text{desired output}}{\text{required input}} = \frac{\text{cooling effect}}{\text{work input}} = \frac{Q_c}{W_c} \tag{2.17}$$

$$COP = \frac{\text{desired output}}{\text{required input}} = \frac{\text{heating effect}}{\text{work input}} = \frac{Q_h}{W_c} \tag{2.18}$$

For both cooling and heating modes, GSHPs are designed to operate over a wide range of inlet fluid and air temperatures coming from the GHX and the internal open loop, respectively. Therefore, the performance coefficients given in (2.17) and (2.18) are obtained only for a specific set of operating conditions. In general, for ENERGY STAR® certified GSHPs, the COP ranges from 3.6 to 5.2, and the EER from 16.2 to 31.1. The rated capacity of a GSHP is provided in terms of its cooling capacity.

2.5.4.4 Operating Cycling

A thermostat is used to monitor indoor air temperature, sending commands to the GSHP controller to turn the compressor ON/OFF, and thus control the heat transfer process to maintain the indoor temperature within adequate limits. Due to the high thermal inertia of the household and the high-power consumption of the HP compressor, a GSHP is an excellent candidate to participate in a DR strategy for frequency control without affecting consumer comfort. The thermal inertia allows control of the compressor power consumption as a function of system frequency variations. GSHPs have the same restriction as conventional ACs, requiring a lockout time when it is turned OFF to avoid compressor stall. Consequently, a DR strategy has to consider this lockout time needed to control the duty cycle of the GSHP in order to provide frequency regulation, being the same as an AC.

2.5.5 Electric Water Heater

An EWH uses electrical energy, 15 to 25% of the total residential load consumption, to increase and control water temperature. Two types of EWHs are available on the market: (1) a tank-type EWH that stores hot water in a tank, and (2) tankless EWH that only heats water as needed. The tank-type EWH is the most common model used in North America [9]; therefore, only this type is considered here.

A residential tank-type EWH has an insulated metal-sheet cylindrical tank where hot water is stored until it is needed. Typically, the storage capacity of a residential tank-type

EWH varies between 20 to 80 gallons (75 to 80 litters), with 50 gallons being the most commercialized [25]. The tank includes one or two heating elements, an inlet pipe for the cold water, and an outlet pipe for the hot water. Each heating element has a thermostat, which is attached to an electrical resistor enclosed by a sheath of stainless steel or copper, as depicted in Figure 2.15. Additionally, there are two standard tank-type EWH models:

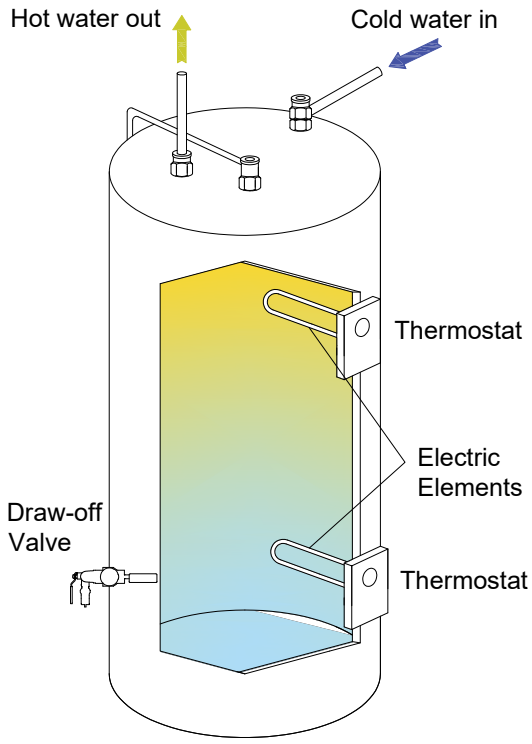

Figure 2.15: Tank-type EWH with two heating elements [53].

- A single-element EWH has only one temperature control element for the whole water mass inside the tank. This element is located close to the bottom of the tank, and it is responsible for maintaining the water temperature according to its thermostat setpoint.
- A dual-element EWH has two temperature control elements (upper and lower) that work alternately to heat and control the water temperature. When hot water is being used, cold water enters the tank and moves to the bottom because of its density. Then, the upper element is turned ON to regulate the water temperature at the top

of the tank according to the predefined setpoint. After that, the lower element is turned ON to heat the water at the bottom of the tank. In this manner, water is heated more uniformly due to the alternative operation of both elements. In terms of operation time, the lower element works more frequently, because it heats the cold water that later is moved up with a higher temperature [9].

After hot water is drawn from the storage tank, cold water refills the tank. As a result, the internal water temperature decreases as a function of both the inlet cold water and the conduction losses (thermal losses through the isolation). Therefore, the water temperature has to be controlled by means of a thermostat whose setpoint can be adjusted according to consumer preferences [34]. The heating elements are switched ON/OFF in a hysteresis fashion, as the temperature varies within the thermostat's dead band, which comprises a few degrees above and below the setpoint. When the temperature hits the dead band's lower limit, the thermostat closes the switch, allowing current flows through the resistor, thus generating heat which is absorbed by the water. The switch remains closed until the water temperature hits the dead band's upper limit. As a heating element basically consists of a resistor, this load does not demand reactive power and has a high electric-thermal efficiency conversion. Therefore, the power consumption accounts for heating the inlet cold water and compensating for the conduction losses.

Hot water consumption, analogously to the electric consumption, differs according to the number of occupants, geographical location of the house, facilities (bath, shower, etc.), appliances (dishwasher, washing machine, etc.), and consumer habits (frequency and duration of consumption). Hot water usage involves activities such as dishwashing, hand washing, cooking, showering, and leaks. In [63], comprehensive research was performed to estimate the daily average hot water usage in North American houses, which was found to be 51.1 gallons (193.4 liters) per day.

According to healthcare societies and organizations, such as the American Society of Sanitary Engineering or the Public Health Agency of Canada, there are two opposing risks when selecting the temperature of water inside the tank: risk for thermal shock and scalding injuries if the temperature is high, and risk of exposure to Legionella (bacteria responsible for Legionnaires' disease – pulmonary legionellosis) if the temperature is low. Thus, the temperature range established to avoid exposure to these health problems can vary between 49 to 60 ℃ [53], since at a temperature higher than 49 ℃, the bacteria Legionella does not survive, whereas with a temperature lower than 60 ℃, the risk of scalding and mineral build up in the EWH tank and pipes is reduced.

An EWH is considered an ideal candidate to participate in a DR strategy. Its high thermal inertia allows storing thermal energy by heating water, thus acting as a thermal

battery (with similar features to any other ESS technology). As the heating element contains a resistor, its power consumption can be controlled as fast and frequently as needed with near instantaneous response in order to provide frequency regulation without affecting consumer comfort.

2.6 Simulators

2.6.1 Smart Residential Load Simulator

The Smart Residential Load Simulator (SRLS) [34] is a freeware based on Matlab-Simulink-GUIDE toolboxes, developed to facilitate the study of EMSs in smart grids. It provides user-friendly interfaces to study the power and energy consumption patterns of typical appliances (i.e., ACs, furnaces, EWHs, refrigerators, stoves, dishwashers, washing machines, dryers, pool pumps and different types of light-bulbs) and their related costs, in a single-family household over a 24-hour horizon. In addition, the simulator models the local power generation from a wind turbine and/or a solar PV panel, as well as a small battery system. The influence of occupants' activity levels, solar radiation, and ambient temperature, on energy consumption patterns, is also considered. The simulator results have been validated by comparing its mathematical models with actual measurements.

2.6.2 CREST Domestic Electricity Demand Model

The CREST simulator [64] is a Microsoft Excel® macro-enabled workbook that provides a high-resolution representation of the domestic demand from a single dwelling. It models the load consumption pattern from a large number of household appliances over 24 hours by considering factors such as the number of occupants and their active occupancy patterns, the month of the year, and solar irradiation. A configuring interface enables users to select up to 33 appliances when performing case studies. The simulator maps occupancy patterns and employs appliance-usage probability to generate the load demand profiles stochastically. It has been validated by contrasting its results with actual measured data sets showing similar demand patterns.

2.6.3 DHW Event Schedule Generator

The DHW Event Schedule Generator [65] is a Microsoft Excel® macro-enabled spreadsheet tool able to stochastically generate hot water schedules over a one-year horizon, based on

the probability distributions of hot water usage (from sinks, showers, baths, clothes washers, and dishwashers), duty cycles, flow rates, water-draw profiles, weather, and seasons. The tool includes a user-friendly interface that allows the generation of random profiles based on the number of rooms, location of the household, and temperature of both the water inside the tank and the water draws. Additionally, the user can select different time-steps between 1 to 360 seconds. As a result, this tool generates realistic residential hot water profiles that can be used to determine the electric power consumption from an EWH.

2.7 Summary

In this chapter, a background of the main concepts required to develop the proposed DR strategy for primary frequency control was introduced. First, the frequency control architecture and different grid support services needed to maintain the demand-supply balance in a microgrid were described. Then, the technical challenges resulting from the mix of RESs and conventional generation sources were reviewed. A synopsis of DR strategies for residential controllable loads was presented next. Then, the components, operation, and restrictions of TCLs, i.e., EWHs, ACs, and GSHPs, were described in detail, as these form the basis for the DR strategy described in the next chapter. Finally, a brief description of the simulators used to model realistic residential load demand and hot water consumption profiles was presented.

Chapter 3

Modeling and Controls

This chapter presents the proposed modeling of the different components of a hybrid PV-diesel microgrid, and discusses the design of the developed DR strategy for primary frequency control. Thus, the droop control model of a diesel genset is presented first, followed by the design and modeling of a solar PV system. Then, the thermo-electrical models of EWHs, ACs, and GSHPs are described, and their simulation results are presented and discussed. Next, the use of the simulators introduced in the previous chapter to generate random load demand and hot water consumption profiles is described. Finally, the characteristics and control logics of the proposed DR strategy are presented. The models developed in this thesis were implemented in a MATLAB/Simulink (R2018a) environment.

3.1 Diesel Gensets

The standard Woodward governor model DEGOV_1 is used here, since it is utilized in several industry-grade transient electromechanical programs, as well as in research works [66, 67]. This governor model consists of three components: an electronic control box, a fuel control actuator, and a droop compensator. Figure 3.1 depicts a block diagram of the DEGOV_1 governor model and its associated parameters, where $\Delta\omega$ is the rotor speed deviation; ω_{ref} is the speed reference; τ_i $\forall_i$ $\in\{1,..6\}$ are the time constants of the control box and actuator; K is the gain of the actuator and must be tuned according to the characteristics of the genset; T_{MAX} and T_{MIN} are the upper and lower torque limits, respectively; τ_D is the engine firing time delay; D is the droop characteristic; and ΔP_{MECH} is the output mechanical power. The gains and time constants used in this model are adopted from [66] and are summarized in Table 3.1

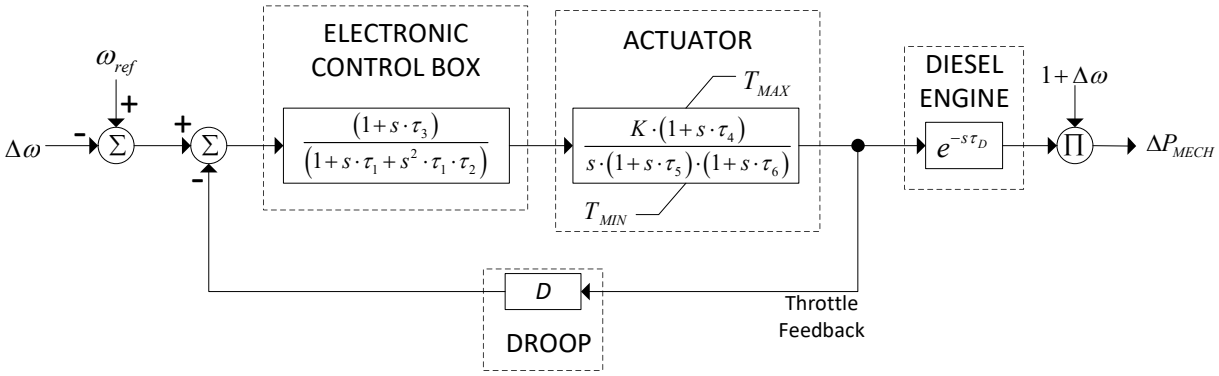

Figure 3.1: Block diagram of the diesel genset DEGOV$_1$ governor model [67].

Table 3.1: Parameters of the DEGOV$_1$ governor model [66].

Parameter	**Value**
τ_1 [s]	0.01
τ_2 [s]	0.02
τ_3 [s]	0.2
τ_4 [s]	0.25
τ_5 [s]	0.009
τ_6 [s]	0.0384
T_{MIN} [p.u.]	0
T_{MAX} [p.u.]	1.1
τ_D [s]	0.01

The droop compensator in Figure 3.1 uses a feedback signal coming from the engine's throttle valve. This valve regulates the supply of fuel intake into the engine, and its position represents the adjusting of mechanical power. Thus, if the speed varies, the governor adjusts the throttle valve position enough to cancel the speed change through the droop compensator [55]. As a result, the objective of this governor model is to regulate the position of the throttle valve in response to a disturbance. The difference between the rotational speed deviation and the droop compensation signal is sent to an electronic control box, whose output drives an actuator. The actuator converts the control signal into a fuel flow rate signal to regulate the throttle valve position, and thus regulate the amount of fuel entering the engine. Finally, a delay τ_D is introduced to represent the time interval from fuel ignition to mechanical torque generation in the engine.

3.1.1 Swing Equation

Any imbalance between power generation and load consumption produces a frequency deviation with respect to the nominal system frequency. As a consequence, the synchronous generators, which were rotating at the same electrical angular speed, will be accelerated or decelerated. Therefore, the mechanical motion equation (swing equation), which describes the dynamics of the movement of the generators' rotors, is used to study system frequency deviations [45].

$$P_{MECH}(p.u.) - P_{ELEC}(p.u.) = \frac{2H}{\omega_s}\frac{d^2\delta}{dt^2} \tag{3.1}$$

where P_{MECH} is the driving mechanical power, P_{ELEC} is the developed electrical power by the generator, H is the inertia constant in p.u., ω_s is the rotor's angular speed, and δ is the power angle. During small perturbations, (3.1) can be expressed as follows:

$$\Delta P_{MECH}(p.u.) - \Delta P_{ELEC}(p.u.) = \frac{2H}{\omega_s}\frac{d\Delta\frac{\omega}{\omega_S}}{dt^2} \tag{3.2}$$

Applying the Laplace transform to (3.2) results in:

$$\frac{1}{2Hs} = [\Delta P_{MECH}(s) - \Delta P_{ELEC}(s)] = \Delta\omega(s) \tag{3.3}$$

This equation describes the synchronous generator motion behavior when an imbalance takes place, and is represented in Figure 3.2 in the form of a block diagram, where ΔP_{MECH} is the output of the governor model depicted in Figure 3.1.

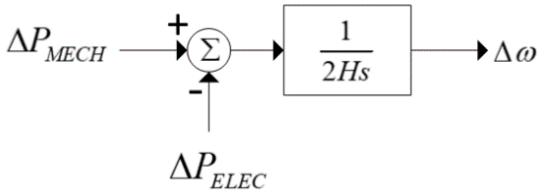

Figure 3.2: Block diagram representation of swing equation.

3.1.2 Dynamic Response

Any change in generation or demand affects system frequency. The dynamics of the short-term response of a diesel genset when an imbalance occurs can be described by connecting

the individual responses of the swing equation and the governor model. Figure 3.3 illustrates both the mechanical and frequency response when a 0.1 p.u. load increase takes place at 10 s, obtained from the models presented in Figures 3.1 and 3.2 for $\omega_{ref} = 1.039$ p.u., $D = 5.39\%$, $H = 1$ p.u., and $f_{nl} = 62.34$ Hz. Note that, before the disturbance occurs, the frequency is constant, and when a sudden change in load takes place, the speed control acts to smoothly change the genset's speed until it is stabilized at a new value according to the droop characteristic.

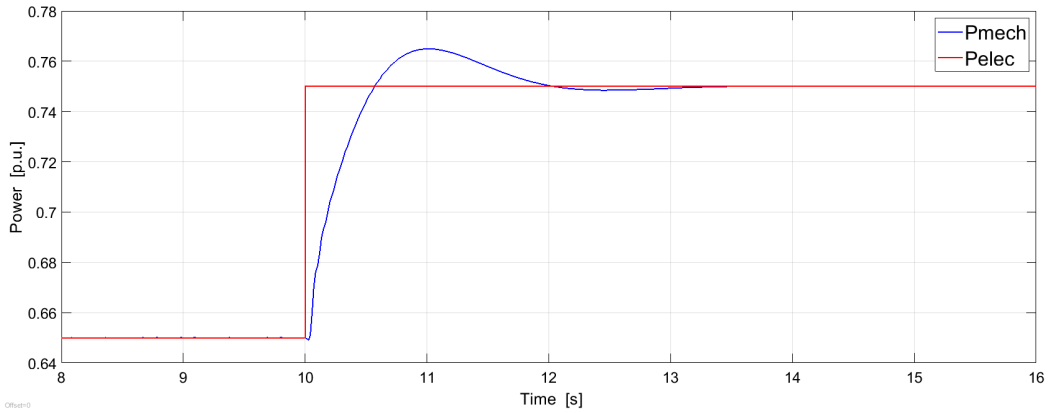

(a)

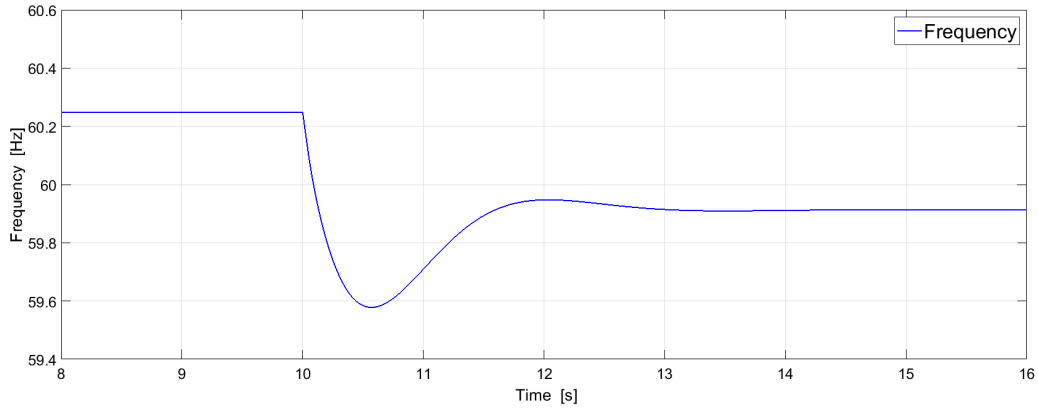

(b)

Figure 3.3: Step response of a diesel genset.

3.2 Solar PV Generation

From a practical standpoint, the integration of solar PV panels into an existing microgrid is relatively simple because they operate as passive generation elements without any control [68]. In other words, the PV panels inject the maximum available power that can be converted from the solar irradiance throughout the day by using a Maximum Power Point Tracking (MPPT) control [69].

A solar PV panel equivalent circuit is depicted in Figure 3.4, where the current supplied by the PV panel is given by:

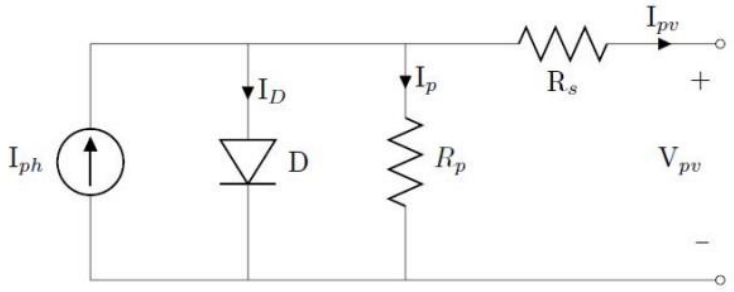

Figure 3.4: Equivalent circuit of one-diode PV cell [69].

$$I_{pv} = I_{ph} - I_0 \left[e^{\frac{q\,(V_{pv} + R_s\, I_{pv})}{N_s\, A\, k\, T_c}} - 1 \right] - \frac{V_{pv} + R_s\, I_{pv}}{R_p} \tag{3.4}$$

$$I_{ph} = \left[I_{sc} + K_i\ (T_c - T_{ref}) \right] \frac{G_s}{G_{ref}} \tag{3.5}$$

$$I_0 = \frac{I_{sc} + K_i\ (T_c - T_{ref})}{e^{\frac{q\left[V_{oc} + K_v\,\left(T_c - T_{ref}\right)\right]}{N_s\, A\, k\, T_c}} - 1} \tag{3.6}$$

where I_{sc} is the short-circuit current; V_{oc} is the open-circuit voltage; K_i is the temperature coefficient of the short-circuit current; K_v is the temperature coefficient of the open-circuit voltage; T_c is the module temperature; G_s is the solar irradiation; T_{ref} is the temperature reference (298 °K); G_{ref} is the irradiation reference (1000 W/m^2); k is the Boltzmann's constant (1.381×10^{-23} J/°K); q is the electron charge (1.602×10^{-19} C); A is the diode ideality factor; R_s is the series resistance; and R_p is the shunt resistance.

Individual PV panels can be readily connected to form an array. Any number of PV strings can be connected in parallel and then, by means of an inverter interface, the array can supply power to the grid. For example, 16 PV panels (180 W) can be arranged in two strings of 8 panels to provide 2.88 kW. By using (3.4) to (3.6), it is possible to determine the I-V and P-V curve characteristics of this PV array. These curves graphically represent the operation of the array in relation to the existing solar irradiation and the ambient temperature conditions.

Table 3.2 summarizes the main parameters of a 180 W solar PV panel, which connected as explained above to form a 2.88 kW PV array, yields the I-V and P-V curves for two solar irradiation conditions, 1000 and 500 W/m^2 at 25 ℃, depicted in Figure 3.5. Observe that there is a maximum power point that changes according to the ambient condition.

Table 3.2: Parameters of the 180 W Day4 48MC Solar PV Module [70].

PV Module	
Day4 48MC 180	
Parameter	**Value**
Rated Power P_{max} [W]	180
Short-circuit current I_{sc} [A]	8.1
Open-circuit voltage V_{oc} [V]	29.4
Temperature coefficient of I_{sc} (K_i) [%/℃]	0.037
Temperature coefficient of V_{oc} (K_v) [%/℃]	-0.321
Series Resistance R_s [Ω]	0.237
Shunt Resistance R_p [Ω]	224.189
Number of cells in series N_s	60
Diode ideality factor A	1.019

An MPPT control tracks the maximum power for any ambient conditions. There are various MPPT techniques, with the Perturbation & Observation (P&O) approach being the most used because of its simplicity. Figure 3.6 shows the P&O algorithm flowchart, where I_{mpp} is the current input to the PV array model, and I_{step} is tipically 0.05 A [69].

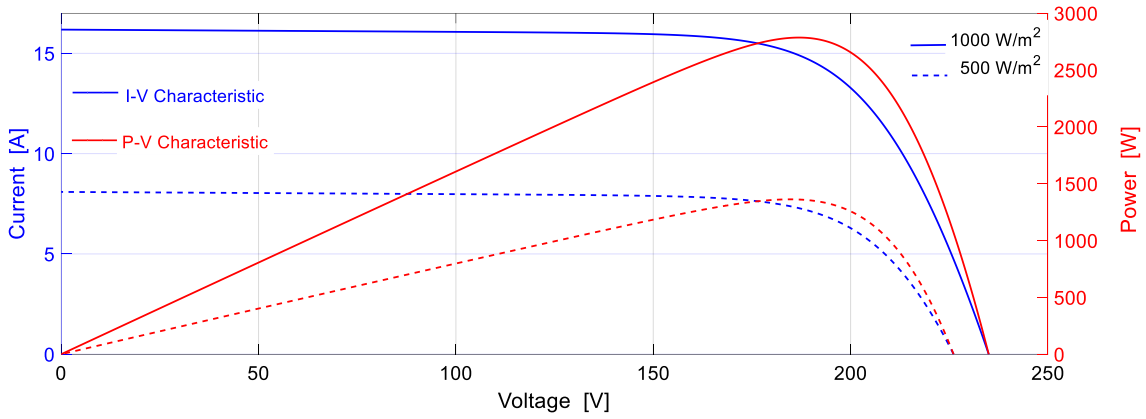

Figure 3.5: Curve characteristics of a solar PV array.

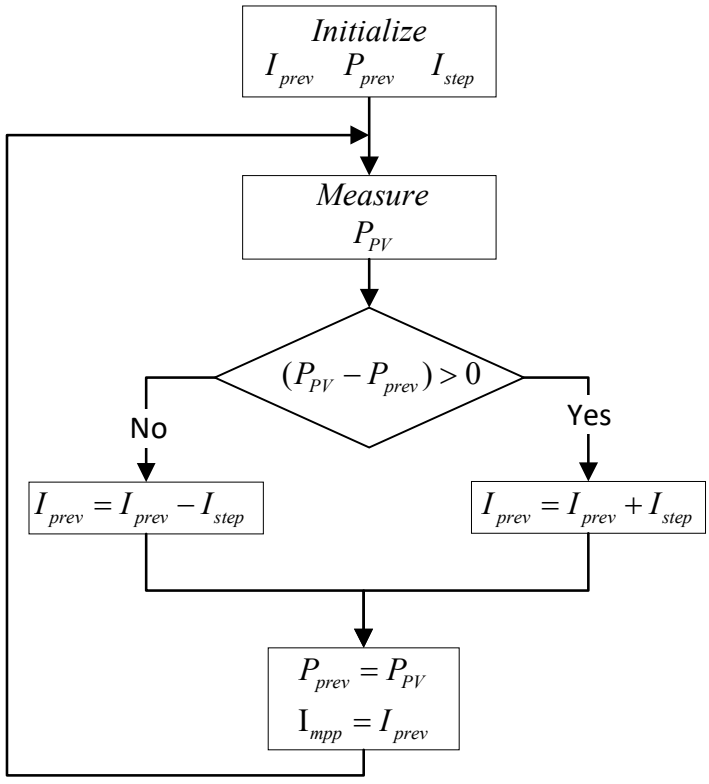

Figure 3.6: Flowchart of the P&O MPPT technique [69].

For the purposes of this thesis, it is not necessary to model the inverter interface. Therefore, it is assumed that the power conversion from DC to AC is lossless, injecting solar PV generation directly into the grid. Figure 3.7 shows a schematic of the relationships between the inputs (red), internal processes (blue), and output (green), used here to model a solar PV array, which for outdoor temperature and solar irradiance curves of a typical summer day in the Nemiah Valley area (British Columbia - Canada), depicted in Figures 3.8 and 3.9 [71], yields the generation curve for the 2.88 kW PV array shown in Figure 3.10.

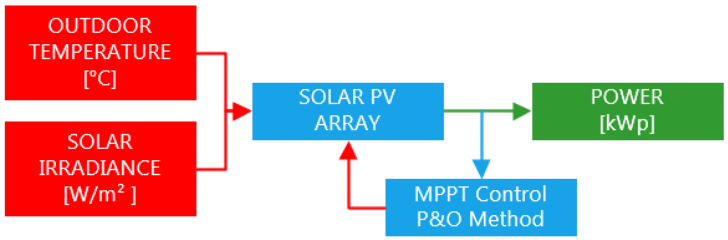

Figure 3.7: Process flowchart of the PV array model.

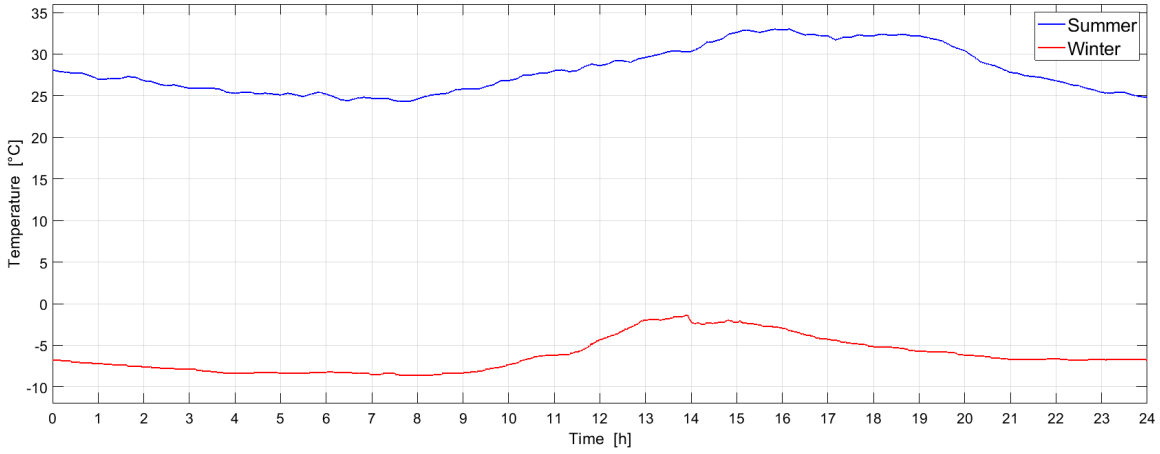

Figure 3.8: Temperature profiles of a typical summer and winter day in the Nemiah Valley area [71].

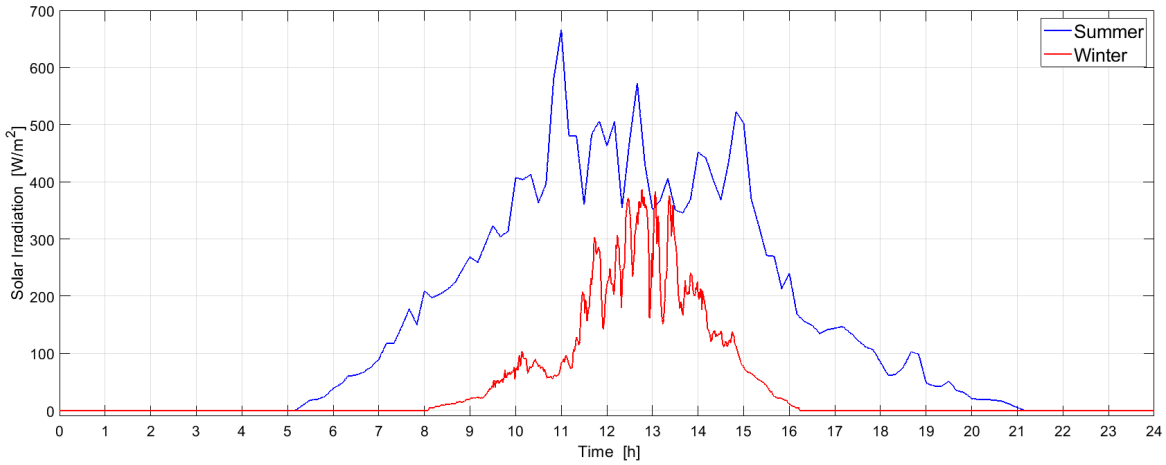

Figure 3.9: Solar irradiation profile of a typical summer day in the Nemiah Valley area [71].

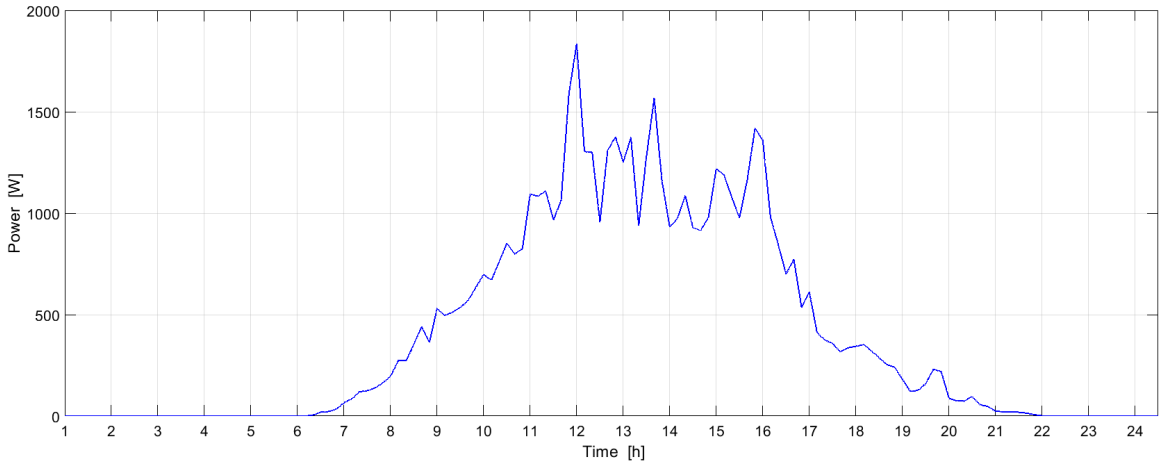

Figure 3.10: Generation curve of a 2.88 kW Solar PV array.

3.3 Thermostatically Controllable Loads

3.3.1 Thermal Model of a Household

Heat transfer in a household is a complex thermodynamic problem that is impractical to model in detail [57]. Thus, the thermal behavior of the household is influenced by: the

outdoor temperature and solar irradiation; the materials of the building envelope of the household (i.e., walls, roof, floor, and glazed surfaces), which affect heat transfer at various rates due to their different thermal properties; and the internal heat gains and moisture levels, which are highly dependent on the number of occupants and their physical activities, and thus vary constantly. Furthermore, although the household is always exchanging heat with the environment, its HVAC system (i.e., AC or GSHP) aims to dynamically control the indoor temperature to maintain occupant comfort. Hence, to design a DR strategy, it is necessary to develop a simplified model able to accurately describe the household s' thermal behavior and the power consumption of its HVAC system, as described next.

3.3.1.1 TEC Model Inputs

The power consumption cycle of an AC and GSHP varies as a function of many changing factors such as ambient temperature, solar irradiance, internal heat loads, thermal properties of the household, among others. Thus, an adequate thermal model of the internal temperature variation and the power consumption of its HVAC system depends on proper assumptions to reduce the complexity of the thermodynamic processes without compromising accuracy, starting with the information needed to build the model.

3.3.1.1.1 Outdoor Temperature. Household thermal behavior and power consumption of its HVAC system largely depend on ambient temperature, which is continuously changing depending on the time of day, season, and location. Hence, the outdoor temperature determines the operating mode of an HVAC system (i.e., heating and/or cooling mode), as well as the heat exchange rate between the household and its surroundings. The temperature profiles for typical summer and winter days in the Nemiah Valley area, used here, are presented in Figure 3.8 [71].

3.3.1.1.2 Solar Irradiance. It denotes the rate at which solar energy is incident on a square meter of the earth's surface, measured in W/m^2, and is highly variable and dependant on the location, orientation, weather, time of day, and season. Solar irradiance directly heats a household through the building envelope (i.e., walls and roof), and partially passes through glazed surfaces to the inner space of the household, regardless of the outdoor temperature. Thus, the intensity of the solar irradiance has an immediate effect on the thermodynamic behavior of the household, since it contributes directly to the internal heat gains when formulating the energy balance (heat transfer) equations. Figure 3.9 depicts a solar irradiance curve for typical summer and winter days in the Nemiah Valley area, used here [71].

3.3.1.1.3 Internal Heat Gains. According to [72], the internal heat gain sources consist primarily of five components: solar irradiance through glazed surfaces, occupants, electric equipment and appliances, lighting, and hot water usage. While latent heat (water vapor) gains generated from hot water, equipment and appliances, and occupants represent an immediate heat gain source, sensible heat (people, lights, and certain equipment) has a time-delay effect, since the heat is first absorbed by the surroundings (inner walls, ceilings, floors) before being gradually released into the air. Internal heat gains have two opposite effects on the operation of an HVAC system: in winter, has a positive effect since the internal gains contribute to reduce the heating demand, whereas during the summer, when it is necessary to cool the household, has a negative effect, since these heat gains increase the cooling demand from the household. For example, Figure 3.11 shows the internal heat gains patterns for a single-family household with five occupants.

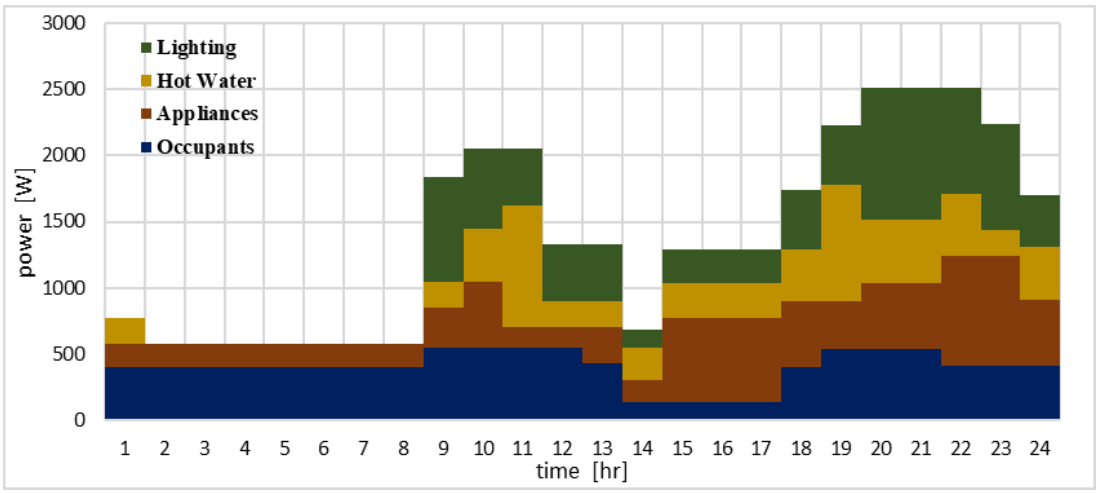

Figure 3.11: Internal heat gains in a household with five occupants [72].

3.3.1.1.4 Thermal Comfort. Thermal comfort of the human body inside a household depends on three ambient factors [59]: indoor temperature, humidity, and air motion. Therefore, an adequate HVAC system must maintain these factors within tolerable limits for the human body to feel comfortable in an environment. To achieve this purpose, the literature proposes the ranges in Table 3.3 used here (Section 2.5.3), where the temperature ranges refer to the indoor dry-bulb temperature T_{db}, which is measured by a thermometer freely exposed to the air. On the other hand, the wet-bulb temperature T_{wb} is measured by a thermometer with his tip covered by a wet cloth and indicates the moisture content of the

air. These two temperatures plus the volumetric air flow rate through the evaporator coil of an AC or GSHP (cooling mode) allows determining their cooling capacity, as observed in Sections 3.3.2 and 3.3.3.1.1.

Table 3.3: Thermal comfort recommended ranges.

	Summer	**Winter**
Temperature	23 to 25 [°C]	21 to 23 [°C]
RH	50%	50%
Air motion	<15 [m/min]	<9 [m/min]

3.3.1.1.5 Heat Injection/Absorption To/From the HVAC. The household exchanges continuously heat with the environment while its HVAC system, i.e., AC or GSHP, aims to control the indoor temperature to keep an adequate comfort level for the occupants. The amount of heat injected/absorbed by the HVAC system is a simultaneous dynamic process that has to be modeled independently and coupled to the TEC model of the household. The heat transfer process between AC+Household and GSHP+Household is presented in Sections 3.3.2 and 3.3.3, respectively.

3.3.1.2 TEC Model

Considering the aforementioned inputs, and in order to reduce the complexity of the analysis of the involved heat transfer processes, while maintaining adequate accuracy of the thermodynamic household model, the following assumptions are made [33, 34] [43], [58]:

- Indoor air temperature is homogeneous.
- Temperature of the building envelope is homogeneous.
- No internal heat transfer, i.e., it is assumed that the HVAC system maintains the same temperature for all rooms inside the house.
- Thermal and mechanical properties of building materials, i.e., k_{th}, c_p, and ρ, defined in Section 2.5.2, are constant.
- Thermal comfort parameters, i.e., temperature, RH%, and air motion, remain within the recommended limits presented in Table 3.3.

- The HVAC system is operating either in cooling or heating mode.
- The thermostat is located in one room and controls the temperature for the entire household.
- The volumetric air flow rate blown through the condenser coil is constant when the HVAC system is operating.

As a result, the lumped parameter TEC model depicted in Figure 3.12 is used to study the thermodynamic processes, which yields the following set of ordinary differential equations describing the heat transfer processes that allows determining the indoor temperature T_i as a function of time:

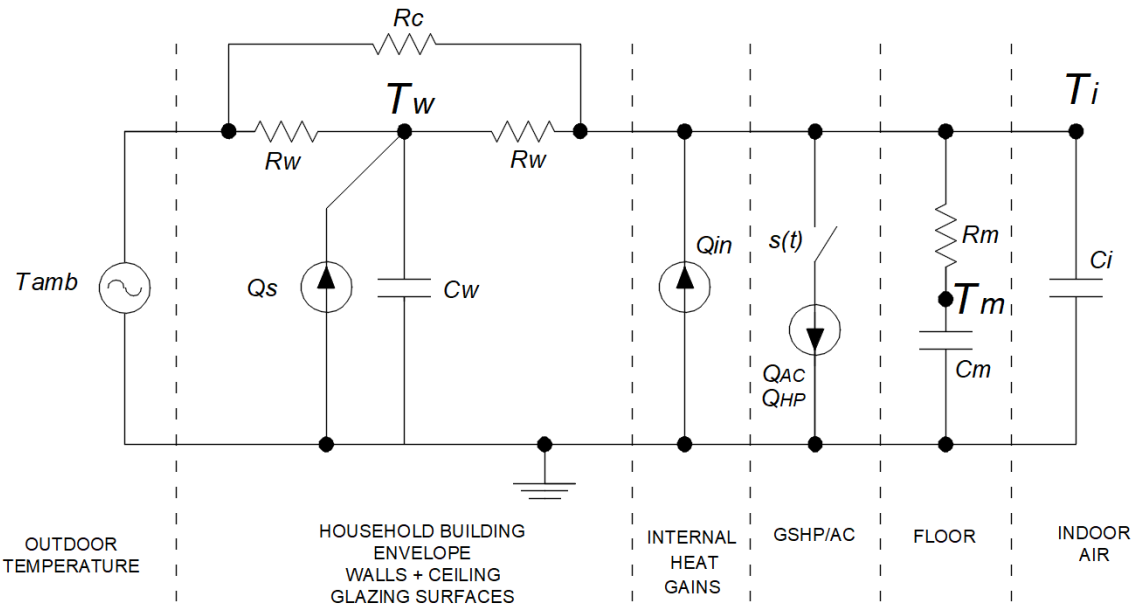

Figure 3.12: TEC network model of a household.

$$C_w \frac{dT_w}{dt} = Q_s + \frac{1}{R_w}\,(T_{amb} - T_w) + \frac{1}{R_w}\,(T_i - T_w) \tag{3.7}$$

$$C_i \frac{dT_i}{dt} = Q_{in} \pm s(t)\, Q_{AC/GSHP} + \frac{1}{R_w}\,(T_w - T_i) + \frac{1}{R_c}\,(T_{amb} - T_i) - \frac{1}{R_m}\,(T_m - T_i) \tag{3.8}$$

$$C_m \frac{dT_m}{dt} = \frac{1}{R_m}\,(T_i - T_m) \tag{3.9}$$

where T_w is the temperature on external walls; Q_s is the solar irradiation on external walls; T_{amb} is the outdoor temperature; T_i is the indoor temperature; C_w is the thermal capacitance of the building envelope (walls+ceiling); R_w is the half thermal resistance of the building envelope (walls+ceiling); Q_{in} is the internal heat gains; $s(t)$ is the thermostat switch position; $Q_{AC/GSHP}$ is the heat injected/extracted by the HVAC system; T_m is the temperature of the concrete slab foundation (floor); C_i is the thermal capacitance of the indoor air; R_c is the thermal resistance of the external glazed surfaces; R_m is the thermal resistance of the concrete slab foundation (floor); and C_m is the thermal capacitance of the concrete slab foundation (floor).

For the present research work, the geometric and thermal characteristics for the household model are adopted from [14], and are summarized in Table 3.4 The single-family household used here has a square floor plan with windows evenly distributed on the external walls, a wood-frame structure, and a conditioned basement.The thermostat monitors the indoor temperature T_i, and according to its dynamic variation, the signal $s(t)$ is sent to the controller of the HVAC system to control the heat injection/absorption; thus, the thermostat switching rule with a temperature dead band T_{i_db} is given by (2.10), in which T_i replaces T_t.

Table 3.4: Household geometric and thermal characteristics [14].

House Characteristics	**Value**
Conditioned area [m^2]	215
Conditioned volume [m^3]	525
Glazing fraction [%]	9.5
Thermal Performance	**Value**
R ceiling [m^2·°C/W]	7.67
R external walls [m^2·°C/W]	4.67
Windows $U - value$ [W/m^2·°C]	1.9
Concrete slab foundation	**Value**
Specific heat c_p [J/kg·°C]	880
Density ρ [kg/m^3]	2300
Thermal conductivity [J/s·m·°C]	1.4

3.3.2 Air Conditioner

The model of an AC system consists of the following components: (1) TEC model of the household (Section 3.3.1.2), (2) equation fit model of the AC, and (3) outdoor temperature profile. Figure 3.13 depicts the correlations between the individual components used to model the thermo-electrical behavior of the household and AC, respectively.

A black box approach is used to determine the thermal and electrical behavior of the AC, since the internal thermodynamic processes of the AC are not relevant to the present work. Therefore, the equation fit model presented in [73] is adopted here, in which the equation fit coefficients are determined by a least-square fit of a manufacturer's catalogue data.

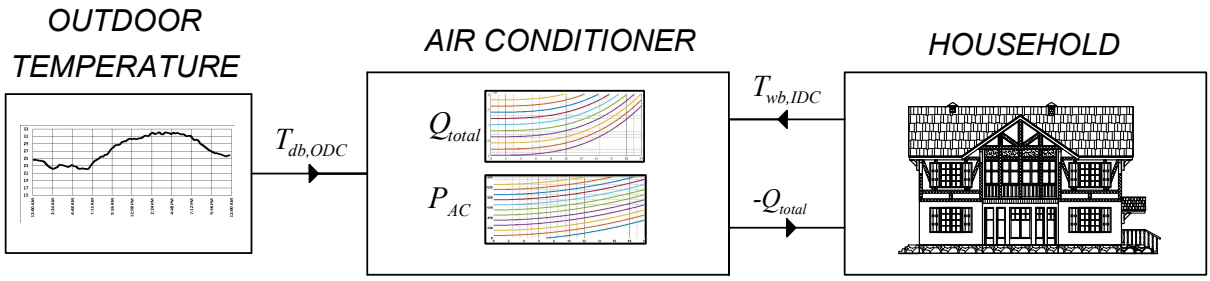

Figure 3.13: Correlations between the sub-models of an AC.

The cooling capacity Q_{AC} and the power consumed by the compressor P_{AC} are functions of the indoor wet-bulb temperature $T_{wb,IDC}$, the outdoor dry-bulb temperature $T_{db,ODC}$, and the volumetric air flow rate V_{air} blown through the condenser coil. Thus, the correlations used to model the thermal and electrical behavior of the AC as a function of the varying operating conditions can be formulated as follows [73]:

$$\frac{Q_{AC}}{Q_{AC,ref}} = X_1 + X_2 \left[\frac{T_{db,ODC}}{T_{ref}}\right] + X_3 \left[\frac{T_{wb,IDC}}{T_{ref}}\right] + X_4 \left[\frac{\dot{V}_{air}}{\dot{V}_{air,ref}}\right] \tag{3.10}$$

$$\frac{P_{AC}}{P_{AC,ref}} = Y_1 + Y_2 \left[\frac{T_{db,ODC}}{T_{ref}}\right] + Y_3 \left[\frac{T_{wb,IDC}}{T_{ref}}\right] + Y_4 \left[\frac{\dot{V}_{air}}{\dot{V}_{air,ref}}\right] \tag{3.11}$$

where Q_{AC} is the cooling capacity of the AC; $Q_{AC,ref}$ is the rated cooling capacity of the AC; X_1-Y_4 are the equation fit coefficients; $T_{db,ODC}$ is the outdoor air dry-bulb temperature;

T_{ref} is the reference temperature (283 °K); $T_{wb,IDC}$ is the indoor air wet-bulb temperature; V_{air} is the indoor air volumetric flow rate; $V_{air,ref}$ is the indoor air volumetric flow rate reference; P_{AC} is the power consumed by the compressor; and $P_{AC,ref}$ is the rated power of the AC. The computed value of Q_{AC} is used as input to the TEC model of the household (Section 3.3.1.2). Furthermore, according to [74], the wet-bulb temperature $T_{wb,IDC}$ can be computed as function of both the dry-bulb temperature $T_{db,IDC}$ and the RH% as follows:

$$T_{wb,IDC} = T_{db,IDC}\left[0.151977\sqrt{(RH\% + 8.313659)}\right] + \arctan\left(T_{db,IDC} + RH\%\right) - \arctan\left(RH\% - 1.676331\right) + 0.00391838\sqrt{RH\%^3}\arctan\left(0.023101\ RH\%\right) - 4.686035 \tag{3.12}$$

3.3.2.1 Household+AC Model

Figure 3.14 shows the relationships between the inputs (red), internal processes (blue), and output (green) used to model the household thermal behavior and AC power consumption. At each time step, the model uses the inputs and simultaneously solves the household and AC sub-models until it converges.

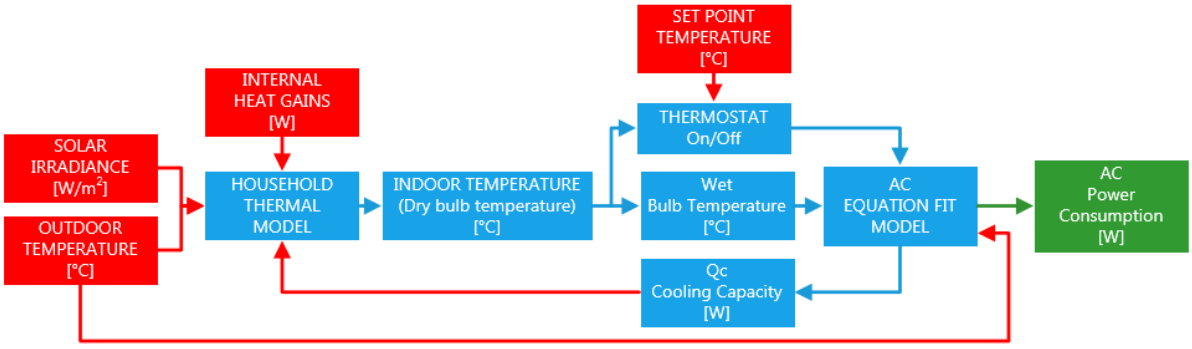

Figure 3.14: Process flowchart of the household+AC model.

In [14], the cooling capacity of the GSHP system used to provide climate control to the household is 1.5 Tons. Therefore, a proper AC was selected among the manufacturers' catalogue with similar cooling capacity, in order to compare the AC and GSHP cycling and power consumptions under the same conditions. The characteristics of the split AC, used here are shown in Table 3.5.

Table 3.5: Characteristics of the 1.5 Tons AC [75].

TRANE AIR CONDITIONER SPLIT SYSTEM	
Model	2TTB3024A1
Coil	2TXCB025A53
Parameter	**Value**
Total Capacity [BTUh]	20800
Power [W]	1930

The inputs to the household model are taken from Section 3.3.1.1. In addition, the AC is controlled by a thermostat which setpoint is 25 ℃, and has a dead band $T_{i,db}$ equal to ± 0.5 ℃. Figure 3.15 shows the simulation results of the thermo-electrical behavior of the household+AC model. The plots of the outdoor (Figure 3.8 - summer) and indoor temperatures are shown in the upper diagram while the cycling and power consumption is shown in the lower diagram. Note that the pattern of the power consumption changes dynamically as the cooling load changes.

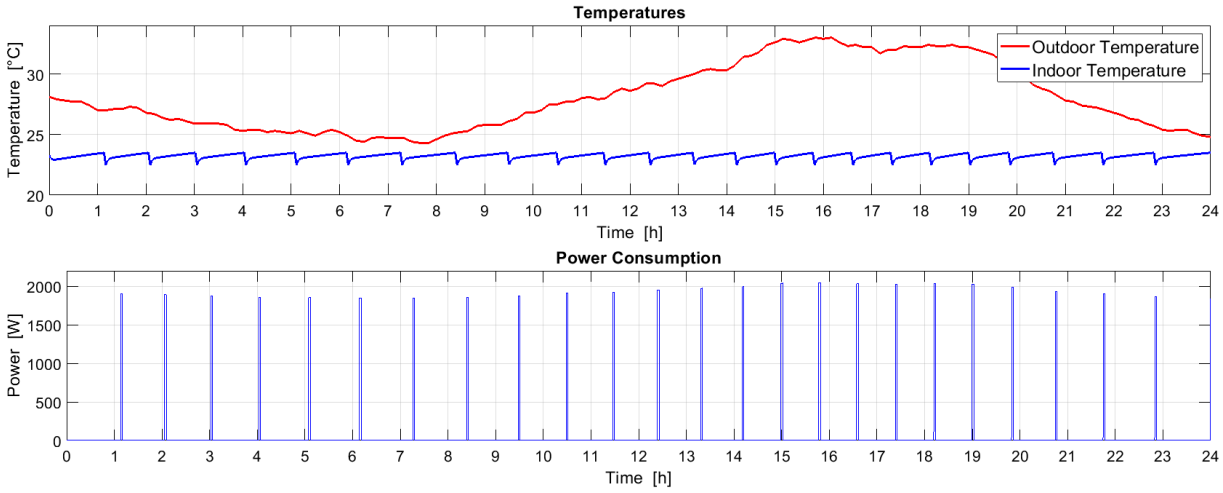

Figure 3.15: Modeling results of the household+AC model.

3.3.3 Ground Source Heat Pump

The model of a GSHP consists of the following components: (1) TEC model of the household (Section 3.3.1.2), (2) equation fit model of the reversible water-to-air HP, and (3) TEC model of the GHX. The dynamics of each sub-model have to be simultaneously connected to reproduce the behavior of the whole system. The models for the HP and the GHX are described next.

3.3.3.1 Water-to-Air Heat Pump

In the same way as for the AC, a black box approach is used here to model the thermo-electrical behavior of the reversible HP, using the equation fit model presented in [76] for both heating and cooling operating modes. The coefficients of the non-dimensional equations are determined by a least-square fit of the manufacturer's catalogue data.

3.3.3.1.1 Cooling Mode. In this operating mode, heat is pumped from the household to the ground in order to provide cooling for climate control. Figure 3.16 depicts the components and the variables used in this model.

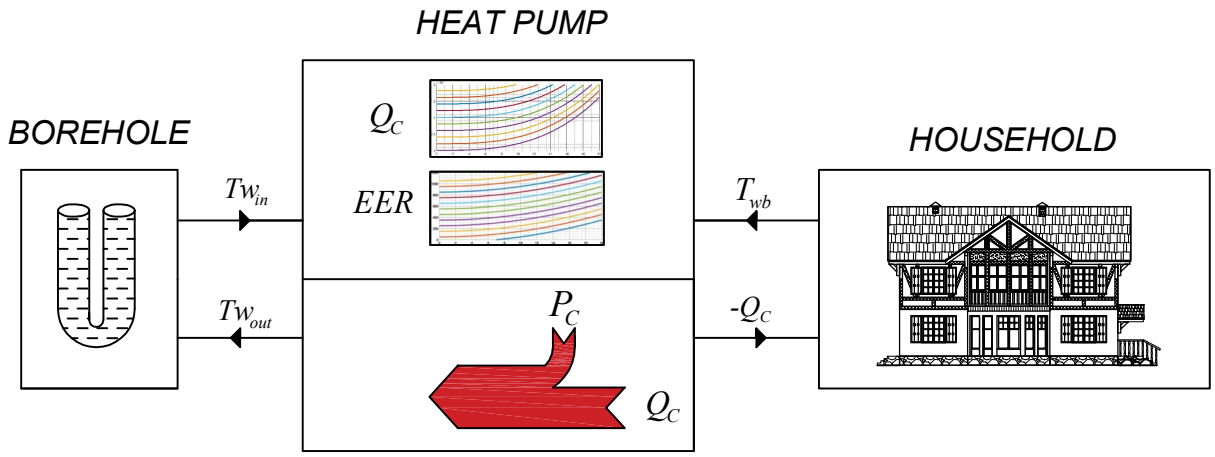

Figure 3.16: Correlations between the sub-models of a GSHP in cooling mode.

The cooling capacity Q_c and the EER of the HP are functions of the indoor wet-bulb temperature T_{wb}, the inlet water temperature Tw_{in} coming from the GHX, and the mass flow rate of the fluid $\dot{m}_W$ inside the GHX loop. The computed value of Q_c is then used

as input to the TEC model of the household (Section 3.3.1.2), whereas the outlet fluid temperature Tw_{out} is used as input for the TEC model of the GHX (Section 3.3.3.2).

The cooling mode equations for computing the performance of the heat pump are:

$$\frac{Q_c}{Q_{c,ref}} = A_1 + B_1 \left[\frac{T_{Win}}{T_{ref}}\right] + C_1 \left[\frac{T_{ref}}{T_{wb}}\right] \left[\frac{\dot{m}_W}{\dot{m}_{W,ref}}\right] \tag{3.13}$$

$$\frac{EER}{EER_{ref}} = D_1 + E_1 \left[\frac{T_{Win}}{T_{ref}}\right] + F_1 \left[\frac{T_{ref}}{T_{db}}\right] \left[\frac{\dot{m}_W}{\dot{m}_{W,ref}}\right] \tag{3.14}$$

where Q_c is the cooling capacity of the HP; $Q_{c,ref}$ is the rated cooling capacity of the HP; A_1-F_1 are the equation fit coefficients; Tw_{in} is the inlet fluid temperature; T_{ref} is the reference temperature (283 °K); T_{wb} is the indoor air wet-bulb temperature; $\dot{m}_W$ is the mass flow rate of fluid through the GHX loop; $\dot{m}_{W,ref}$ is the mass flow rate reference; EER is the calculated efficiency ratio of the HP; and EER_{ref} is the rated efficiency ratio of the HP. The wet-bulb temperature T_{wb} is computed as a function of both the indoor air dry-bulb temperature obtained from the TEC model of the household and RH%, using (3.12).

The power consumed by the compressor P_c of the HP is computed as follows:

$$P_c = \frac{Q_c}{EER} \tag{3.15}$$

And the amount of heat rejected to the ground is:

$$Q_{rejected} = Q_c + P_c \tag{3.16}$$

Finally, the outlet fluid temperature Tw_{out} is computed by using the energy balance equation for a heat exchanger operating as an evaporator [58]:

$$Tw_{out} = \frac{Q_{rejected}}{\dot{m}_W \, c_{pw}} + Tw_{in} \tag{3.17}$$

3.3.3.1.2 Heating Mode. In this operating mode, the flow of the refrigerant through the HP is reversed in order to absorb and pump heat form the ground to be household. Figure 3.17 shows the correlations between the components of this model.

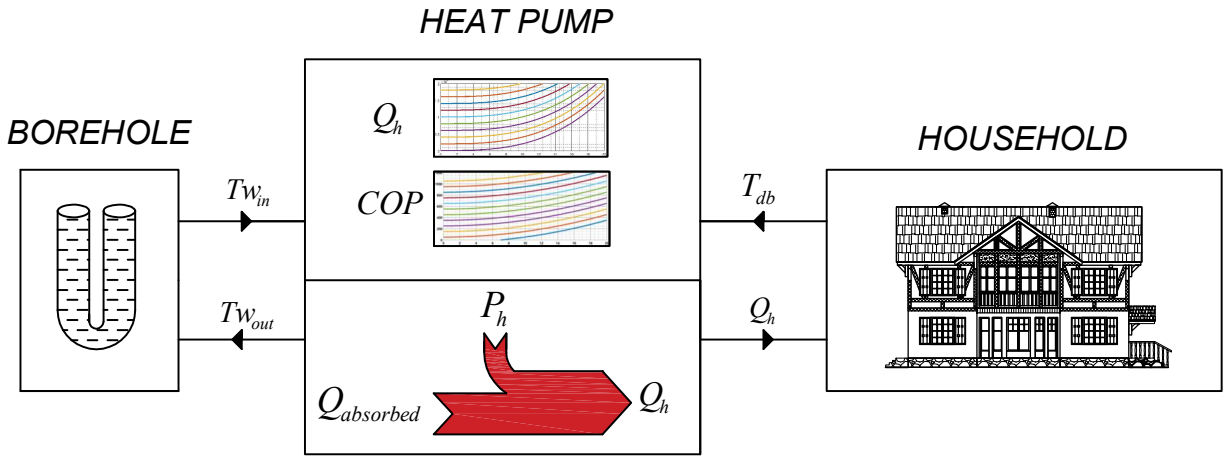

Figure 3.17: Correlations between the sub-models of a GSHP in heating mode.

The heating capacity Q_h and the COP of the HP are functions of the indoor air dry-bulb temperature T_{db}, the inlet fluid temperature Tw_{in} coming from the GHX, and the mass flow rate of the fluid $\dot{m}_{W,ref}$ inside the GHX loop. The computed value of Q_h is used as input to the TEC model of the household (Section 3.3.1.2) whereas the outlet fluid temperature Tw_{out} is used as input for the TEC model of the GHX (Section 3.3.3.2).

The heating mode equations for computing the performance of the HP are:

$$\frac{Q_h}{Q_{h,ref}} = A_2 + B_2 \left[\frac{T_{Win}}{T_{ref}}\right] + C_2 \left[\frac{T_{ref}}{T_{db}}\right] \left[\frac{\dot{m}_W}{\dot{m}_{W,ref}}\right] \tag{3.18}$$

$$\frac{COP}{COP_{ref}} = D_2 + E_2 \left[\frac{T_{Win}}{T_{ref}}\right] + F_2 \left[\frac{T_{ref}}{T_{db}}\right] \left[\frac{\dot{m}_W}{\dot{m}_{W,ref}}\right] \tag{3.19}$$

where Q_h is the heating capacity of the HP; $Q_{h,ref}$ is the rated heating capacity of the HP; A_2-F_2 are the equation fit coefficients; T_{db} is the indoor air dry-bulb temperature; COP is the calculated efficiency ratio of the HP; and COP_{ref} is the rated efficiency ratio of the HP.

The power consumed by the compressor P_h of the HP can then be computed as follows:

$$P_h = \frac{Q_h}{COP} \tag{3.20}$$

And the amount of heat absorbed from the ground can be determined as:

$$Q_{absorbed} = Q_h - P_h \tag{3.21}$$

Finally, the outlet fluid temperature Tw_{out} can be computed by using the energy balance equation for a heat exchanger operating as a condenser [58] as follows:

$$Tw_{out} = Tw_{in} - \frac{Q_{absorbed}}{\dot{m}_W \, c_{pw}} \tag{3.22}$$

3.3.3.2 GHX Thermal Model

In order to capture the dynamics of the heat exchange between the borehole and its surrounding ground in a short-term basis, the TEC model developed in [77] is adopted. This model has been validated in [78], and is able to accurately reproduce the dynamic behavior of the GHX under transient operating conditions (ON/OFF operations) for cooling and heating modes. As this model is aimed to reproduce the thermal response of the GHX for one operational day, only takes into account the dynamics of the surrounding ground directly affected by the heat extraction/rejection. Thus, a vertical discretization of the borehole is used to represent the borehole by means of n segments with height dz. Then, for each segment, a TEC is built to describe the vertical and radial heat transfer processes along the borehole depth. Figure 3.18 depicts the thermal network and the variables used for a segment j. In this model, the lumped parameters of the TEC network for a single segment are first computed; then, the heat flow equations are defined. It should be noted that the parameters are the same for all the n segments, while the temperature at each node changes as a function of time and depth of the borehole.

3.3.3.2.1 Parameter Calculation. The grout inside the borehole is split into two equal regions, which yields a thermal network with five nodes for each segment (Figure 3.18). Each node represents a specific temperature, with T_1 and T_2 representing the temperatures of the fluid inside each leg of the U-pipe (one leading the fluid up and the other down), T_{b1} and T_{b2} corresponding to the temperatures of the grout regions, and T_g representing the temperature of the surrounding ground. Since the borehole has a depth L, the height dz for each segment n is given by:

$$dz = \frac{L}{n-1} \tag{3.23}$$

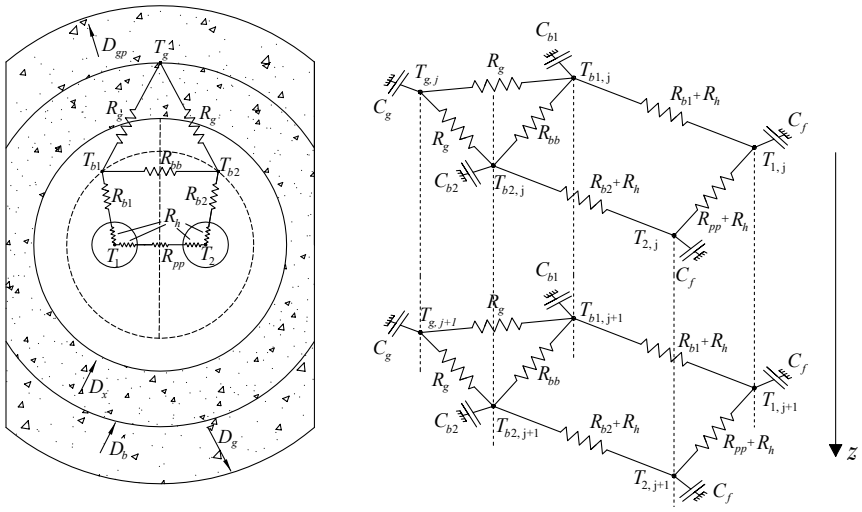

Figure 3.18: TEC network model of the GHX [77].

Each node has a thermal capacitance and shares a thermal resistance with every adjacent node. Therefore, the network consists of five capacitances and six resistances and their values can be calculated as follows, with the required parameters being defined in Table 3.6:

- The thermal capacitance of the nodes T_{b1} and T_{b2} is:

$$C_{b1} = C_{b2} = CV_b \frac{\pi}{8} \left(d_b^2 - 2d_{p,e}^2\right) dz \tag{3.24}$$

- The thermal capacitance of the node T_g depends on the penetration ground diameter d_{gp}, and is related to the extension of the ground around the GHX from which heat is absorbed/rejected:

$$C_g = CV_g \frac{\pi}{4} \left(d_{gp}^2 - d_b^2\right) dz \tag{3.25}$$

- The thermal capacitance of the nodes T_1 and T_2 is:

$$C_f = c_w \, \rho_w \frac{\pi}{4} \, d_{p,i}^2 \, dz \tag{3.26}$$

Table 3.6: Geometric-Thermal properties of the GHX [77].

THERMAL PROPERTIES	**Value**
Ground thermal conductivity k_g [W/m·℃]	3.1
Grout thermal conductivity k_b [W/m·℃]	1.675
Ground volumetric thermal capacitance CV_g [kJ/m^3·℃]	2160
Grout volumetric thermal capacitance CV_b [kJ/m^3·℃]	4186
Experimental mean borehole thermal resistance R_{bl} [m·℃/W]	0.062
GEOMETRICAL CHARACTERISTICS	**Value**
Borehole diameter d_b [mm]	140
External U-pipe diameter $d_{p,e}$ [mm]	40
Internal U-pipe diameter $d_{p,i}$ [mm]	35.2
Shank spacing (center-to-center) S_h [mm]	75
Depth L [m]	260
MODEL PARAMETERES	**Value**
Number of nodes n	254
Grout node thermal capacitance C_{b1}, C_{b2} [J/℃]	53.73
Ground node thermal capacitance C_g [J/℃]	1100
Borehole conductive thermal resistance R_{b1}, R_{b2} [℃/W]	0.06131
Pipe to pipe thermal resistance R_{pp} [℃/W]	0.291
Grout-to-grout thermal resistance R_{bb} [℃/W]	0.2389
Grout-to-ground thermal resistance R_{bg} [℃/W]	0.05075
Equivalent pipes diameter d_{eq} [mm]	74.65
Grout node position d_x [mm]	140
Ground radial penetration diameter d_{gp} [mm]	593.6
Ground nodes position d_g [mm]	366.8
FLUID PROPERTIES	**Value**
Density ρ_w [kg/m^3]	974.1
Specific heat c_w [J/kg·℃]	4361
Thermal conductivity k_w [W/m·℃]	0.464
Kinematic viscosity μ_w [m^2/s]	3.17x10^{-6}

- The thermal resistance between the nodes T_{b1} and T_{b2} is:

$$R_{bb} = \frac{S_h}{k_b \left(d_b - d_{pe}\right) dz} \tag{3.27}$$

- The thermal resistance between the nodes T_1 and T_2 has a conductive (R_{pp}) and a convective term[1] (R_h):

$$R_{T_1T_2} = R_{pp} + 2R_h \tag{3.28}$$

$$R_{pp} = \frac{S_h - d_{p,e}}{d_{p,e}\, k_b\, dz} \tag{3.29}$$

R_h is the convective resistance of the fluid inside the pipes and is calculated as:

$$R_h = \frac{1}{\pi\, Nu\, k_w\, dz} \tag{3.30}$$

where, Nu represents the Nusselt number, which is calculated according to the relationship of the flow regime of the fluid inside the U-pipe as [58]:

$$Nu = x\, Nu_{laminar} + (1 - x)\; Nu_{turbulent} \tag{3.31}$$

where x is defined depending on whether the fluid is laminar, turbulent or mixed for a circular pipe:

$$x = \begin{cases} 1 & Reynolds < 2300 \\ 0 & Reynolds > 10000 \\ \frac{10000 - Reynolds}{7700} & \end{cases} \tag{3.32}$$

and:

$$Nu_{la\,\min ar} = \frac{3.657}{\arctan\left(2.264\sqrt[3]{Z} + 1.7\sqrt[3]{Z^2}\right)} + \frac{0.0499}{Z}\arctan(Z) \tag{3.33}$$

$$Nu_{turbulent} = 0.024\, Reynolds^{0.8}\; \sqrt[3]{Prandtl} \tag{3.34}$$

[1] The convection heat transfer occurs when a solid surface is in contact with a moving fluid. In the case of the GHX, this energy transfer mode takes place between the solid surface of the U-pipe and the internal fluid that is in motion due to the action of the pump connected in this circuit.

where:

$$Z = \frac{dz}{d_{p,i}\, Reynolds\, Prandtl} \tag{3.35}$$

Equations (3.32) to (3.35) are functions of the Reynolds and Prandtl numbers, which are calculated as follows:

$$Reynolds = \frac{w\, d_{p,i}}{\mu_w} \tag{3.36}$$

$$Prandtl = \frac{\mu_w\, \rho_w\, c_w}{k_w} \tag{3.37}$$

where the velocity of the fluid inside the U-pipe is:

$$w = \frac{\dot{m}_W}{\rho_W\, \frac{\pi}{4}\, d_{p,i}^2} \tag{3.38}$$

- The thermal resistance between the nodes T_1 and T_{b1} is given by:

$$R_{T_1 T_{b1}} = R_{T_2 T_{b2}} = R_{b1} + R_h \tag{3.39}$$

$$R_{b1} = R_{b2} = \frac{\log\left(\frac{d_x}{d_{eq}}\right)}{\pi\, k_b\, dz} \tag{3.40}$$

where R_h is calculated with (3.30), and d_x depends on the shank space between the centers of the legs of the U-pipe and has to be determined by means of a sensitivity analysis; however, in [78], it is shown that if the pipes are very close to the borehole wall, it can be assumed that $d_x = d_b$. Finally, in (3.40), d_{eq} is:

$$d_{eq} = d_{p,e}\sqrt{\frac{4S_h}{\pi\, d_{p,e}} + 1} \tag{3.41}$$

- The thermal resistance between the nodes T_{b1} and T_g is:

$$R_{T_{b1} T_g} = R_{T_{b2} T_g} = \frac{1}{\pi\, k_g\, dz} \log\left(\frac{d_g}{d_b}\right) \tag{3.42}$$

where d_g is calculated as the mean diameter between the penetration diameter d_{gp} and the borehole diameter d_b.

According to [62], most boreholes use an aqueous solution as the circulating fluid inside the GHX. Therefore, the thermal characteristics of a solution with 20% volume fraction ethanol are used here (see Table 3.6).

3.3.3.2.2 Heat Flow Equations. For each node, the heat flow differential equations are built using the parameters described previously. However, for the nodes T_1 and T_2, an extra term is added to capture the temperature variation as a function of the borehole depth and the flow velocity v of the fluid inside the U-pipe as follows:

$$\frac{\partial T_1(z)}{\partial t} = -v\frac{\partial T_1(z)}{\partial z} - \frac{1}{C_f}\left(\frac{T_1(z) - T_{b1}(z)}{R_{b1}} + \frac{T_1(z) - T_2(z)}{R_{pp}}\right) \tag{3.43}$$

$$\frac{\partial T_2(z)}{\partial t} = -v\frac{\partial T_2(z)}{\partial z} - \frac{1}{C_f}\left(\frac{T_2(z) - T_{b2}(z)}{R_{b2}} + \frac{T_2(z) - T_1(z)}{R_{pp}}\right) \tag{3.44}$$

$$C_{b1}\frac{\partial T_{b1}(z)}{\partial t} = \frac{T_1(z) - T_{b1}(z)}{R_{b1}} + \frac{T_{b1}(z) - T_{b2}(z)}{R_{bb}} - \frac{T_{b1}(z) - T_g(z)}{R_g} \tag{3.45}$$

$$C_{b2}\frac{\partial T_{b2}(z)}{\partial t} = \frac{T_2(z) - T_{b2}(z)}{R_{b2}} - \frac{T_{b1}(z) - T_{b2}(z)}{R_{bb}} - \frac{T_{b2}(z) - T_g(z)}{R_g} \tag{3.46}$$

$$C_g\frac{\partial T_g(z)}{\partial t} = \frac{T_{b1}(z) - T_{b2}(z)}{R_g} - \frac{T_{b2}(z) - T_g(z)}{R_g} \tag{3.47}$$

The procedure to solve these equations is explained next.

3.3.3.2.3 Numerical Solution. In order to solve this set of heat-flow equations, a spatial-temporal discretization of the problem is performed, using the Lax-Wendroff approximation method [79] . According to this method, the temperature of a certain segment j at certain time t^{n+1} is calculated by using the temperature of the same segment at a previous step t^n and the temperatures of two equidistant points separated by a distance equal to Δz as illustrated in Figure 3.19. Therefore, the temperature of each point j can be computed as follows:

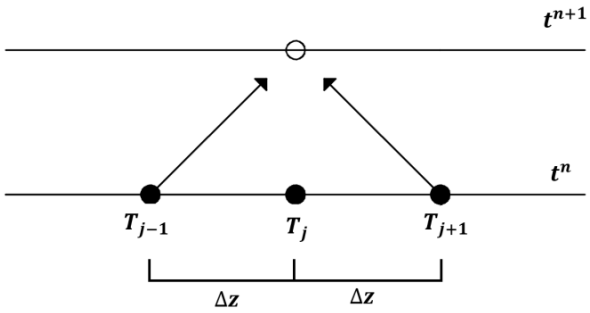

Figure 3.19: Lax-Wendroff approximation method [79].

$$T_j^{n+1} = \frac{1}{2}\left(T_{j+1}^n + T_{j-1}^n\right) - \frac{v\Delta t}{2\Delta z}\left(T_{j+1}^n + T_{j-1}^n\right) \tag{3.48}$$

where $\Delta z = dz$ according to (3.23), and Δt must satisfy the Courant–Friedrichs–Lewy condition (CFL), which requires that the fluid displacement must be less than the distance between two consecutive segments during the interval Δt, i.e.:

$$CFL \leq 1 \tag{3.49}$$

$$\Delta t = CFL\frac{\Delta z}{v} \tag{3.50}$$

By applying the Lax-Wendroff method to (3.43)-(3.47) the following set of equations can be obtained:

$$T_1^{n+1}(j) = T_1^n(j) - \frac{v\Delta t}{2\Delta z}[(T_1^n(j+1) - T_1^n(j-1)) - \frac{v\Delta t}{\Delta z}(T_1^n(j+1) - 2T_1^n(j) + T_1^n(j-1))] - \frac{\Delta t}{C_f}\left(\frac{T_1^n(j) - T_{b1}^n(j)}{R_{b1}} + \frac{T_1^n(j) - T_2^n(j)}{R_{pp}}\right) \tag{3.51}$$

$$T_2^{n+1}(j) = T_2^n(j) - \frac{v\Delta t}{2\Delta z}[(T_2^n(j+1) - T_2^n(j-1)) - \frac{v\Delta t}{\Delta z}(T_2^n(j+1) - 2T_2^n(j) + T_2^n(j-1))] - \frac{\Delta t}{C_f}\left(\frac{T_2^n(j) - T_{b2}^n(j)}{R_{b2}} - \frac{T_1^n(j) - T_2^n(j)}{R_{pp}}\right) \tag{3.52}$$

$$T_{b1}^{n+1}(j) = T_{b1}^{n}(j) - \frac{\Delta t}{C_{b1}} \left(\frac{T_1^n(j) - T_{b1}^n(j)}{R_{b1}} + \frac{T_{b1}^n(j) - T_{b2}^n(j)}{R_{bb}} - \frac{T_{b1}^n(j) - T_g^n(j)}{R_g} \right) \tag{3.53}$$

$$T_{b2}^{n+1}(j) = T_{b2}^{n}(j) - \frac{\Delta t}{C_{b2}} \left(\frac{T_2^n(j) - T_{b2}^n(j)}{R_{b2}} - \frac{T_{b1}^n(j) - T_{b2}^n(j)}{R_{bb}} - \frac{T_{b2}^n(j) - T_g^n(j)}{R_g} \right) \tag{3.54}$$

$$T_{g}^{n+1}(j) = T_{g}^{n}(j) + \frac{\Delta t}{C_{g}} \left(\frac{T_{b1}^n(j) - T_g^n(j)}{R_g} + \frac{T_{b2}^n(j) - T_g^n(j)}{R_g} \right) \tag{3.55}$$

where the temperature of the segment $j = 1$ is the temperature of the fluid entering the GHX given by (3.17) or (3.22) for cooling and heating mode, respectively. For each iteration, the temperatures of all N segments at a time t^n are known; then, for the next time step, the new temperatures are calculated for the time $t^{(n+1)}$. Finally, the temperature of the segment $j = N$ corresponds to the temperature of the fluid leaving the GHX. This temperature is used as input to the HP model (Sections 3.3.3.1.1 and 3.3.3.1.2).

3.3.3.3 Modeling Results of the Household+GSHP

Figure 3.20 shows a schematic of the relationships between the inputs (red), internal processes (blue), and output (green) used to model the thermal behavior and power consumption of the household and GSHP for cooling and heating modes, respectively. For comparison purposes, a GSHP with a cooling capacity of 1.5 Tons was selected from a manufacturers' catalogue, in order to approximately have the same conditions than the AC. The characteristics of this GSHP are depicted in Table 3.7.

The inputs to the household model are taken from Section 3.3.1.1. The GSHP is controlled by a thermostat with a setpoint of 25 ℃, and a ± 0.5 ℃ dead band. The GHX has the geometric and thermal characteristics presented in Table 3.6, which results in the fluid traveling through the U-pipe in $\omega = 2.88$ minutes (with $\dot{m}_W = 1135.62$ kg/hr). Thus, the thermal behavior of the household and the ON/OFF cycling of the GSHP are illustrated in Figure 3.21 for cooling and heating modes, respectively. The ambient temperature mostly governs the cycling and power consumption of the GSHP; as a result, the heating load is much higher than the cooling load. This premise is validated by comparing the cycling frequency, the magnitude of the power consumption, and the time the GSHP remains ON

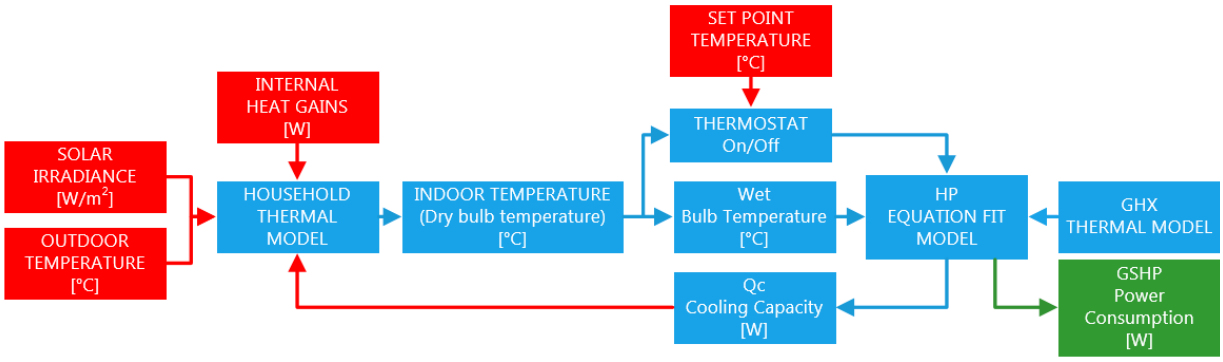

(a) Cooling mode.

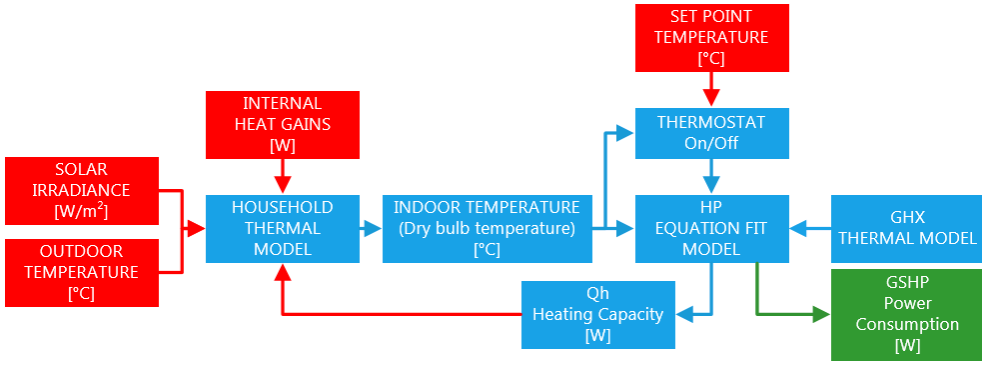

(b) Heating mode.

Figure 3.20: Process flowchart of the household+GSHP model.

Table 3.7: Characteristics of the GSHP [80].

BOSCH Residential GSHP	
Model	BP018
Parameter	**Value**
Cooling Capacity [BTUh]	20500
EER	19
Heating Capacity [BTUh]	14800
COP	3.8

for both operating modes. The compressor cycles are reflected in the temperatures of the fluid Tw_{in} and Tw_{out} for the GHX, and the internal household air temperature T_i. For the cooling mode, Tw_{out} is lower than Tw_{in}, since as the fluid flows through the U-pipe, heat is transferred to the surrounding ground, and therefore, the fluid temperature decreases. On the other hand, for the heating mode, Tw_{out} is higher than Tw_{in}, since as the fluid flows through the U-pipe, heat is absorbed from the surrounding ground, with the fluid increasing in temperature.

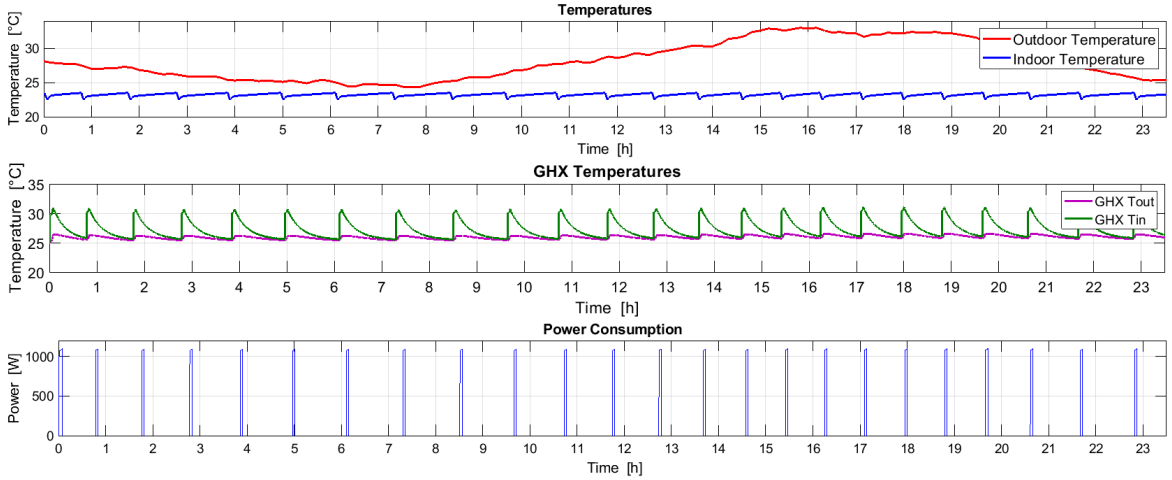

(a) Cooling mode.

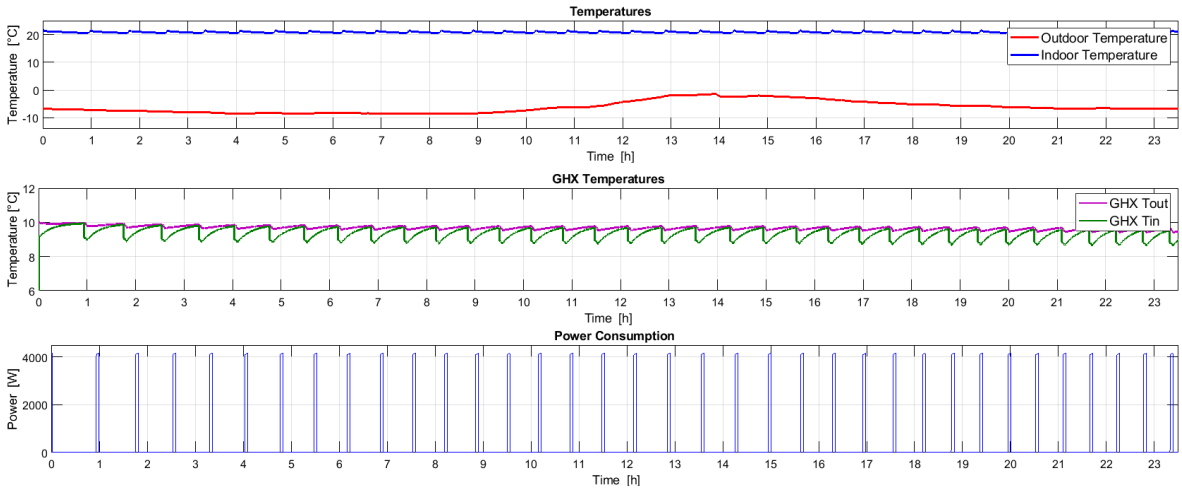

(b) Heating mode.

Figure 3.21: Modeling results of the household+GSHP model.

3.3.4 Electric Water Heater

A single-element EWH is used to model the thermo-electrical behavior of a tank-type EWH for daily operation, based on heat transfer processes and considering a variable hot water consumption. This model is adopted since in a dual-element EWH, the upper element is activated no more than 5% of the time [9]. To simplify the analysis of the heat transfer processes, but maintaining adequate accuracy of the thermo-electrical behavior of the EWH, the following assumptions are made:

- The water temperature inside the tank is uniform.
- The heating element heats the entire water mass inside the tank.
- The inlet cold water has a constant temperature.
- The thermal properties of the water mass remain unchanged.
- The thermal and mechanical properties of the tank remain unchanged.

Based on these assumptions, a first-order ordinary differential equation is used to model the heat transfer processes which consists of two parts [34]: (a) heating cold water (due to hot water usage), and (b) standby losses. Figure 3.22 depicts the lumped parameter TEC model of the EWH under study.

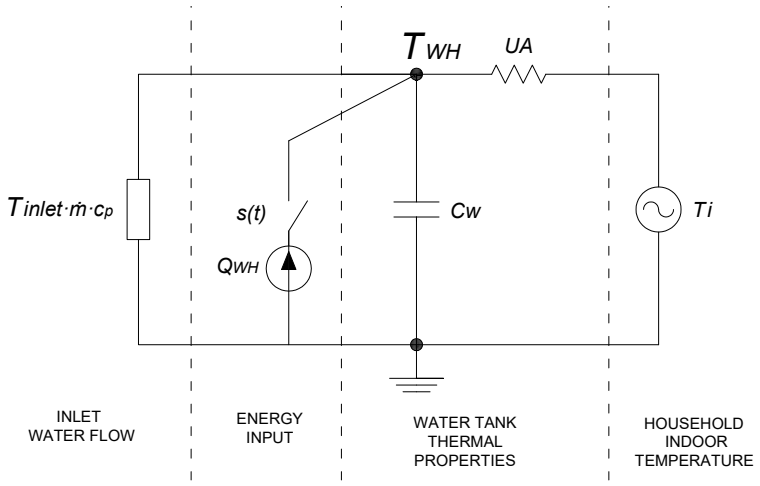

Figure 3.22: TEC network model of a single-element tank-type EWH [34].

The following ordinary differential equation describes the heat transfer processes presenting from Figure 3.22, and allows determining the temperature of the water inside the tank T_{EWH} as a function of time:

$$C_{wt}\frac{dT_{EWH}}{dt} = \dot{m_{EWH}}\, c_{pw}\,(T_{inlet} - T_{EWH}) + UA_{EWH}\,(T_i - T_{EWH}) + s_{EWH}(t)\,Q_{EWH} \quad (3.56)$$

where:

$$\dot{m_{EWH}} = W_d(t)\,\rho_w \quad (3.57)$$

$$Q_{EWH} = P_{EWH}\,\eta_{EWH} \quad (3.58)$$

whit $\dot{m_{EWH}}$ representing the inlet water mass flow rate; c_{pw} being the specific heat capacity of water; $W_d(t)$ being the average hot water drawn per hour; ρ_w being the density of water; T_{EWH} being the temperature of the water inside the tank; T_{inlet} being the inlet cold water temperature; T_i being the ambient temperature around the tank; C_{wt} being the thermal capacitance of water inside the tank; UA_{EWH} being the thermal conductance of the tank shell; $s_{EWH}(t)$ being the thermostat switch position; Q_{EWH} being the heat injected into the tank; P_{EWH} being the rated power of the EWH; and η_{EWH} being the efficiency of the EWH.

In the model illustrated in Figure 3.22, T_{EWH} is monitored to control the switching action of the heating element. The rate at which the temperature T_{EWH} drops depends on the amount of the hot water drawn $W_d(t)$ and the standby thermal losses. Generally, the thermostat's temperature dead band T_{EWH_db} has a hysterisis range of ±1.4 ℃, and depending on the technology and building material properties, P_{EWH} varies in the range of 3 to 5.5 kW, and η_{EWH} is in the range of 85 – 94% [34]. The power consumption P_{EWH} depends on the switch position signal $s_{EWH}(t)$ whose status is governed by a thermostat switching rule. Since the EWH provides heating, the status of the signal $s_{EWH}(t)$ is inverted with respect to (2.10) as follows:

$$s_{EWH}(t) = \begin{cases} 0 & T_{EWH} > (T_0 + \Delta T_{EWH}) \\ 1 & T_{EWH} < (T_0 - \Delta T_{EWH}) \\ keeping & (T_0 - \Delta T_{EWH}) \leq T_{EWH} \leq (T_0 + \Delta T_{EWH}) \end{cases} \quad (3.59)$$

where T_0 is the setpoint temperature, ± ΔT_{EWH} is the dead band temperature, and T_{EWH} is the water temperature inside the tank. Therefore, based on the dynamics of the hot water temperature T_{EWH} and the switch position $s_{EWH}(t)$, the EWH consumes either full rated power or none. The methodology used to determine the hot water usage is explained next.

3.3.4.1 Hot Water Consumption Profile

An hourly average hot water drawn profile represents the use of an EWH with a storage tank, which decouples the hot water demand from the cold water supply; in this way, the EWH does not require to be turned on instantaneously with every hot water consumption drawn [81]. Hence, the DHW Event Schedule Generator (Section 2.6.3) is used to generate an hourly hot water usage profile for a 50 gallons capacity EWH over a 24-hour horizon based on the number of bedrooms (2 and 4), thermostat setpoint temperature (54 and 50 °C), temperature of shower, sink, and bath draw (39 °C), and location of the household. The simulator allows generating a hot water usage profile with a maximum time step of 6 minutes; therefore, after generating the profile, this was adjusted to obtain an average hourly profile. Figure 3.23 depicts the hot water profiles for a household with three and five occupants, respectively.

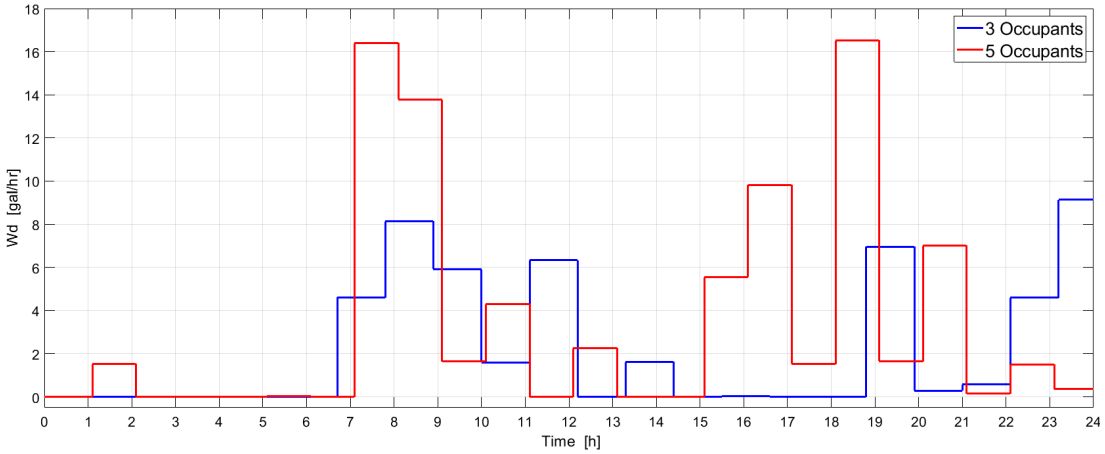

Figure 3.23: Water draw profiles for a 24-hour horizon.

3.3.4.2 Modeling Results of the EWH

Figure 3.24 shows a schematic of the relationships between the inputs (red), internal processes (blue), and output (green) used to model the thermo-electrical behavior of the EWH. The parameters of the EWH are adopted from [34], and are summarized in Table 3.8.

The EWH is controlled by a thermostat which setpoint is 50 °C and has a ±1.4 °C dead band. Thus, the thermo-electrical behavior and the ON/OFF cycling of an EWH for a family of five are illustrated in Figure 3.25. The heat transfer processes due to the hot

water consumption and standby losses are reflected in the temperature variation (green), hot water draw profile (red), and power consumption cycling (blue). The rate at which the temperature T_{EWH} decreases depends on the amount of the hot water being used, however, even if there is no consumption, T_{EWH} decreases as a result of the standby losses. The duty cycle of the power consumed by the EWH depends on T_{EWH}; thus, as soon as this temperature hits the lower dead band limit, the heating element of the EWH is turned ON, remaing in this state until T_{EWH} hits the upper dead band limit.

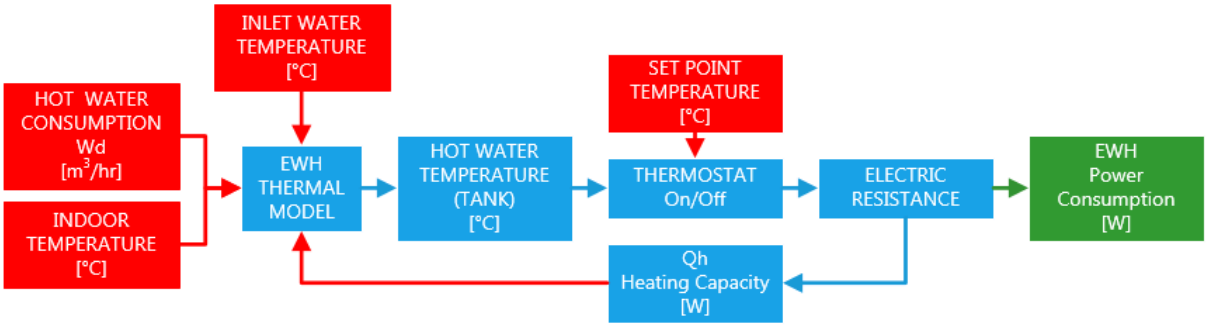

Figure 3.24: Process flowchart of the EWH model.

Table 3.8: Characteristics of the EWH [34].

Parameter	**Value**
ρ_w [kg/m^3]	998
c_{pw} [J/kg·°C]	4180
T_{inlet} [°C]	16
UA [W/°C]	6847.483
P_{EWH} [W]	4000
η_{EWH} [%]	94

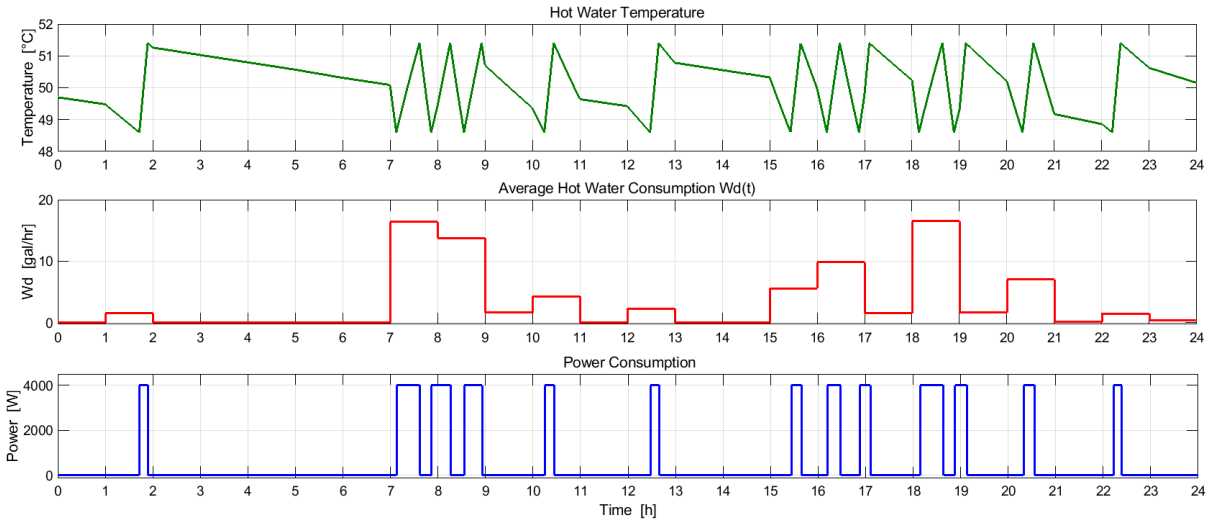

Figure 3.25: Modeling results of the EWH model.

3.4 Non-Thermostatically Controllable Loads

Modeling realistic residential non-TCLs demand profiles plays a fundamental role on the design and evaluation of a DR strategy. Therefore, by combining the characteristics of the simulators presented in Sections 2.6.1 and 2.6.2, it is possible to generate a 1-minute resolution demand profile over a 24-hour horizon for a single-family dwelling. Thus, from the SRLS the ambient temperature and solar irradiation curves are obtained, as well as the power rating and efficiencies from the available appliances (without considering the AC and furnace), to be used as complementary inputs for the CREST simulator (Section 2.6.2). Then, at the beginning of the simulation, the CREST simulator randomly allocates the group of appliances for a particular dwelling based on the number of occupants, day, and month. If the simulator allocates an EWH, storage heater, or other space heating devices, they must be manually deselected. Then, the active occupancy model is run to generate an occupancy profile. Finally, the electricity demand model is run, and according to the occupancy pattern, the non-TCLs load profile is generated.

The purpose of generating a load profile with a 1-minute resolution is to represent the sudden and random demand variation of individual households. Two examples of demand profiles for non-TCLs are shown in Figure 3.26, for a household of three and five occupants, respectively.

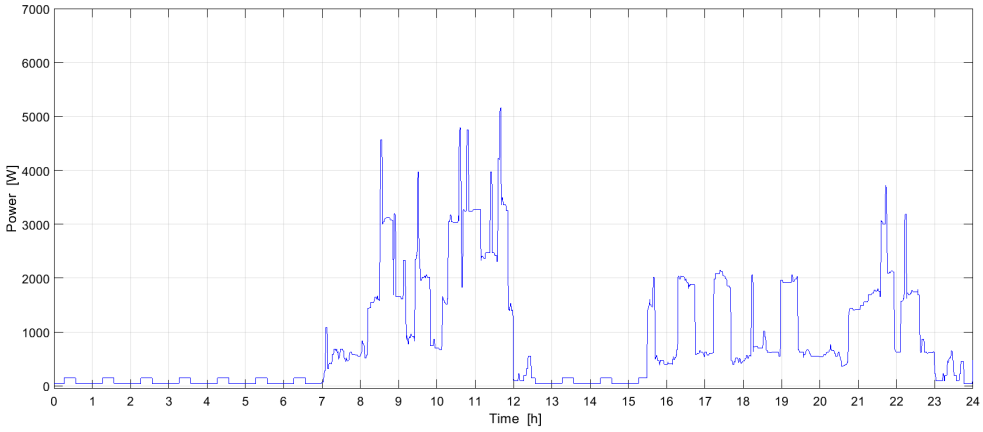

(a) Three occupants.

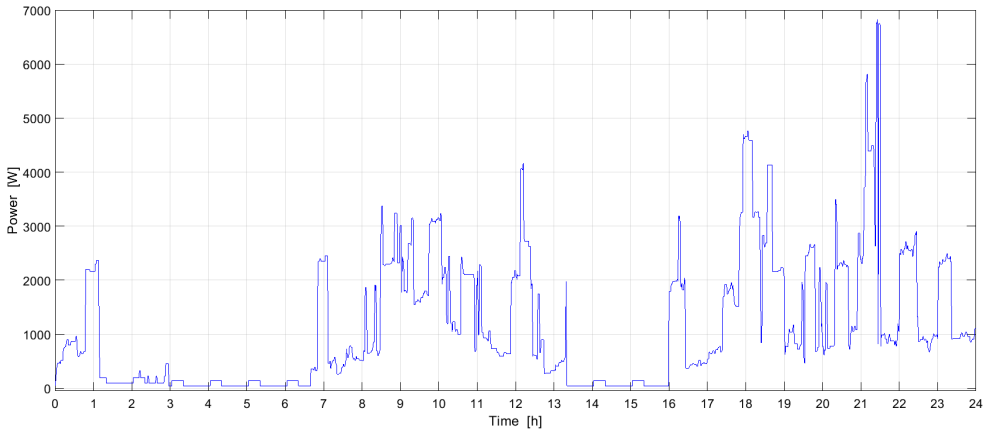

(b) Five occupants.

Figure 3.26: Demand profile from non-TCLs in a single-family household.

3.5 Primary Frequency Control Strategy

Since frequency is a global parameter that can be observed at any point in a power system, providing information to determine the instantaneous demand-supply balance, a DR strategy for TCLs using a decentralized control architecture is proposed here. Thus, a communication channel for frequency regulation signals is unnecessary, since each TCL controller can measure the system frequency locally. Therefore, by means of a frequency sensor and an adequate control logic, TCLs can be autonomously turned ON/OFF while

considering consumer comfort [15], [41].

Power consumption cycles of TCLs, i.e., EWHs, ACs, and GSHPs, respond to temperature variations monitored by thermostats. In this context, an LFC method is designed to control a cluster of TCLs and provide primary frequency control by adjusting their thermostat setpoint temperatures as a function of system frequency deviations. Thus, the thermostat temperature setpoint T_0 is dynamically adjusted according to the system frequency deviation by means of the following linear relationship [15]:

$$T_0 = T_{base} \pm k_f \left(f_{sys} - f_0\right) \tag{3.60}$$

where T_{base} is the target temperature, k_f is the coefficient of temperature-frequency change in ℃/Hz, f_{sys} is the measured system frequency, f_0 is the target frequency, and the $\pm$ sign depends on the operating mode of the TCL, i.e., cooling or heating mode. For each TCL, $T_{control}$ and k_f must be appropiately adjusted to avoid excessive wear. In addition, k_f can also be regulated according to the magnitude of the frequency deviations. Furthermore, due to comfort and health restrictions, the control must limit T_0 to bypass the max/min recommended temperatures for each type of TCL.

3.5.1 LFC for EWHs

As the heating element of an EWH contains a resistor, its power consumption can be controlled as frequently and rapidly as needed. Thus, the parameters of the temperature-frequency characteristic given by (3.60) are only determined based on system frequency limits plus comfort and health restrictions, as follows:

- T_{base} is calculated as the central hot water temperature from the safe range established to provide comfort and avoid health problems, i.e.:

$$T_{base} = \frac{T_{EWH,min} + T_{EWH,max}}{2} \tag{3.61}$$

- f_0 is calculated as the central frequency of the frequency limits established for normal operating conditions of the microgrid:

$$f_0 = \frac{f_{lim,min} + f_{lim,max}}{2} \tag{3.62}$$

- k_f denotes the slope of the curve in a temperature-frequency framework; therefore, it can be calculated according to the temperature and frequency limits given in (3.61) and (3.62), as follows:

$$k_f = \frac{T_{EWH,max} - T_{EWH,min}}{f_{lim,max} - f_{lim,min}} \tag{3.63}$$

For example, as for Section 2.5.5, $T_{EWH,max} = 60$ ℃ and $T_{EWH,min} = 49$ ℃, and assuming $f_{lim,max} = 61.37$ Hz and $f_{lim,min} = 60.33$ Hz as the frequency limits, the graphical representation of (3.60) for an EWH is shown in Figure 3.27, where the correlation between frequency and temperature is shown, as well as the thermostat temperature dead band curves $T_{db} = T_0 \pm \Delta T$ as given by (2.8) and (2.9). Thus, if the system frequency changes, the thermostat setpoint temperature will vary accordingly, and as a result, the EWH can be turned ON/OFF. However, as the system frequency varies continuously, this condition will cause excessive wear, and thus, shortening the lifetime of the EWHs. Additionally, all EWHs equipped with this control may affect each other, as each will try to follow its temperature-frequency characteristic independently of the actions of other EWHs, even if frequency changes slightly. Therefore, the temperature-frequency characteristic must be complemented by a control logic in order to limit the switching operations, as explained next.

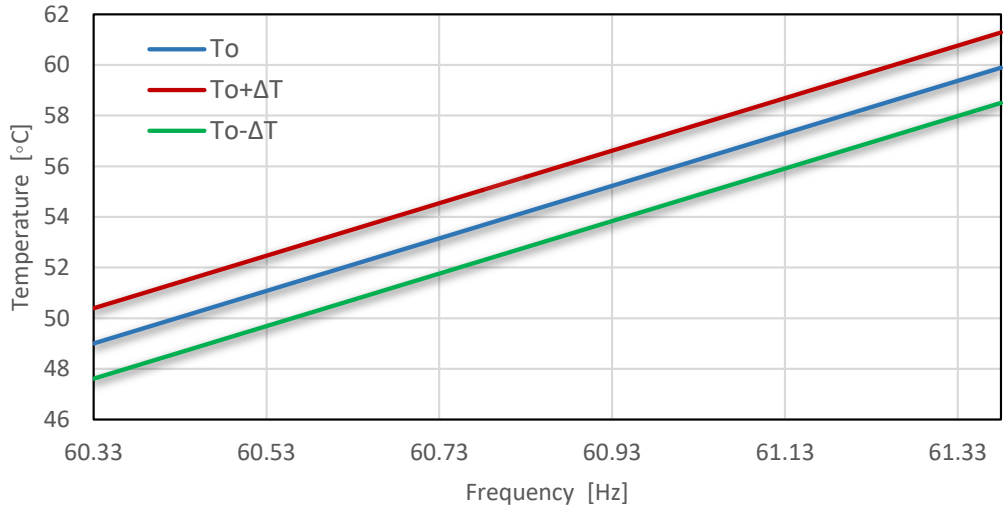

Figure 3.27: Temperature-frequency characteristic of the LFC control for an EWH.

At each time step, the control measures f_{sys}, T_{EWH}, and $s_{EWH}(t)$, and also reads the

previous value of the thermostat setpoint $T_{0,prev}$. If f_{sys} varies with respect to f_0, the control will increase/decrease the thermostat setpoint temperature by a factor $\Delta T_0 = k_f(f_{sys} - f_0)$. The following control logic is modified from [40] to obtain a better performance when EWHs are providing primary frequency control:

- If $\Delta T_0 < 2\Delta T$ the control is activated. This condition allows that only the EWHs with $T_{EWH} < (T_0 + \Delta T)$ and $s_{EWH}(t) = 0$ are turned ON. For the rest of cases, the EWHs will maintain their states.
- If $-2\Delta T < \Delta T_0$ the control is activated. This condition allows that only the EWHs with $T_{EWH} > (T_0 + \Delta T)$ and $s_{EWH}(t) = 1$ are turned OFF. For the rest of cases, the EWHs will maintain their states.
- If $\Delta T_0 > 2\Delta T$:
  - If $T_{EWH} < T_{0,prev}$ and $s_{EWH}(t) = 0$ the control is activated. This condition allows reducing the number of EWHs to be turned ON.
  - If $s_{EWH}(t) = 1$ the control is activated. This condition allows EWHs to maintain their same states.
- If $\Delta T_0 < -2\Delta T$:
  - If $T_{EWH} > T_{0,prev}$ and $s_{EWH}(t) = 1$ the control is activated. This condition allows reducing the number of EWHs to be turned OFF.
  - If $s_{EWH}(t) = 0$ the control is activated. This condition allows EWHs to maintain their same states.
- Two intermediate limits (f_{low} and f_{up}) within and close to the system frequency limits are defined as follows:

$$f_{lim,min} < f_{low} < f_0 \tag{3.64}$$

$$f_0 < f_{up} < f_{lim,max} \tag{3.65}$$

  If $f_{sys} < f_{low}$ or $f_{sys} > f_{up}$, the control is activated. As the frequency deviation is unknown at each time step, these limits help to avoid that f_{sys} exceeding frequency limits, resulting in better performance compared to the logic proposed in [40].

- If $f_{sys} \leq f_{lim,min}$ or $f_{sys} \geq f_{lim,max}$, the slope k_f is increased to allow a higher number of EWHs counteract the frequency deviation, which improve performance compared to the logic in [40].
- If the logic leads to disable the control, the thermostat setpoint temperature will be equal to that of the previous time step, i.e., $T_0 = T_{0,prev}$.

Based on the conditions mentioned above, the flowchart of the control logic for an EWH is depicted in Figure 3.28 The proposed modifications to the control logic in [40] are shown in yellow, which were introduced to improve performance, as previously explained.

3.5.2 LFC for ACs and GSHPs

ACs and GSHPs are restricted by a lockout time after being turned OFF to avoid compressor stall. Consequently, the control logic has to consider this lockout time when controlling the duty cycle of these TCLs to provide frequency regulation. As both TCLs operate in a similar way, they have the same control logic. Therefore, the parameters of the temperature-frequency characteristic for ACs and GSHPs given by (3.60) are determined based on operating and comfort restrictions in addition to system frequency limits as follows:

- T_{base} is calculated as the central indoor temperature from the comfort range established to provide comfort and avoid health problems, i.e.:

$$T_{base} = \frac{T_{i,min} + T_{i,max}}{2} \tag{3.66}$$

- f_0 is calculated as the central frequency of the frequency limits established for normal operating conditions of the microgrid, i.e.:

$$f_0 = \frac{f_{lim,min} + f_{lim,max}}{2} \tag{3.67}$$

- k_f is calculated according to the temperature and frequency limits given in (3.66) and (3.67), as follows:

$$k_f = \frac{T_{i,max} - T_{i,min}}{f_{lim,max} - f_{lim,min}} \tag{3.68}$$

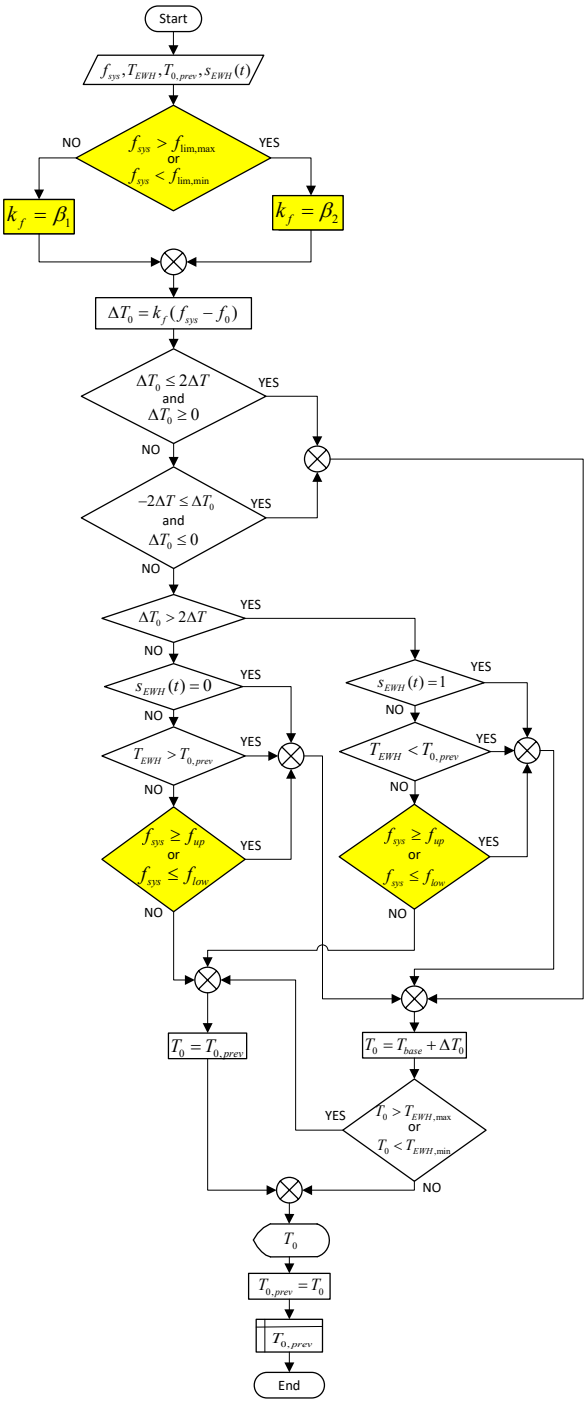

Figure 3.28: LFC logic for EWHs.

- In the case of ACs and GSHPs in cooling mode, (3.60) has a negative sign.

For example, according to Section 2.5.3, $T_{i,max} = 25$ ℃ and $T_{i,min} = 23$ ℃, and assuming $f_{lim,max} = 61.37$ Hz and $f_{lim,min} = 60.33$ Hz as the frequency limits, the graphical representation of (3.60) for an AC/GSHP is shown in Figure 3.29. This Figure shows the temperature-frequency characteristic for ACs and GSHPs in cooling mode, and the dead band $T_{db} = T_0 \pm \Delta T$ according to (2.8) and (2.9). This temperature-frequency characteristic is complemented by some logics to determine if the control must be activated or not. In this regard, the control logic is the same than for an EWH (Section 3.5.1), but are complemented by the lockout time $t_{lockout}$ when the AC/GSHP is turned OFF. Thus, a flag t_f is used to determine if the time these TCLs have remained OFF is greater than the lockout time, as follows:

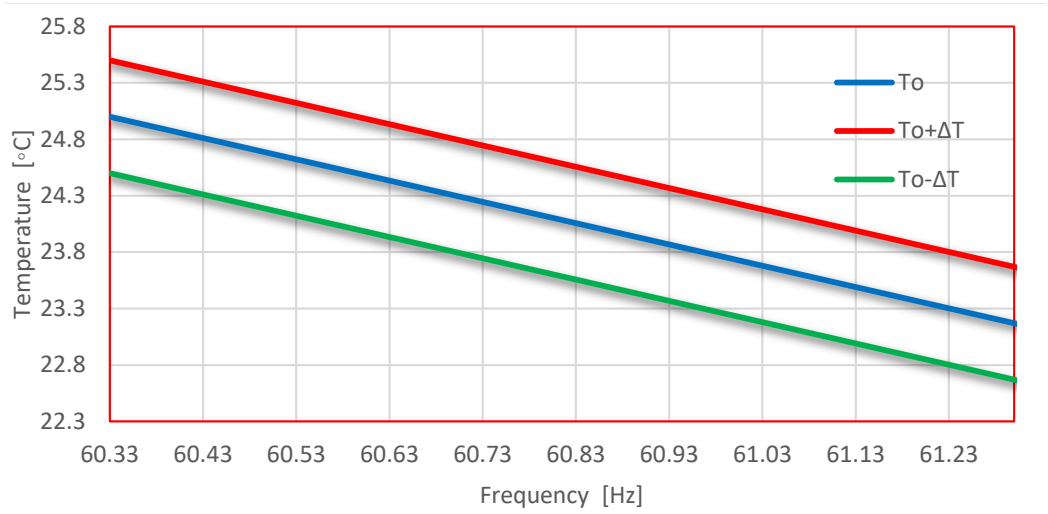

Figure 3.29: Temperature-frequency characteristic of an AC/GSHP (cooling mode).

$$t_f = \begin{cases} 0 & t_f \leq t_{lockout} \\ 1 & t_f > t_{lockout} \end{cases} \tag{3.69}$$

This equation is used to determine if an AC or GSHP can be turned ON. Based on this, the flowchart of the control logic for an AC/GSHP is shown in Figure 3.30.

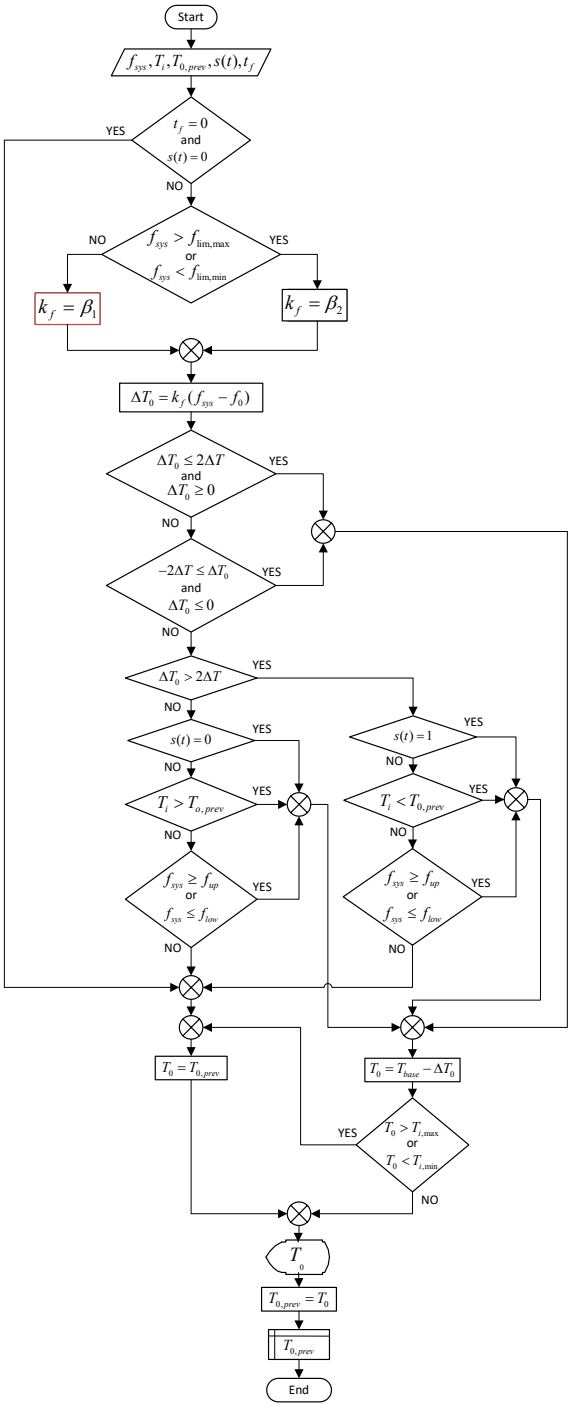

Figure 3.30: LFC logic for ACs and GSHPs in cooling mode.

3.6 Summary

In this chapter, the models for the different components of a hybrid PV-diesel microgrid were presented, followed by the control logic for the proposed DR strategy for primary frequency control. Thus, the modeling of a diesel genset and a solar PV system was described first. Then, the thermo-electrical models of TCLs, i.e., EWHs, ACs, and GSHPs, were developed, presenting some illustrative simulation results. The use of the SRLS, CREST, and DHW simulators to generate realistic non-TCLs demand and hot water consumption profiles was presented next. Finally, the control logic of the proposed DR based on an LFC method for TCLs was described in detail.

Chapter 4

Case Studies

In this chapter, the proposed decentralized DR strategy for controlling TCLs, i.e., EWHs, ACs, and GSHPs, is implemented and its performance is evaluated. First, the characteristics and components of a benchmark hybrid microgrid are described. Then, the electrical and thermal models developed in Chapter 3 are adapted to the components of this test system. Load and hot water consumption profiles are generated and randomly allocated among the households to represent realistic conditions. Next, several case studies are performed, and relevant results are presented and discussed. Finally, the performance of the proposed DR strategy is analized.

4.1 Test System Configurations

In Canada, remote communities rely largely on diesel gensets with high costs for electricity generation ($0.13 to $2.45 per kWh [5]). In contrast, solar PV generation costs are up to $0.75 per kWh nowadays, and have been decreasing continuously [4]. Therefore, hybrid solar PV-diesel generation offers a promising cost-effective alternative for both reducing greenhouse emissions and lowering electricity costs in some regions, and thus such a system is studied here.

4.1.1 Test System

The microgrid of the Xeni Gwet'in First Nation community of British Columbia's remote Nemiah Valley, depicted in Figure 4.1, has been extensively adopted as a test system to

perform power systems studies, since it was Canada's first battery-free PV-diesel off-grid network installed in 2007 [6], [40], [68], [82]. It is located about 250 km north of Vancouver and close to 100 km from the nearest national grid interconnection. The microgrid is divided into two areas: (1) a commercial complex supplied by underground low voltage lines, and (2) residential customers served by an aerial single-phase medium voltage (MV-1Ph) feeder divided into two laterals, the north lateral has a length of 1.47 km while the length of the south lateral is 0.92 km.

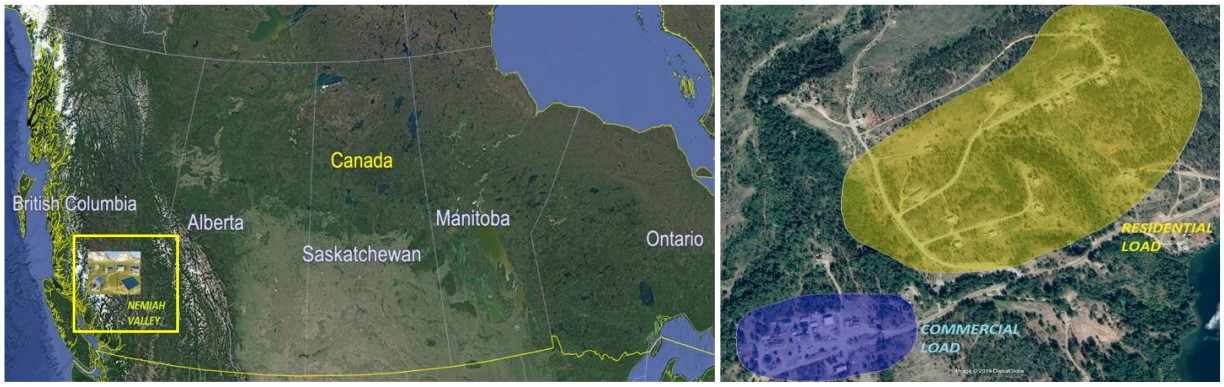

Figure 4.1: Location and aerial view of the hybrid PV-diesel microgrid in the Nemiah Valley.

The commercial zone is operated from two different busses: the first bus serves a commercial complex which comprises a band office, a daycare, a health center, water pumps, a gas station, and the diesel generation station, whereas the second bus serves critical loads that must remain powered at all times [82]. The residential zone has 22 housing units (14 single-detached houses and 2 fourplexes). The generation plant houses three diesel gensets: two gensets with 95 kW rated power, and one with 30 kW. The two 95 kW gensets are operated one at a time, on a rotational basis, to supply the weekday demand, whereas the 30 kW genset is operated at weeknight and on weekends. Additionally, 27.36 kW of distributed PV generation provide electricity during weekdays as follows: a set of two 5.4 kW roof-top PV systems are installed on each of the fourplexes, and two 2.88 kW roof-top PV systems are installed on two different houses along the distribution feeder. A schematic of the microgrid is shown in Figure 4.2.

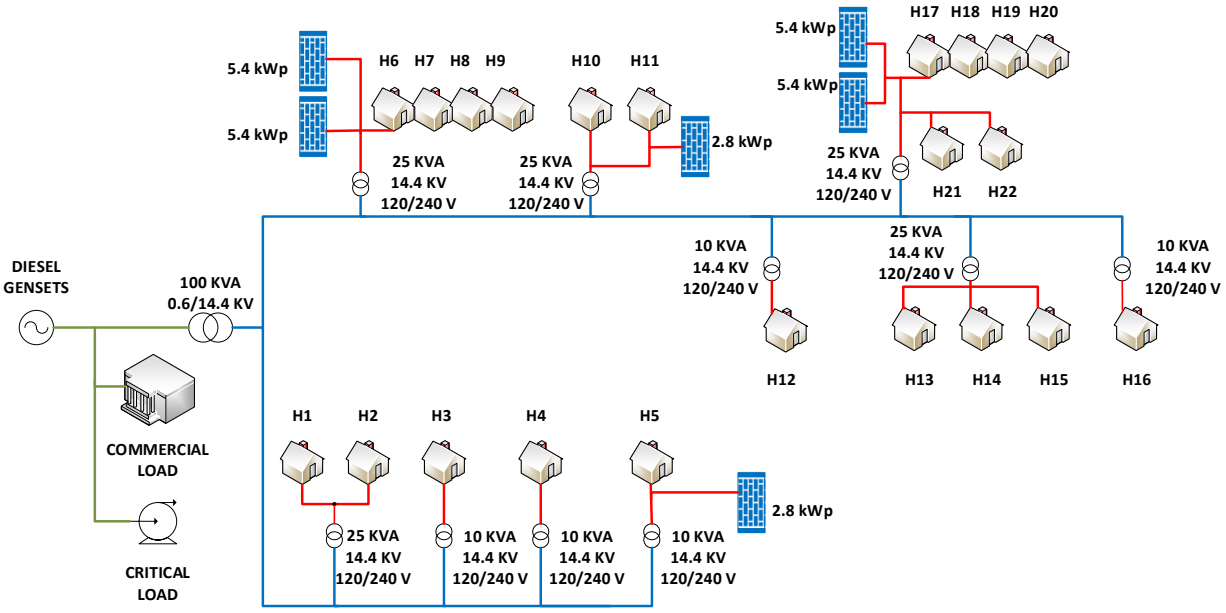

Figure 4.2: Single-phase diagram of the Nemiah Valley's microgrid.

4.1.2 Diesel Gensets

No specific frequency limits for normal operation in isolated microgrids have been defined. In this regard, the limits imposed by the recommended operation range of diesel gensets can be adopted as the operational frequency limits in a microgrid, since, as presented in Section 2.3, the generation costs, fuel consumption, and efficiency is the highest when gensets operate within these limits.

The 30 kW genset from the Nemiah Valley's microgrid supplies the critical commercial load plus the residential load at weeknights and weekends. The critical load plus the residential load have a 14 kW average power consumptions that remain fairly constant [82]. Thus, this genset is constantly operating within their efficient limits, and thus, the operation of this genset is not considered in this thesis to evaluate the performance of the proposed DR strategy.

The 95 kW gensets serves the loads through a single-phase feeder; thus, in practice, only 2/3 of the generator power is available. Therefore, the efficient operating range of these gensets is from 28 to 64 kW, which corresponds to 30 to 90% of their available power, respectively. In a typical weekday, the day's peak load is 75 kW with an average

load of 29 kW without considering PV generation, which could be up to 27.36 kW. In this regard, the load variation plus the intermittent PV generation makes it challenging to efficiently operate these gensets on weekdays [82]. The characteristics of the 95 kW genset and its droop parameters, according to (2.2), are presented in Table 4.1. Thus, from the characteristics of the 95 kW genset (Table 4.1) and (2.2), the droop curve illustrated in Figure 4.3 can be obtained.

Table 4.1: Characteristics of the 95 kW Deutz genset [82].

DEUTZ Air-Cooled Diesel Genset	
Engine BF69L13G	
Parameter	**Value**
P_G [kW]	95
V_T [V]	600
s_p [kW/Hz]	29.4
f_{nl} [Hz]	62.34

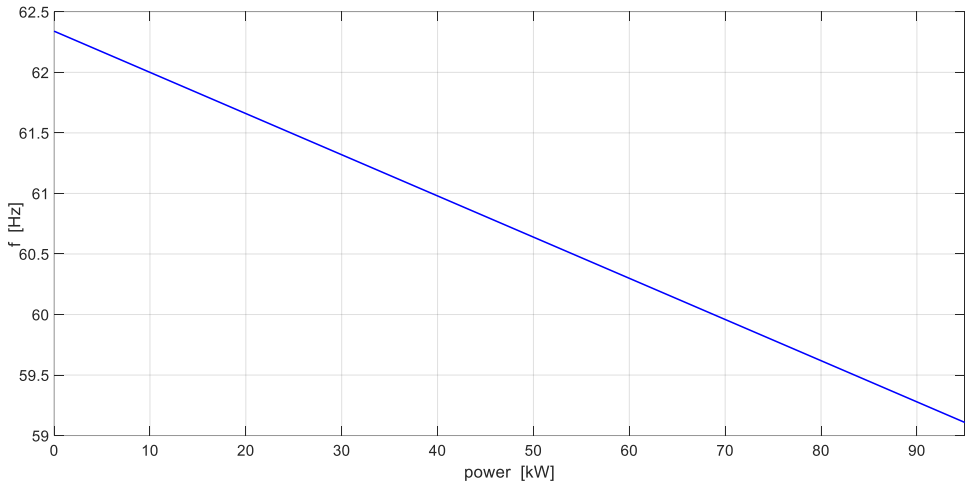

Figure 4.3: Droop characteristic of the 95 kW Deutz diesel genset.

Table 4.2 depicts the specific fuel consumption at certain percentages of the output power of the 95 kW genset, provided by the manufacturer. Using this data and (2.4) with

$\rho_f = 0.835$ kg/dm^3 and $\sigma = 1000$, the FCR at the same percentages of the output power can be obtained. Then, in order to obtain the FCR for the entire operating range of the 95 kW genset, the following second order function FCR can be approximated:

$$FCR_{95kW} = 0.0004522\, P_G^2 + 0.1617\, P_G + 3.619 \tag{4.1}$$

Table 4.2: Specific fuel consumption of the 95 kW Deutz diesel genset [82]

	Consumption	
Power	[g/kWh]	[L/h]
25 %	280	7.721
50 %	223	12.298
75 %	211	17.455
100 %	209	23.053

Finally, with (4.1), (2.5), and (2.6), the efficiency curve of the genset can be obtained (with $LHV_{fuel} = 43.2$ MJ/kg). Figure 4.4 depicts the FCR and efficiency curves of the 95 kW genset.

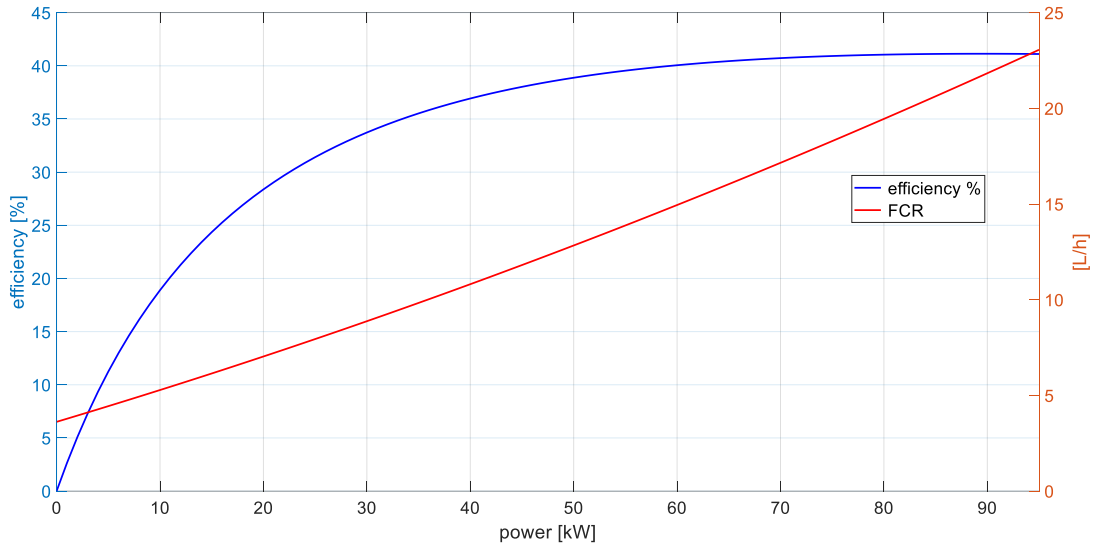

Figure 4.4: FCR and efficiency curves of the 95 kW Deutz genset.

4.1.3 Solar PV Generation

The total PV generation capacity of the 6 roof-top PV systems is 27.36 kW, which represents 36% of the peak load (75 kW) in a typical weekday. These panels operate as passive generation elements without any control, which means that their generation only depends on ambient conditions, i.e., temperature and solar irradiation. Therefore, for the purposes of this thesis, the aggregated solar PV generation is obtained by adding the individual capacity of the roof-to panels according to the model presented in Section 3.2. The ambient temperature and solar irradiation profiles, inputs to the solar PV array model, correspond to the curves depicted in Figures 3.8 and 3.9 for a typical summer day, respectively. Table 3.2 shows the parameters of the individual PV modules that are connected to form the PV systems. Therefore, the total aggregated solar PV generation for a typical summer day is depicted in Figure 4.5.

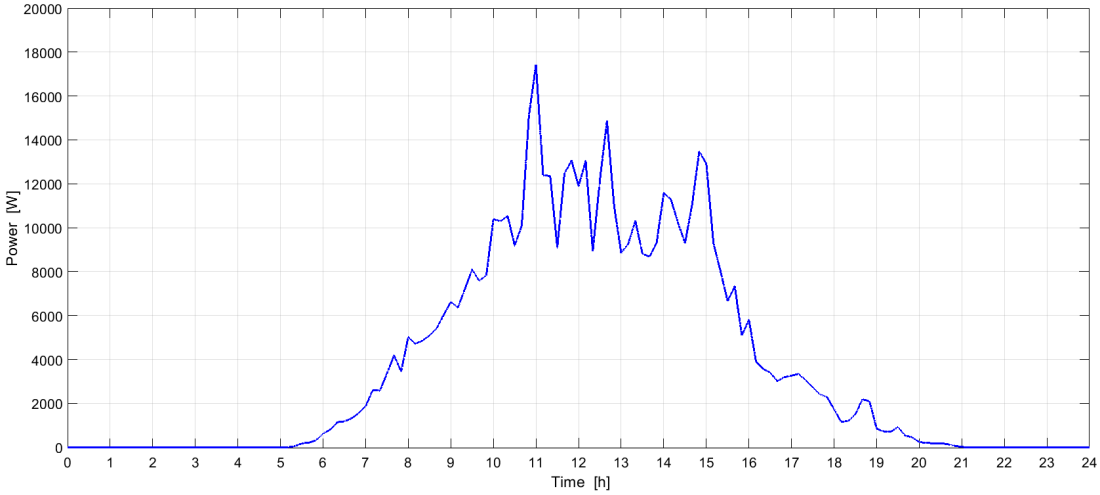

Figure 4.5: Aggregated solar PV generation.

4.1.4 Residential Loads

The load profile of the residential zone of the Nemiah Valley's microgrid must represent the natural sudden and random demand variation among different households. Since this zone has 22 housing units, it is necessary to model individual load profiles that reflect realistic conditions. Since occupants in a household is one of the main factors that determines the demand profiles of residential loads, the number of occupants in each household is

randomly assigned between 2 to 5 occupants. Additionally, the setpoint temperatures of TCLs highly influence their consumption cycles. Thus, the setpoint temperatures for HAVC systems, i.e., ACs and GSHPs, and EWHs are also randomly assigned among the households, corresponding the recommended temperatures in Sections 2.5.3 and 2.5.5 due to safety restrictions for indoor air and hot water (between 23 and 25 ℃ during summer, and 49 to 60 ℃, respectively). Table 4.3 shows the results of the random assignments, which together with the methodology described in Sections 3.3.4.1 and 3.4, yields realistic hot water consumption and non-TCLs demand profiles for all households. This yields the load profile of the test system households used in this thesis and depicted in Figure 4.6, with a peak load of 63 kW, which is consistent with the system data provided in [82].

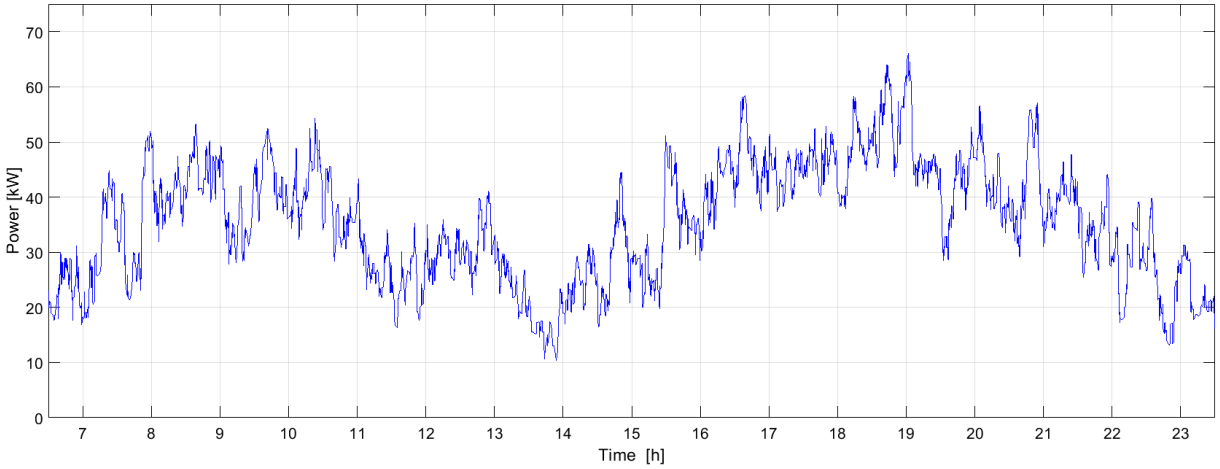

Figure 4.6: Aggregated residential load.

4.1.5 Commercial Load

The commercial load demand is adopted from [83, 84], where the typical daily load profile shown in Figure 4.7 is used for analysis of low-voltage microgrids. This profile has been scaled to fit the 12 kW peak load demand of the test system [82].

Table 4.3: Summary of the random operating condition assignments.

House	**Occupants**	**Indoor setpoint Temperature [°C]**	**Hot Water setpoint Temperature [°C]**
H1	3	25	54
H2	3	24	50
H3	5	23	51
H4	5	23	59
H5	2	24	50
H6	3	23	58
H7	3	25	55
H8	4	24	60
H9	4	25	49
H10	5	25	54
H11	3	23	50
H12	4	24	49
H13	4	23	58
H14	2	24	53
H15	2	25	57
H16	3	23	59
H17	5	24	50
H18	3	25	53
H19	4	25	52
H20	2	24	55
H21	5	24	58
H22	3	23	56

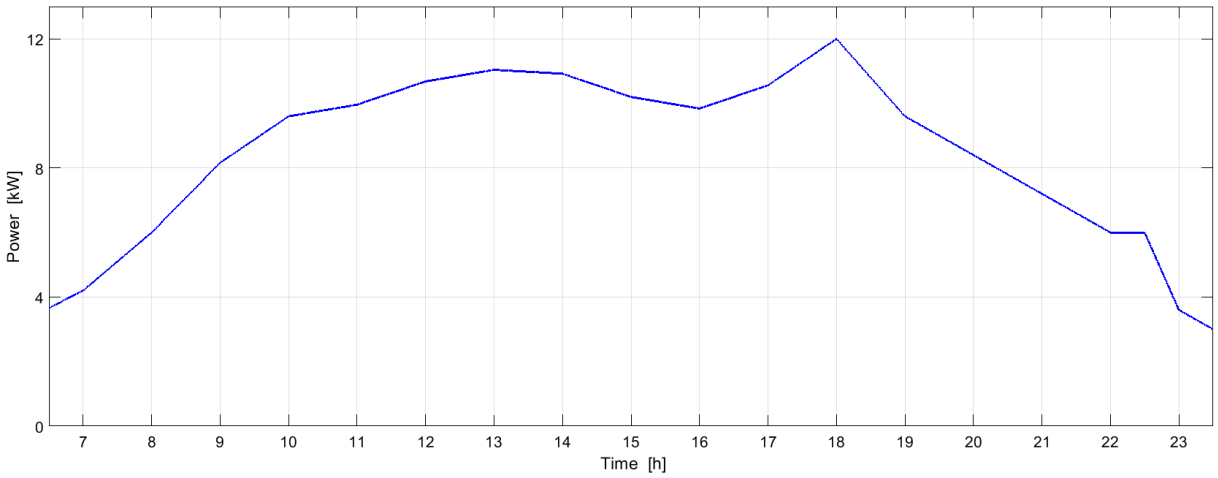

Figure 4.7: Commercial load [83].

4.2 DR Control Logic

The DR strategy for the provision of frequency control presented in Sections 3.5.1 and 3.5.2 for EWHs and ACs/GSHPs, respectively, is applied here. Thus, the parameters of (3.60) and the variables of the control logic are defined according to the characteristics of the Nemiah Valley's microgrid as follows:

- The limits of the safe operating temperature range for EHWs are $T_{EWH,max} = 60$ ℃ and $T_{EWH,min} = 49$ ℃, whereas for ACs and GSHPs are $T_{i,max} = 25$ ℃ and $T_{i,min} = 23$ ℃.
- The central temperature for EWHs is $T_{base} = 54.5$ ℃, whereas for ACs and GSHPs is $T_{base} = 24$ ℃.
- The frequency limits established for normal operating conditions are defined based on the operating range of the 95 kW genset, which corresponds to 30 to 90% of its available power. As this genset supplies power through a single-phase feeder, only 2/3 of the generator power is available; thus, the operating range of this generator is 28 to 64 kW. Hence, using its droop characteristic, the frequency limits are found to be $f_{lim,max} = 61.37$ Hz and $f_{lim,min} = 60.33$ Hz, which yields a central frequency of $f_0 = 60.85$ Hz in (3.62) and (3.67). These values are high compared to the standards

defined by some utilities [85]; however, the droop characteristic of the 95 kW diesel genset and the restriction imposed by the single-phase feeder, yield these high values for this particular system, as also observed in [68].

- Based on these temperature and frequency limits, the slope of the temperature-frequency characteristics for EWHs is $k_f = 10.377$ ℃/Hz, whereas for ACs and GSHPs is $k_f = 10.886$ ℃/Hz. These values correspond to β_1 according to the control logic presented in Figures 3.28 and 3.30. If f_{sys} exceeds the frequency limits, the new slope β_2 increases in 10% with respect to β_1. The value of β_2 was found by trial and error.

- The dead band temperature for EWHs is $\Delta T = \pm 1.4$ ℃, whereas for ACs and GSHPs is $\Delta T = \pm 0.5$ ℃.

- The intermediate limits are defined according to the higher rated power of the TCLs. Therefore, the power of an EWH (P_{EWH}) is used to determine these limits by adding/subtracting P_{EWH} to the operating power limits of the genset, which yields $f_{up} = 61.25$ Hz and $f_{low} = 60.47$ Hz.

- A delay $t_D = 5$ min in the initial activation and final deactivation of the LFC control among the TCLs' controllers is used to complement the control logic presented in Sections 3.5.1 and 3.5.2 for EWHs and GSHPs, respectively. This delay allows having a smoother transition when the 30 kW and 95 kW gensets are switched.

- In order to somewhat represent realistic conditions, it is assumed that three households (about 14%) do not participate for the provision of frequency control in the Nemiah Valley's microgrid. The assignment of these households was performed randomly, resulting in households H1, H7, and H16, not considered as part of the DR strategy.

4.2.1 Frequency Control Architecture

In microgrids, voltage and frequency, i.e., active and reactive power, are coupled due to the large R/X ratio of distribution feeders, and specially voltage dependent loads. However, in this thesis, the voltage dependency of load active power is not considered, thus assuming more limiting and hence challenging frequency control conditions.

The frequency control architecture used to study the performance of the DR strategy for the provision of primary frequency control is shown in Figure 4.8. This architecture

consists of aggregated non-TCL load demand, aggregated solar PV generation, TCLs with LFC controllers, and a diesel genset (governor action plus inertia). The controllers of the EWHs and ACs/GSHPs monitor the system frequency and turn ON/OFF these TCLs according to the logic described in the previous chapter.

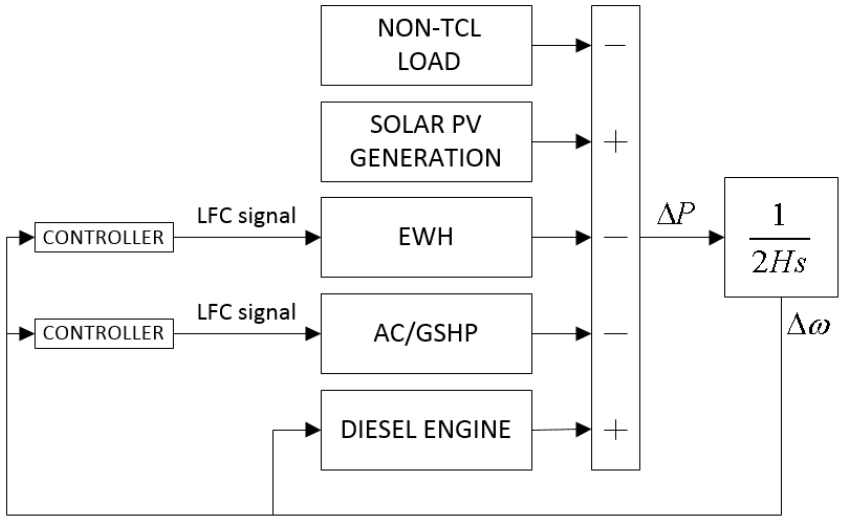

Figure 4.8: Control architecture for primary frequency regulation.

4.3 Case Studies and Simulation Results

The performance of the thermo-electrical models of TCLs, i.e., EWHs, ACs, and GSHPs, along with the proposed DR strategy for primary frequency control are evaluated on the Nemiah Valley's microgrid based on the following case studies:

Case 1 No control: In this case, only the diesel genset is responsible for balancing the demand plus the aggregated PV generation.

Case 2 EWHs' control: This study case is performed by using the control logic for EWHs proposed in [40].

Case 3 Proposed EWHs' control: In this case, the control logic for EWHs developed in Section 3.5.1 is used.

Case 4 Proposed EWHs + ACs' control: In this case, the frequency control presented in Case 3 is complemented by the control logic for ACs developed in Section 3.5.2.

Case 5 Proposed EWHs + GSHPs' control: In this case, the performance of GSHPs replacing ACs for primary frequency control is evaluated. Hence, the primary frequency control is shared between EWHs (**Case 3**) and GSHPs (Section 3.5.2).

All these cases are studied during the working hours of the 95 kW diesel gensets, as discussed in Section 4.1.2, which correspond to 6:30 a.m. to 11:30 p.m. on weekdays [82].

4.3.1 System Frequency

Figure 4.9 depicts the system frequency response for all case studies considering identical thermal and electrical demand conditions. Note that the performance of the frequency control of the proposed EWH DR strategy (**Case 3**) compared to that in [40] (**Case 2**) is improved. In addition, as more TCLs, i.e., ACs (**Case 4**) or GSHPs (**Case 5**), are used to provide frequency control, the overall system response is better.

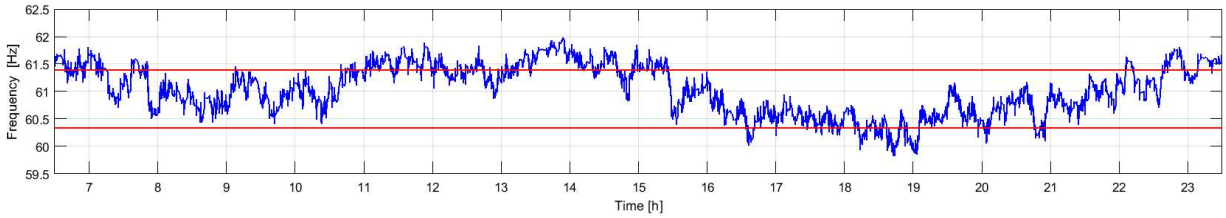

(a) **Case 1**: No control.

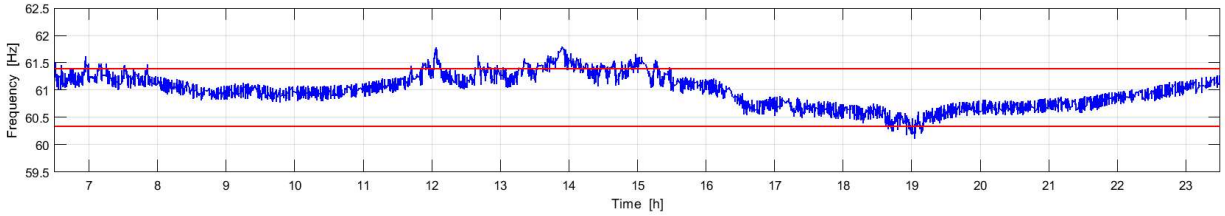

(b) **Case 2**: EHWs' control [40].

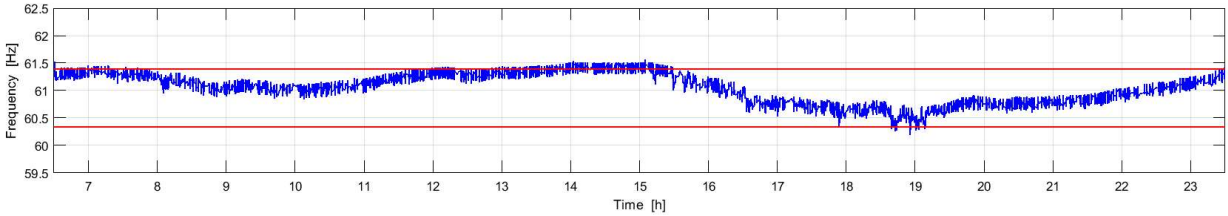

(c) **Case 3**: Proposed EWHs' control.

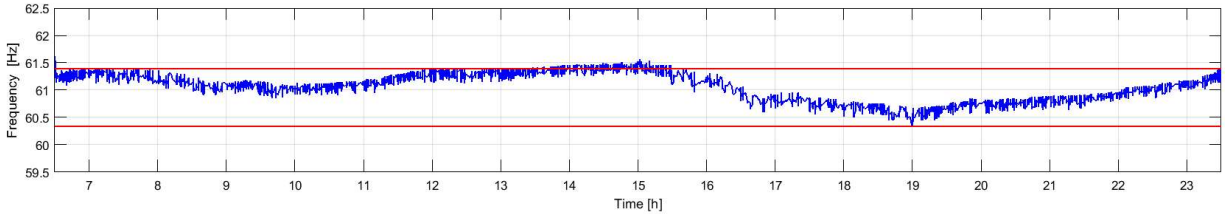

(d) **Case 4**: Proposed EWHs+ACs' control.

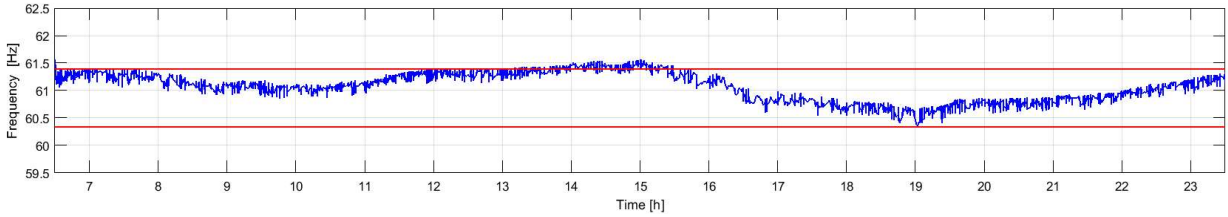

(e) **Case 5**: Proposed EWHs+GSHPs' control.

Figure 4.9: System frequency response.

4.3.2 Active Power

The active power generated by the 95 kW diesel genset is depicted in Figure 4.10 for the different study cases. Observe that as frequency control is added from the demand side, by means of the TCLs, the steep ramps are reduced significantly, thus helping the genset to respond more smoothly and very close, or within, its efficient operating limits as defined in Section 4.2.

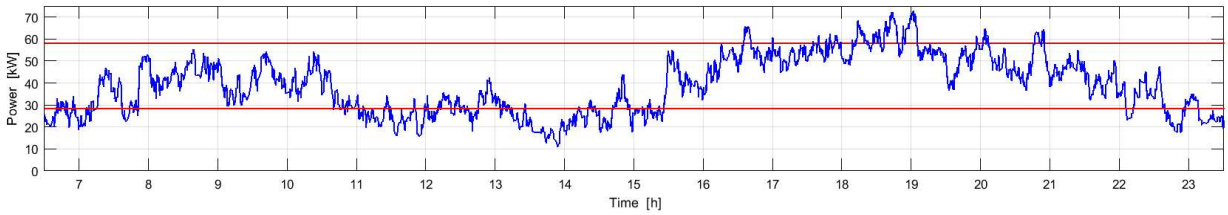

(a) **Case 1**: No control.

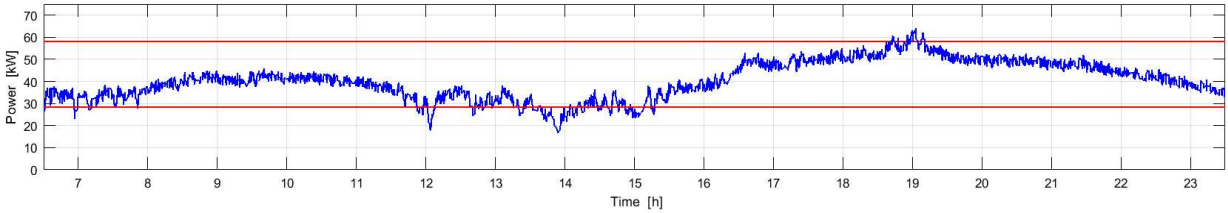

(b) **Case 2**: EHWs' control [40].

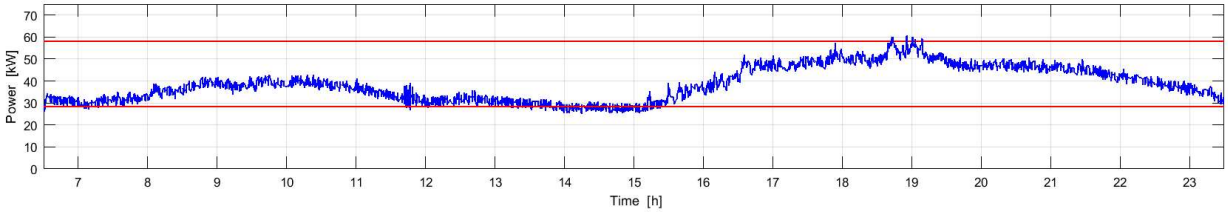

(c) **Case 3**: Proposed EWHs' control.

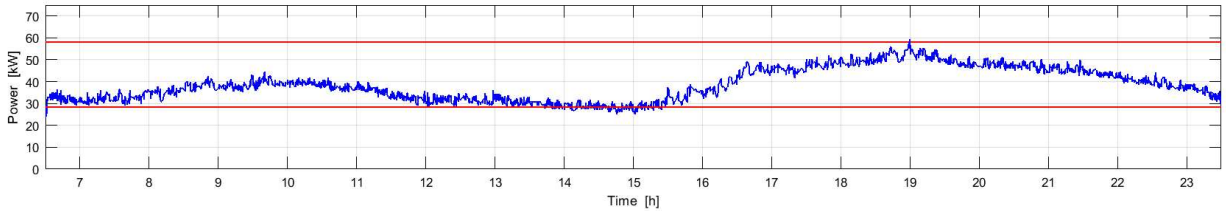

(d) **Case 4**: Proposed EWHs+ACs' control.

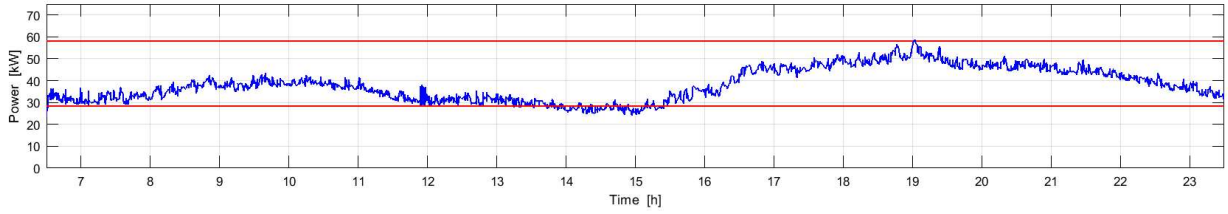

(e) **Case 5**: Proposed EWHs+GSHPs' control.

Figure 4.10: Diesel genset active power.

4.3.3 Efficiency

The efficiency curves over the operating time of the 95 kW diesel genset are depicted in Figure 4.11 for all case studies. According to Figure 4.4, the maximum efficiency that this genset can reach is close to 40%. Thus, as the DR response attempts to maintain the diesel operating as close as possible to this point, observe that the efficiency of the supply over the full range of load variations is improved, which can be directly translated into fuel savings and cost reductions.

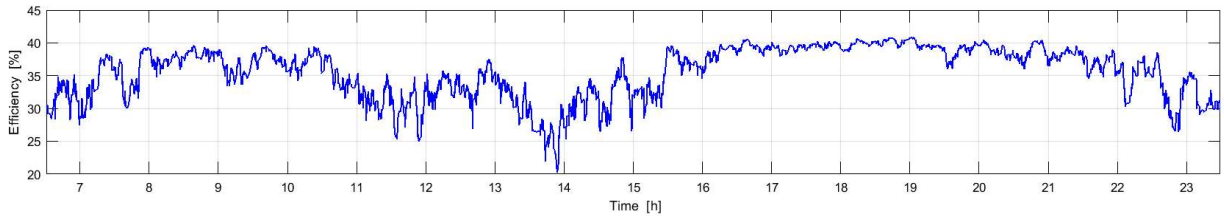

(a) **Case 1**: No control.

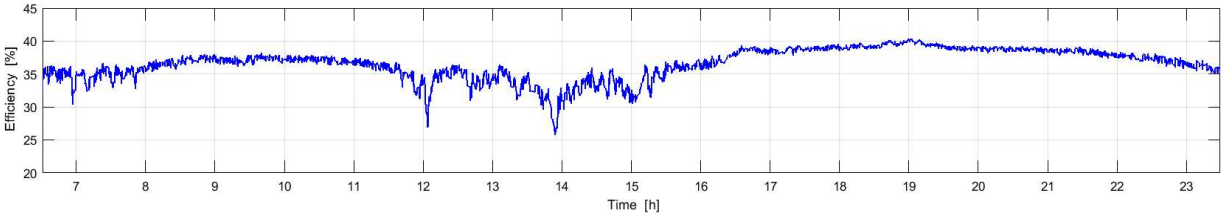

(b) **Case 2**: EHWs' control [40].

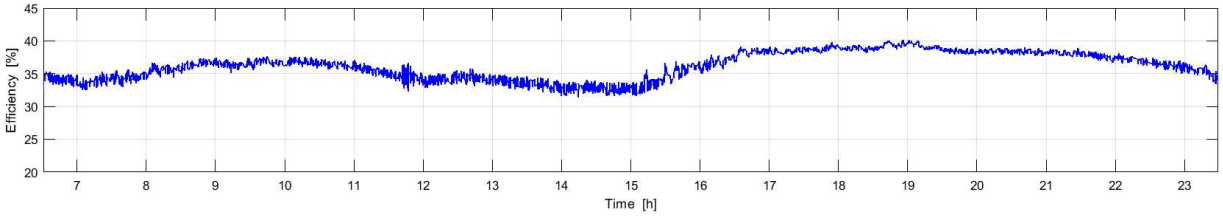

(c) **Case 3**: Proposed EWHs' control.

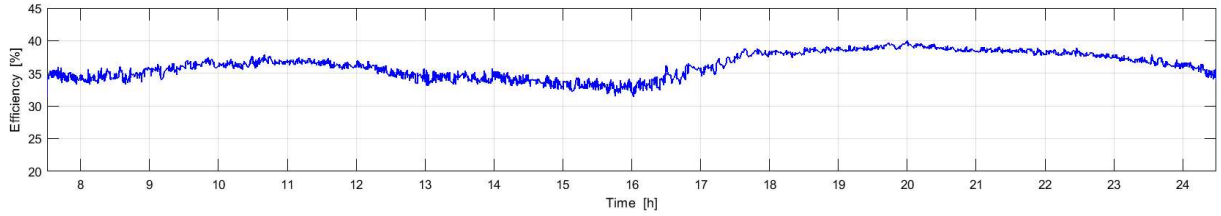

(d) **Case 4**: Proposed EWHs+ACs' control.

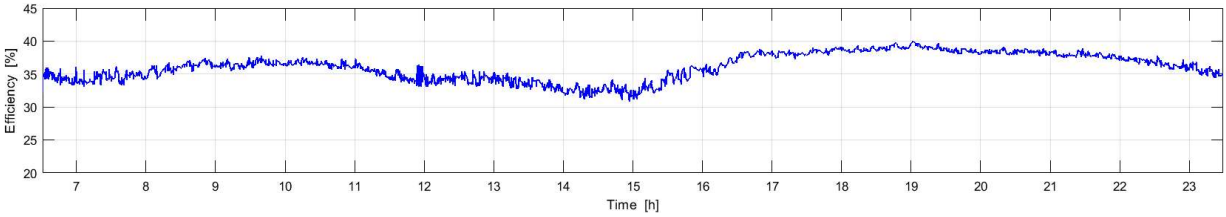

(e) **Case 5**: Proposed EWHs+GSHPs' control.

Figure 4.11: Diesel genset efficiency.

4.3.4 Temperature Variations

The proposed DR strategy for primary frequency control, adjusts the thermostat setpoint temperatures as a function of system frequency deviations. Therefore, the operation of the DR strategy on the TCLs can be illustrated as follows:

- Figures 4.12 and 4.13 depict the EWHs' temperatures and temperature setpoints for **Case 1**, **Case 2**, and **Case 3**. In the first case, no control for EWHs is used, resulting in each individual customer selecting a setpoint temperature within the safety range, as per Table 4.3. For **Case 2**, adopted from [40], and **Case 3**, note that the setpoints constantly vary over the operating time, meaning that EWHs are turned ON/OFF to provide frequency control; however, for **Case 3**, the temperatures are closer to each other, thus resulting in more operations to control the system frequency.
- Figures 4.14 and 4.15 illustrate the indoor temperatures and temperature setpoints for all households. Since the DR strategy for ACs and GSHPs is the same, only two cases are presented. In **Case 1**, the customers select their setpoints as per Table 4.3, and no control is activated, whereas for **Case 4**, the setpoints vary over time. As the safety range is narrow, and considering that both ACs and GSHPs are compressor-based loads restricted by a lockout time after being turned OFF, observe that the setpoint adjustment is smother than that of EWHs.

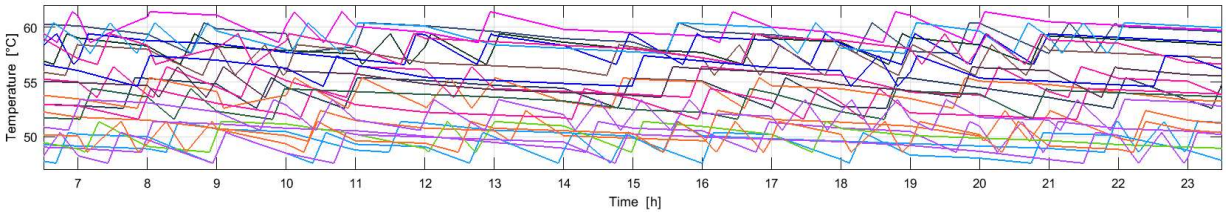

(a) **Case 1**: No control.

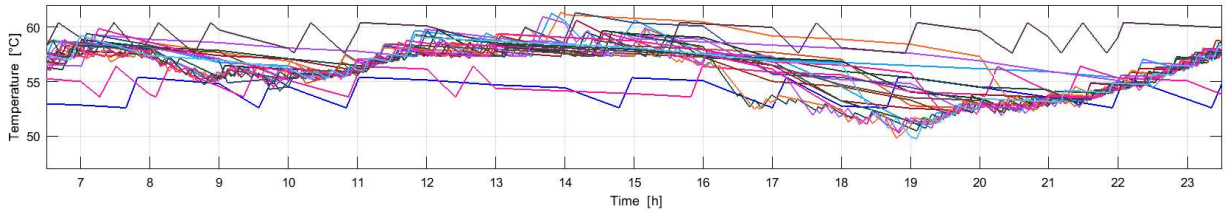

(b) **Case 2**: EHWs' control [40].

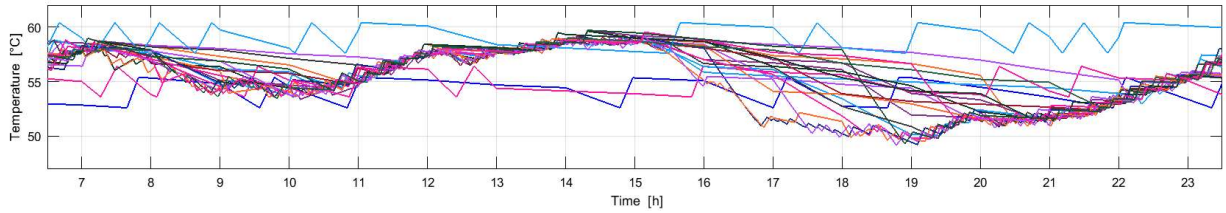

(c) **Case 3**: Proposed EWHs' control.

Figure 4.12: EWHs' temperatures for all households.

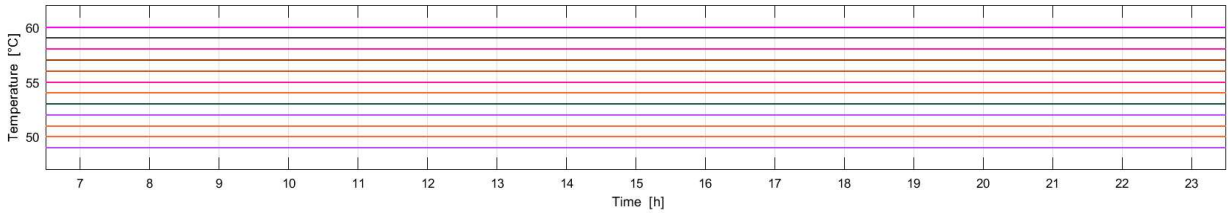

(a) **Case 1**: No control.

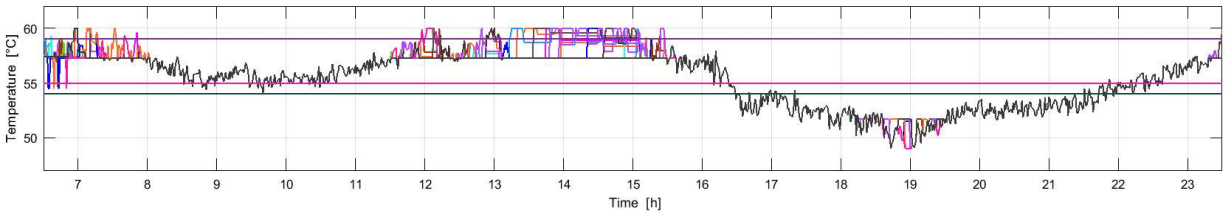

(b) **Case 2**: EHWs' control [40].

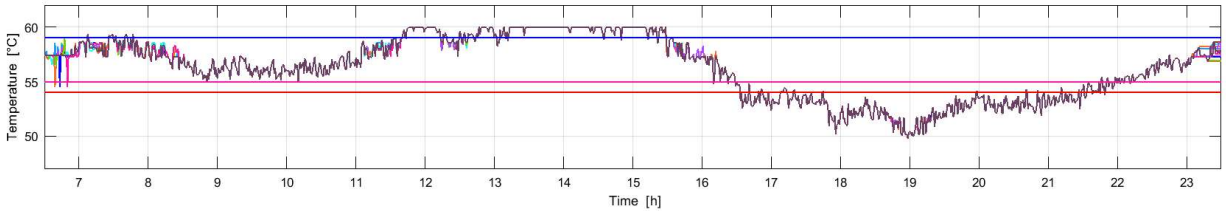

(c) **Case 3**: Proposed EWHs' control.

Figure 4.13: EWHs' temperature setpoints for all households.

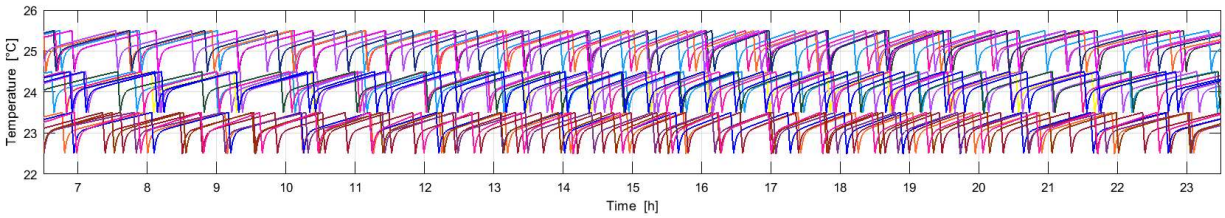

(a) **Case 1**: No control.

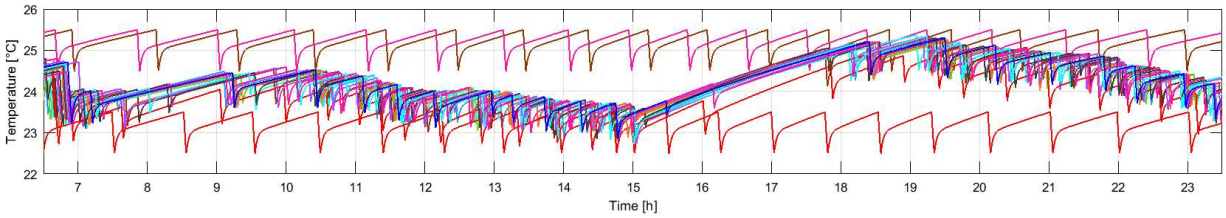

(b) **Case 4**: Proposed EWHs+ACs' control

Figure 4.14: Households' indoor temperatures.

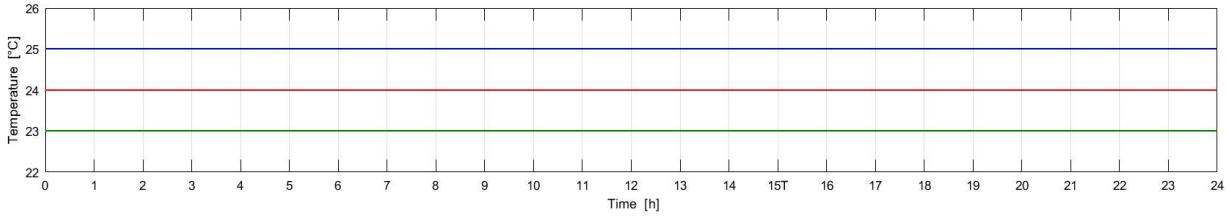

(a) **Case 1**: No control.

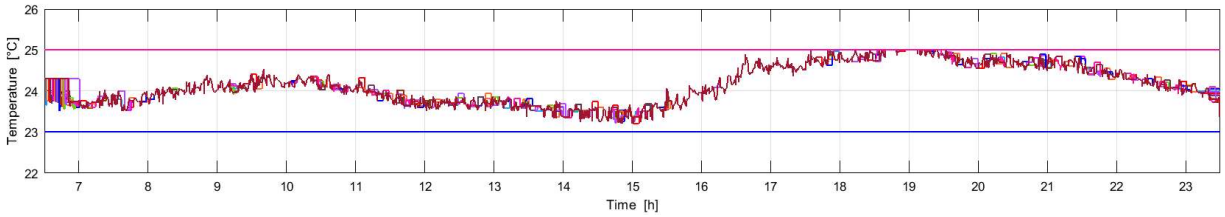

(b) **Case 4**: Proposed EWHs+ACs' control

Figure 4.15: Households' indoor temperature setpoints.

4.3.5 Power Cycling

The power cycling of TCLs, i.e., EWHs, ACs, and GSHPs, when subject to the proposed DR strategy are each compared to the base case, as follows:

- Figure 4.16 shows the power cycling of an EWH in a household. Note how the hot water temperature inside the tank differs with respect to the base case (**Case 1**), due to the ON/OFF operations of the EWH (**Case 2** and **Case 3**). Thus, in **Case 1**, the hot water temperature varies within the dead band of the thermostat, while in **Case 2** and **Case 3**, the DR strategy frequently activates the heating element of the EWH (more often in **Case 3**), resulting in a broader hot water temperature variation. The aggregated power of all EWHs for all 5 cases are shown in Figure 4.17.

- The indoor and outdoor temperature variations of a household equipped with an AC is shown in Figure 4.18, as well as the power cycling of this appliance. In the base case (**Case 1**), note that the AC is limited to provide thermal comfort with its power consumption being ruled by a thermostat switching rule, whereas in **Case 4**, observe how the DR strategy adjusts the power cycling in order to provide frequency control while maintaining indoor thermal comfort. The aggregated powers of ACs for **Case 1** to **Case 4** are shown in Figure 4.19.

- Since the DR strategy for GSHPs and ACs is the same, a similar response from the GSHP to that of an AC can be observed, as shown in Figure 4.20, but with lower powers, due to the characteristics of the GSHPs. Again, in the base case (**Case 1**), the AC controls the indoor temperature without contributing to frequency control, while in **Case 5**, the DR strategy forces the GSHP to modify its power consumption for primary frequency control. Furthermore, to show the dynamics of the GHX model, Figure 4.21 depicts the temperature variation of the fluid inside the borehole. Note how the fluid temperature varies, according to the requirements imposed by the GSHP. Thus, as the DR strategy adjusts the power consumption of the GSHP, the GHX must respond accordingly. Finally, the aggregated AC and GSHP powers for **Case 1** and **Case 5** are shown in Figure 4.22; observe that the total power of the GSHPs is significantly lower than with ACs, as expected.

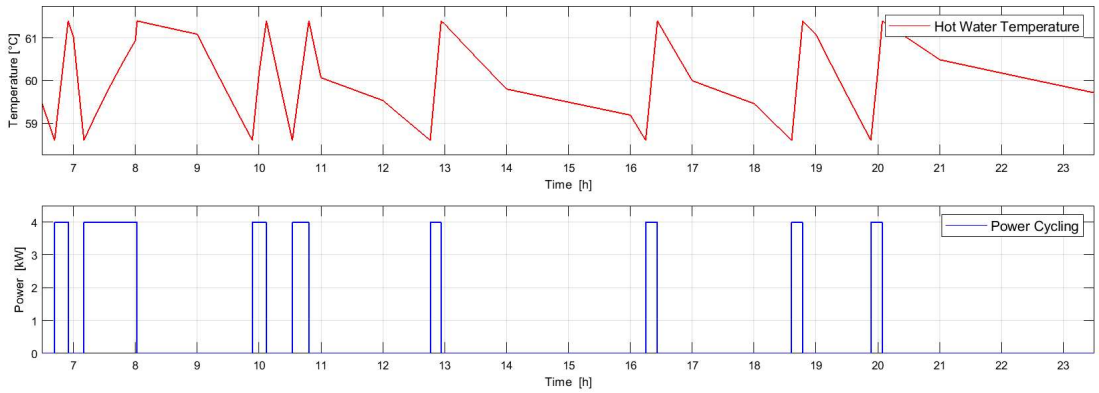

(a) **Case 1**: No control.

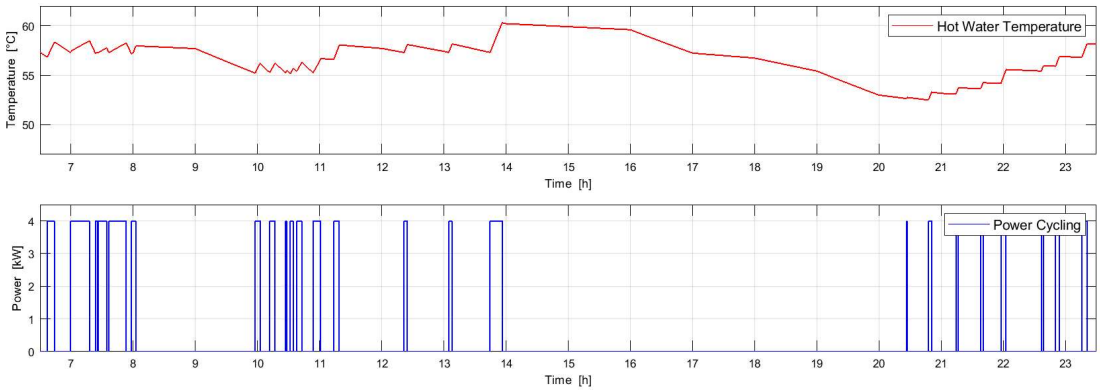

(b) **Case 2**: EHWs' control [40].

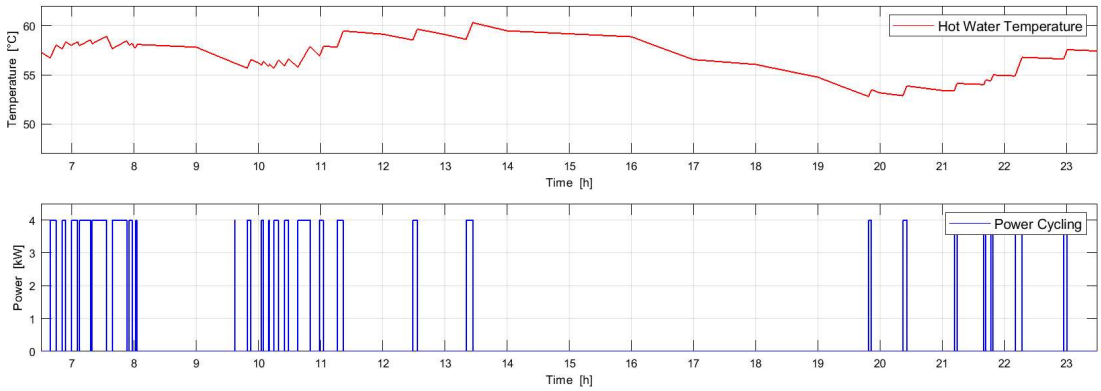

(c) **Case 3**: Proposed EWHs' control

Figure 4.16: EWHs' power cycling for one household.

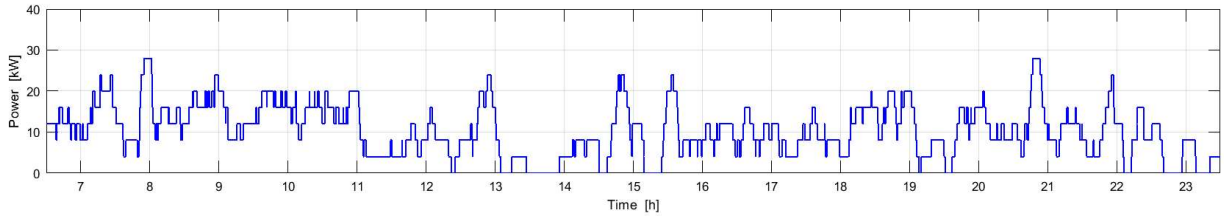

(a) **Case 1**: No control.

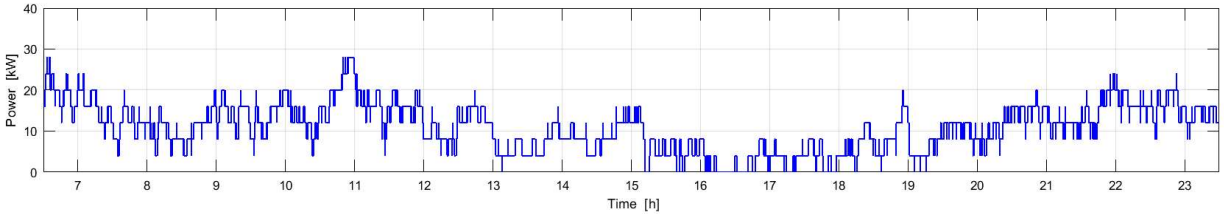

(b) **Case 2**: EHWs' control [40].

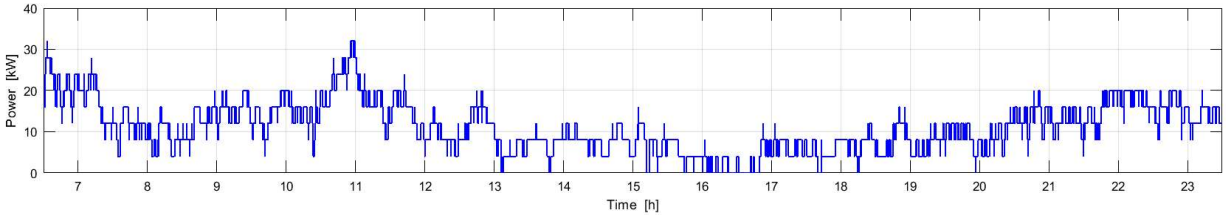

(c) **Case 3**: Proposed EWH's control.

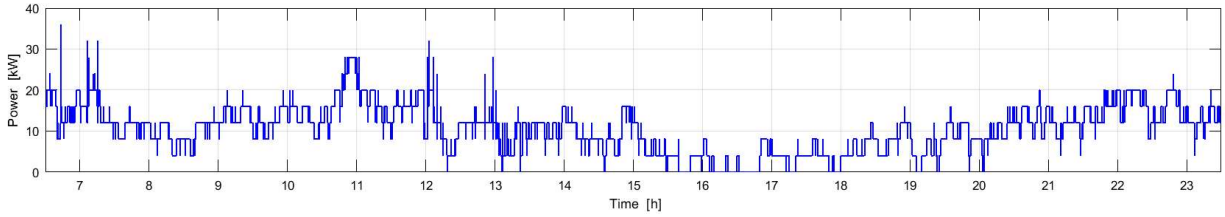

(d) **Case 4**: Proposed EWHs+ACs' control.

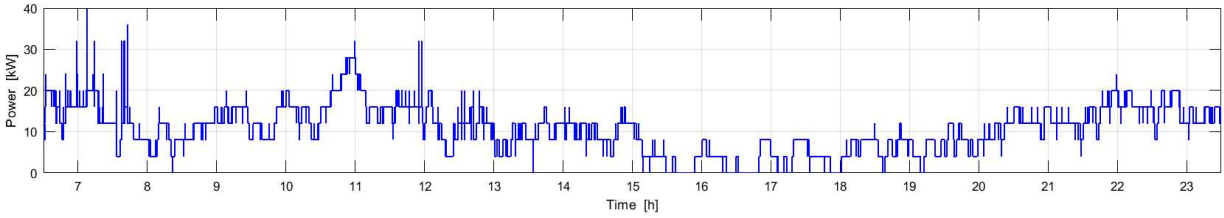

(e) **Case 5**: Proposed EWHs+GSHPs' control.

Figure 4.17: EWHs' aggregated powers.

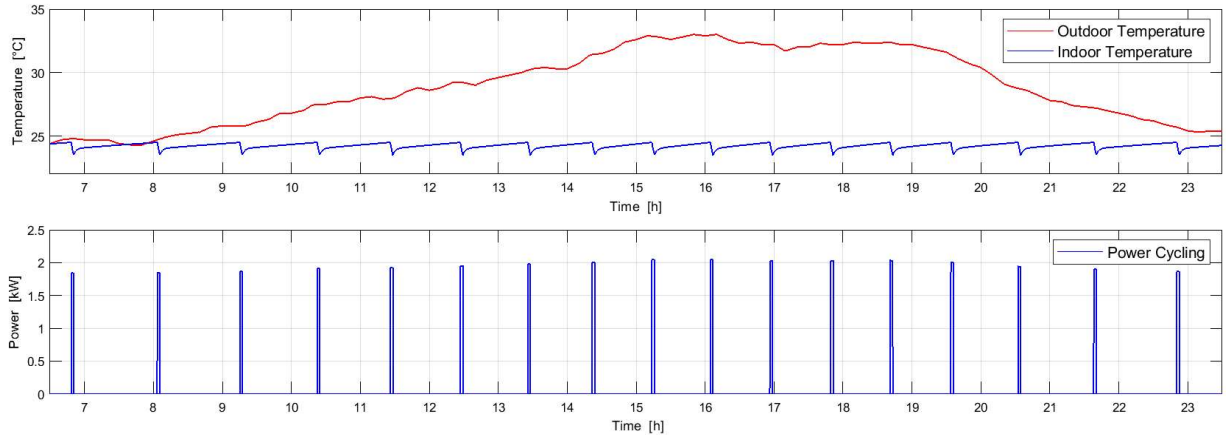

(a) **Case 1**: No control.

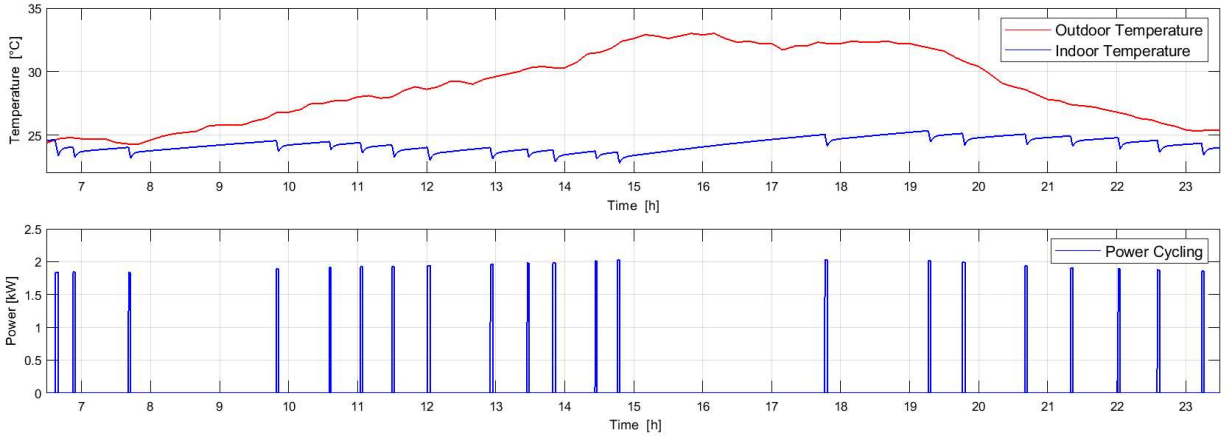

(b) **Case 4**: Proposed EWHs+ACs' control.

Figure 4.18: ACs' power cycling for one household.

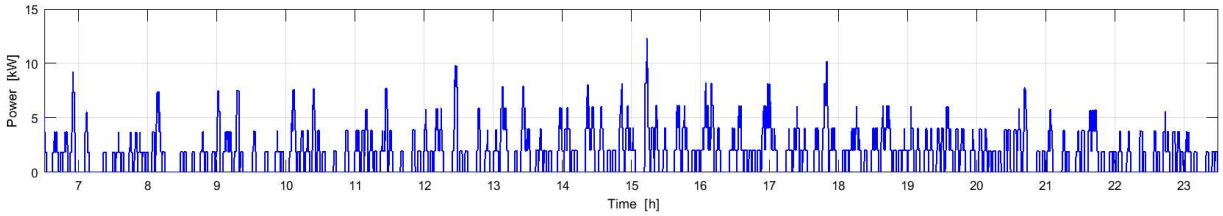

(a) **Case 1**: No control.

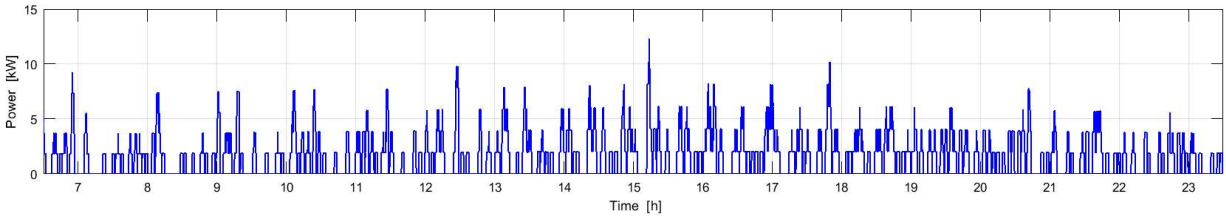

(b) **Case 2**: EHWs' control [40].

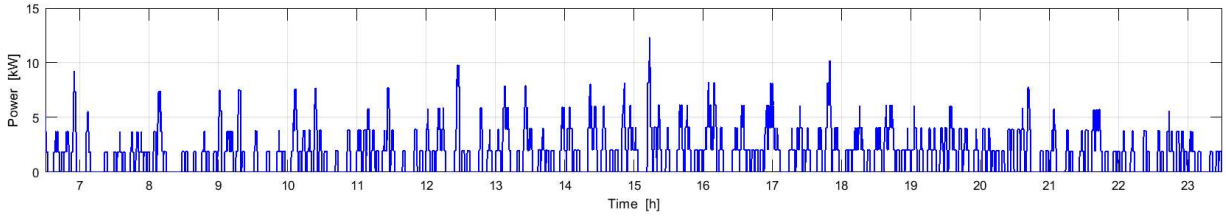

(c) **Case 3**: Proposed EWHs' control.

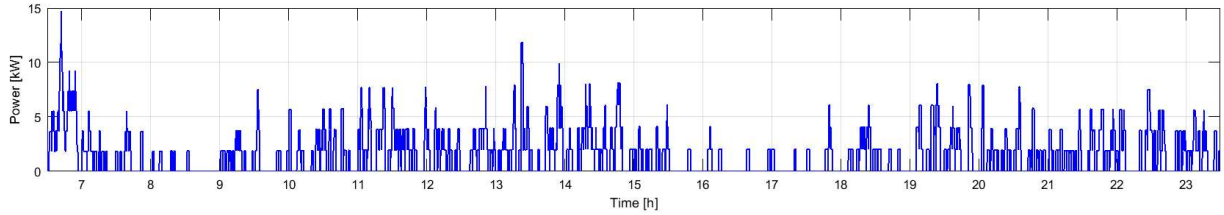

(d) **Case 4**: Proposed EWHs+ACs' control.

Figure 4.19: ACs' aggregated powers.

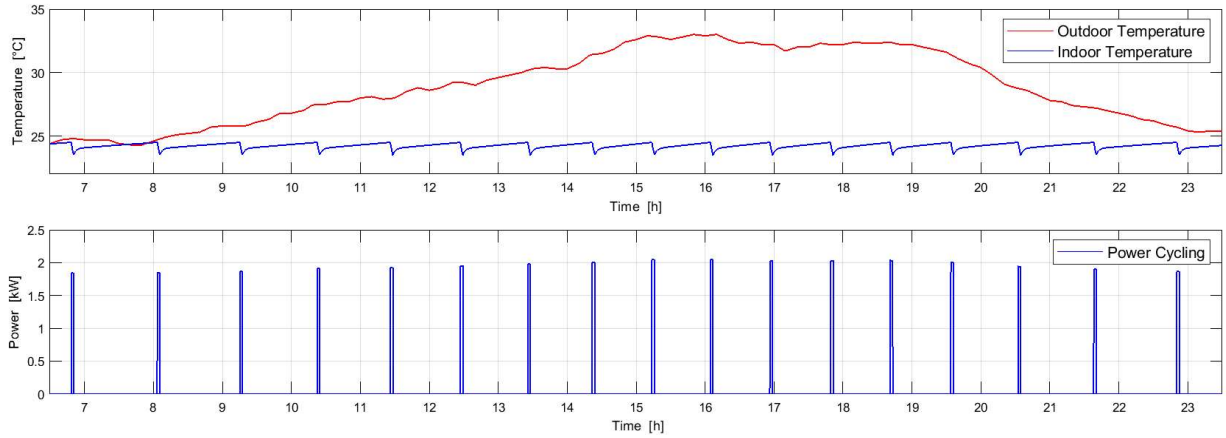

(a) **Case 1**: No control with AC.

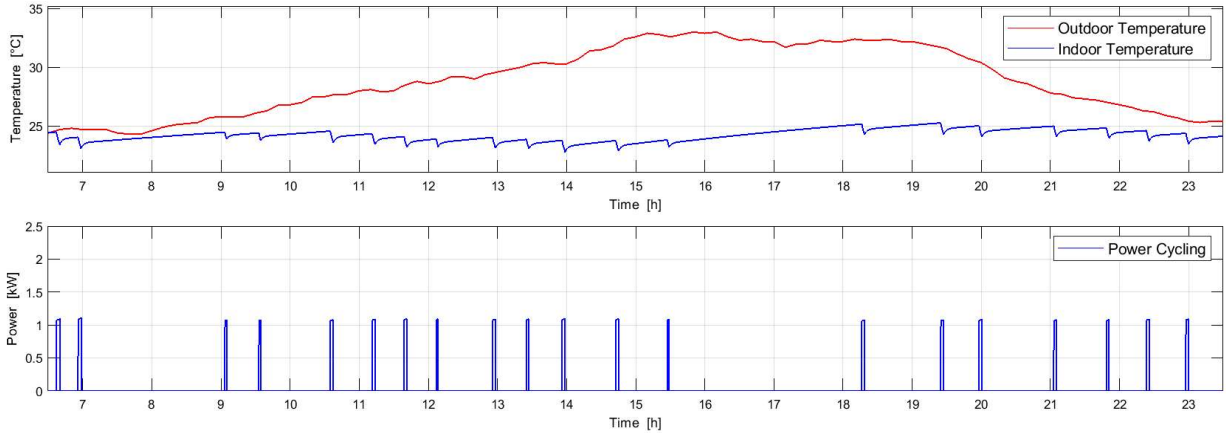

(b) **Case 5**: Proposed EWHs+GSHPs' control.

Figure 4.20: GSHPs' power cycling for one household.

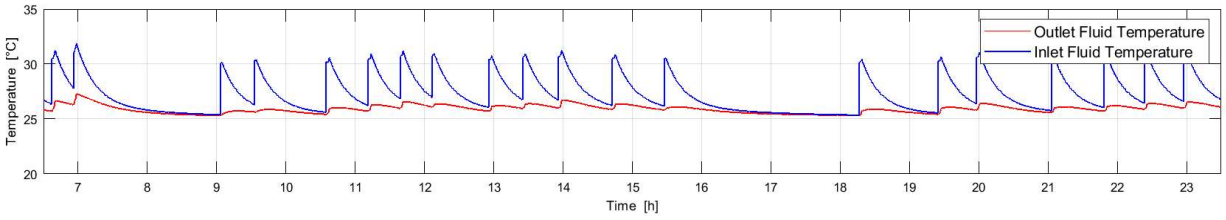

Figure 4.21: GHX fluid temperatures for **Case 5** (Proposed EWHs+GSHPs' control).

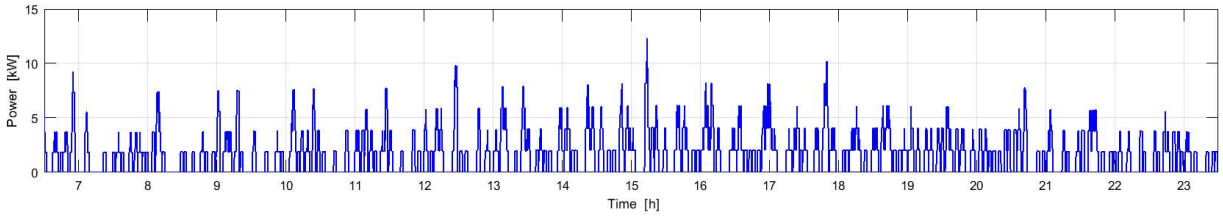

(a) **Case 1**: No control with AC.

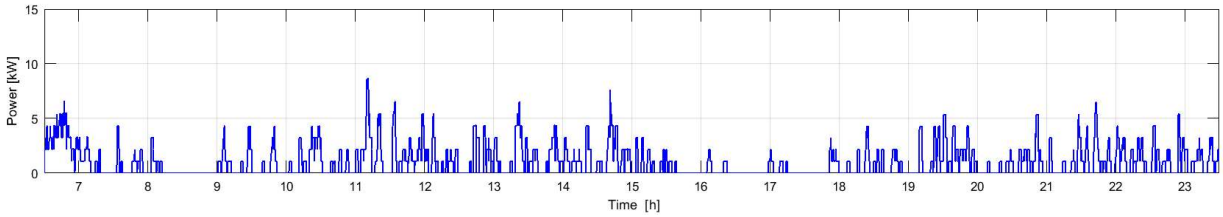

(b) **Case 5**: Proposed EWHs+GSHPs' control.

Figure 4.22: GSHPs' aggregated powers.

4.3.6 Results Comparison and Validation

A summary of the simulation results of the five case studies is shown in Table 4.4, presenting some performance parameters to evaluate the effectiveness of the proposed DR strategy for primary frequency control. Thus, first, observe that a DR strategy significantly improves the system performance irrespective of the TCLs used. In terms of DR for EWHs in **Case 2** and **Case 3**, the DR strategy proposed in this thesis shows a better performance than that of [40], since the frequency variation range is narrower, and the energy consumed by the EWHs over the operating period, as well as the fuel consumption are smaller. By including ACs and GSHPs in **Case 4** and **Case 5**, the overall system performance is improved, as these TCLs increase the demand flexibility for primary frequency control.

The results in Table 4.4 show that the fuel comsuption is reduced when applying the proposed DR strategy. Furthermore, note that the time the genset operates beyond its efficient limits is significantly improved. Observe also that GSHPs consume less energy than ACs, due to their energy storage capacity. In conclusion, a proper management of TCLs leads to enhance the operating conditions in hybrid RESs-diesel microgrids.

Table 4.4: Simulation result comparison.

		Case 1	**Case 2**	**Case 3**	**Case 4**	**Case 5**
Frequency	f_{max} [Hz]	61.98	61.77	61.57	61.62	61.57
	f_{min} [Hz]	59.83	60.04	60.2	60.33	60.35
	σ [Hz]	0.4459	0.2969	0.2547	0.2507	0.2443
Power	P_{max} [kW]	72.77	64.08	60.61	59.45	58.79
	P_{min} [kW]	11.61	16.72	25.5	25.01	23.97
Energy	EWHs [kWh]	174.8	184.4	175.3	177.6	178.8
	ACs [kWh]	28.91	28.7	28.7	27.88	-
	GSHPs [kWh]	-	-	-	-	18.06
Fuel consumption [l]		207	210.8	205	205.2	203.6
Time f_{sys} exceeds limits [%]		32.22	10.58	7.55	4.16	7.15

4.4 Summary

In this chapter, the models of the components of a hybrid PV-diesel isolated microgrid developed in Chapter 3 were applied to the benchmark Nemiah Valley's microgrid, to evaluate the performance of the proposed DR strategy for primary frequency control. First, an overview of the electrical characteristics of the test system was presented. Next, detail descriptions of the parameters used for each of the components (diesel genset, PV system, and TCLs) and for the DR strategy were provided. Then, random occupancy and temperature setpoint assignments were defined to use the simulators described in the previous chapter, resembling realistic residential load and hot water profiles. Finally, five case studies were conducted and their results were summarized and compared in detail, demonstrating the effectiveness of the proposed DR strategy for primary frequency regulation based on the developed thermo-electrical models of EWHs, ACs, and GSHPs.

Chapter 5

Conclusions

5.1 Summary and Conclusions

The research conducted in this thesis focuses on the provision of primary frequency control in isolated microgrids by means of TCLs, i.e., EWHs, ACs, and GSHPs, developing novel thermodynamic models and implementing a DR strategy that allows controlling these TCLs based on decentralized system frequency measurements. Five different study cases were performed on a benchmark hybrid PV-diesel microgrid to validate and demonstrate the effectiveness of the proposed models and control logics.

In Chapter 1, a synopsis of the literature related to DR strategies for primary frequency control was presented first, followed by a review of the features of residential TCLs for the provision of regulation services. Based on this literature review, the motivations and main objectives of the presented research were identified.

In Chapter 2, the main background required to develop the proposed DR strategy for primary frequency control was presented, followed by a comprehensive review of the components, operation, and restrictions of TCLs. The concepts reviewed in this part of the thesis formed the basis for the design of the thermo-electrical models of these TCLs, and the controls of the DR strategy to respond to frequency deviations while minimizing the effects on consumer comfort. In the last part of this chapter, a brief description of the simulators used to model realistic residential load demand and hot water consumption profiles was presented.

In Chapter 3, the models for the different components of a hybrid PV-diesel microgrid were presented, starting from the droop control model of a disel genset, followed by the

modeling of a solar PV system, concluding with the thermo-electrical models of TCLs. Next, the design of the controls of the proposed DR strategy based on an LFC method was described in detail. Finally, the application of the SRLS, CREST,and DHW simulators to generate realistic non-TCLs demand and hot water consumption profiles was presented.

In Chapter 4, the performance of the thermo-electrical models of TCLs for the provision of primary frequency control through proposed DR strategy was evaluated. A benchmark hybrid PV-diesel microgrid was used to conduct five test cases and analyze the system's frequency response under different controls, summarizing and discussing the results.

The main conclusions and findings of the presented research work are as follows:

- The proposed simplified thermo-electrical models of TCLs, i.e., EWHs, ACs, and GSHPs, capture the relevant thermodynamic phenomena at reasonable computational costs, which allows these models to be used in dynamic studies.
- The DR strategy for EWHs presented in [40] was improved to allow a faster frequency recovery by introducing new controls. In addition, based on operating and comfort restrictions, a DR strategy of ACs and GSHPs for the provision of primary frequency control in hybrid isolated microgrids was developed.
- The results of the implementation of the thermo-electrical models of TCLs, subject to the proposed DR strategy, demonstrated the potential to provide primary frequency control, and thus facilitating higher penetration of RES, reducing costs, and improving fuel savings.

5.2 Contributions

The main contributions of this thesis are:

- Developed computationally efficient, simple, and accurate thermo-electrical models of TCLs, i.e., EWHs, ACs, and GSHPs, to resemble their thermodynamic behavior adequately, in order to be used in dynamic studies.
- Developed a decentralized DR strategy based on an LFC method for controlling TCLs, and providing primary frequency control in isolated microgrids with a significant penetration of RES.

- Evaluated and demonstrated the adequacy of the developed thermo-electrical models of TCLs, along with the proposed DR strategy for primary frequency control in hybrid PV-diesel isolated microgrids under realistic conditions.

5.3 Future Work

Based on the work presented in this thesis, the following potential pathways for future work are proposed:

- Improve the DR control architecture by including a synthetic droop control for solar PV systems, in order to increase the flexibility in the system, thus allowing a higher share of RES.
- The TEC method adopted to develop the thermo-electrical models of TCLs, i.e., EWHs, ACs, and GSHPS, can be readily expanded to include additional TCLs with similar characteristics such as refrigerators, freezers, and ESHs. In addition, the proposed DR strategy for TCLs can be adapted for the provision of other regulation services such as peak shaving and load leveling in isolated microgrids with an energy supply mix.
- Develop optimization-based control models of the TCL-based DR strategy, for power and energy management.

Bibliography

[1] O. P. Malik, "Evolution of power systems into smarter networks," *Journal of Control, Automation and Electrical Systems*, vol. 24, no. 1, pp. 139–147, Apr 2013.

[2] D. E. Olivares, A. Mehrizi-Sani, A. H. Etemadi, C. A. Cañizares, R. Iravani, M. Kazerani, A. H. Hajimiragha, O. Gomis-Bellmunt, M. Saeedifard, R. Palma-Behnke, G. A. Jiménez-Estévez, and N. D. Hatziargyriou, "Trends in microgrid control," *IEEE Transactions on Smart Grid*, vol. 5, no. 4, pp. 1905–1919, July 2014.

[3] E. Hossain, E. Kabalci, R. Bayindir, and R. Perez, "Microgrid testbeds around the world: State of art," *Energy Conversion and Management*, vol. 86, pp. 132 – 153, 2014.

[4] J. Royer, "Status of remote/off-grid communities in Canada," August 2011. [Online]. Available: http://publications.gc.ca/collections/collection_2013/rncan-nrcan/M154-71-2013-eng.pdf

[5] M. Arriaga, C. A. Cañizares, and M. Kazerani, "Northern lights: Access to electricity in Canada's northern and remote communities," *IEEE Power and Energy Magazine*, vol. 12, no. 4, pp. 50–59, July 2014.

[6] F. Katiraei, D. Turcotte, A. Swingler, and J. Ayoub, "Modeling and dynamic analysis of a medium penetration PV-Diesel Mini-Grid system," *4th European Conference on PV-Hybrid and Mini-Grid*, May 2008.

[7] F. Katiraei, R. Iravani, N. Hatziargyriou, and A. Dimeas, "Microgrids management," *IEEE Power and Energy Magazine*, vol. 6, no. 3, pp. 54–65, May 2008.

[8] G. Fuchs, B. Lunz, M. Leuthold, and D. Sauer, "Technology overview on electricity storage," June 2012. [Online]. Available: http://www.sefep.eu/activities/projects-studies/120628_Technology_Overview_Electricity_Storage_SEFEP_ISEA.pdf

[9] Z. Xu, R. Diao, S. Lu, J. Lian, and Y. Zhang, "Modeling of electric water heaters for demand response: A baseline pde model," *IEEE Transactions on Smart Grid*, vol. 5, no. 5, pp. 2203–2210, Sep. 2014.

[10] Hydroquebec. (2019) Breakdown of a household's electricity use. [Accessed on 2019-06-10]. [Online]. Available: http://www.hydroquebec.com/residential/customer-space/electricity-use/electricity-consumption-by-use.html

[11] M. Liu, S. Peeters, D. S. Callaway, and B. J. Claessens, "Trajectory tracking with an aggregation of domestic hot water heaters: Combining model-based and model-free control in a commercial deployment," *IEEE Transactions on Smart Grid*, pp. 1–8, 2019.

[12] NRCan. (2017) Ground-source heat pumps (earth-energy systems). [Accessed on 2019-06-10]. [Online]. Available: https://www.nrcan.gc.ca/energy/publications/efficiency/heating-heat-pump/6833

[13] V. Minea, Y. Chen, and A. K. Athienitis, "Canadian low-energy housing: National energy context, and a case study of a demonstration house with focus on its ground-source heat pump," *Science and Technology for the Built Environment*, vol. 23, no. 4, pp. 651–668, 2017.

[14] M. Kummert and M. Bernier, "Sub-hourly simulation of residential ground coupled heat pump systems," *Building Services Engineering Research and Technology*, vol. 29, no. 1, pp. 27–44, 2008.

[15] Z. Xu, J. Ostergaard, and M. Togeby, "Demand as frequency controlled reserve," *IEEE Transactions on Power Systems*, vol. 26, no. 3, pp. 1062–1071, Aug 2011.

[16] T. Masuta and A. Yokoyama, "Supplementary load frequency control by use of a number of both electric vehicles and heat pump water heaters," *IEEE Transactions on Smart Grid*, vol. 3, no. 3, pp. 1253–1262, Sep. 2012.

[17] D. S. Olawuyi, "Renewable energy sources -legal barriers and potential-," *Environmental Policy and Law*, vol. 43, no. 4, pp. 233–238, 10 2013.

[18] P. J. Douglass, R. Garcia-Valle, P. Nyeng, J. Østergaard, and M. Togeby, "Smart demand for frequency regulation: Experimental results," *IEEE Transactions on Smart Grid*, vol. 4, no. 3, pp. 1713–1720, Sep. 2013.

[19] M. Farrokhabadi, C. A. Cañizares, and K. Bhattacharya, "Frequency control in isolated/islanded microgrids through voltage regulation," *IEEE Transactions on Smart Grid*, vol. 8, no. 3, pp. 1185–1194, May 2017.

[20] S. A. Pourmousavi, S. N. Patrick, and M. H. Nehrir, "Real-time demand response through aggregate electric water heaters for load shifting and balancing wind generation," *IEEE Transactions on Smart Grid*, vol. 5, no. 2, pp. 769–778, March 2014.

[21] R. Miller, B. Venkatesh, and D. Cheng, "Overview of FERC Order No. 755 and proposed MISO implementation," in *2013 IEEE Power Energy Society General Meeting*, July 2013, pp. 1–5.

[22] F. C. Ruz and M. G. Pollitt, "Overcoming barriers to electrical energy storage: comparing California and Europe," *Competition and Regulation in Network Industries*, vol. 17, no. 2, pp. 123–149, 2016.

[23] A. Castillo and D. F. Gayme, "Grid-scale energy storage applications in renewable energy integration: A survey," *Energy Conversion and Management*, vol. 87, pp. 885 – 894, 2014.

[24] ESMAP, "Energy storage trends and opportunities in emerging markets," 2017. [Online]. Available: https://www.ifc.org/wps/wcm/connect/ed6f9f7f-f197-4915-8ab6-56b92d50865d/7151-IFC-EnergyStorage-report.pdf?MOD=AJPERES

[25] J. Kondoh, N. Lu, and D. J. Hammerstrom, "An evaluation of the water heater load potential for providing regulation service," *IEEE Transactions on Power Systems*, vol. 26, no. 3, pp. 1309–1316, Aug 2011.

[26] A. Molina-Garcia, F. Bouffard, and D. S. Kirschen, "Decentralized demand-side contribution to primary frequency control," *IEEE Transactions on Power Systems*, vol. 26, no. 1, pp. 411–419, Feb 2011.

[27] J. A. Short, D. G. Infield, and L. L. Freris, "Stabilization of grid frequency through dynamic demand control," *IEEE Transactions on Power Systems*, vol. 22, no. 3, pp. 1284–1293, Aug 2007.

[28] Q. Shi, F. Li, Q. Hu, and Z. Wang, "Dynamic demand control for system frequency regulation: Concept review, algorithm comparison, and future vision," *Electric Power Systems Research*, vol. 154, pp. 75 – 87, 2018.

[29] U. Moslem, F. R. Mohd, and F. A. Mohd, "A review on peak load shaving strategies," *Renewable and Sustainable Energy Reviews*, vol. 82, pp. 3323 – 3332, 2018.

[30] F. E. Consulting, "Electric water heaters as grid energy storage," 2017. [Online]. Available: https://www.energytrust.org/wp-content/uploads/2017/11/Water_Heater_Energy_Storage_wStaffResponse.pdf

[31] P. S. Sauter, B. V. Solanki, C. A. Cañizares, K. Bhattacharya, and S. Hohmann, "Electric thermal storage system impact on northern communities' microgrids," *IEEE Transactions on Smart Grid*, vol. 10, no. 1, pp. 852–863, Jan 2019.

[32] H. Hao, B. M. Sanandaji, K. Poolla, and T. L. Vincent, "Potentials and economics of residential thermal loads providing regulation reserve," *Energy Policy*, vol. 79, pp. 115 – 126, 2015.

[33] D. J. Hammerstrom, J. Brous, D. P. Chassin, G. R. Horst, R. Kajfasz, P. Michie, T. V. Oliver, T. A. Carlon, C. Eustis, O. M. Jarvegren, W. Marek, R. L. Munson, and R. G. Pratt, "Pacific northwest gridwise™ testbed demonstration projects; Part II. Grid friendly™ appliance project," October 2007.

[34] J. M. G. López, E. Pouresmaeil, C. A. Cañizares, K. Bhattacharya, A. Mosaddegh, and B. V. Solanki, "Smart residential load simulator for energy management in smart grids," *IEEE Transactions on Industrial Electronics*, vol. 66, no. 2, pp. 1443–1452, Feb 2019.

[35] EPA. (2017) Geothermal heating and cooling technologies. [Accessed on 2019-06-10]. [Online]. Available: https://www.nrcan.gc.ca/energy/publications/efficiency/heating-heat-pump/6833

[36] NRCan, "Heating and cooling with a heat pump," 2004. [Online]. Available: https://www.nrcan.gc.ca/sites/oee.nrcan.gc.ca/files/pdf/publications/infosource/pub/home/heating-heat-pump/booklet.pdf

[37] M. Gouda, S. Danaher, and C. Underwood, "Building thermal model reduction using nonlinear constrained optimization," *Building and Environment*, vol. 37, no. 12, pp. 1255 – 1265, 2002.

[38] M. D. Rosa, F. Ruiz-Calvo, J. M. Corberán, C. Montagud, and L. A. Tagliafico, "A novel TRNSYS type for short-term borehole heat exchanger simulation: B2G model," *Energy Conversion and Management*, vol. 100, pp. 347 – 357, 2015.

[39] H.-J. Diersch, D. Bauer, W. Heidemann, W. Rühaak, and P. Schätzl, "Finite element modeling of borehole heat exchanger systems: Part 2. numerical simulation," *Computers Geosciences*, vol. 37, no. 8, pp. 1136 – 1147, 2011.

[40] K. Elamari and L. A. C. Lopes, "Frequency based control of electric water heaters in small pv-diesel hybrid mini-grids," in *2012 25th IEEE Canadian Conference on Electrical and Computer Engineering (CCECE)*, April 2012, pp. 1–4.

[41] Ning Lu and Hammerstrom, "Design considerations for frequency responsive grid friendly appliances," in *2005/2006 IEEE/PES Transmission and Distribution Conference and Exhibition*, May 2006, pp. 647–652.

[42] J. A. Short, D. G. Infield, and L. L. Freris, "Stabilization of grid frequency through dynamic demand control," *IEEE Transactions on Power Systems*, vol. 22, no. 3, pp. 1284–1293, Aug 2007.

[43] N. Lu, "An evaluation of the HVAC load potential for providing load balancing service," *IEEE Transactions on Smart Grid*, vol. 3, no. 3, pp. 1263–1270, Sep. 2012.

[44] A. Molina-Garcia, F. Bouffard, and D. S. Kirschen, "Decentralized demand-side contribution to primary frequency control," *IEEE Transactions on Power Systems*, vol. 26, no. 1, pp. 411–419, Feb 2011.

[45] P. Kundur, *Power System Stability and Control*. McGraw-Hill Education, 1994.

[46] D. Peralta, "Primary frequency control with flywheel energy storage technologies," Master's thesis, University of Waterloo, Canada, 2017.

[47] B. Kirby, "Frequency regulation basics and trends," 2004. [Online]. Available: http://www.consultkirby.com/files/TM2004-291_Frequency_Regulation_Basics_and_Trends.pdf

[48] J. Dagel and R. Brady, *Diesel Engine and Fuel System Repair*. Prentice Hall, 2002.

[49] G. Papaioannou, I. Talavera, and J. Hanson, "The influence of diesel generators on frequency stability for isolated grids with high wind power penetration," *International Conference on Renewable Energies and Power Quality (ICREPQ'15)*, vol. 1, no. 13, pp. 616–621, March 2015.

[50] M. Arriaga, C. A. Cañizares, and M. Kazerani, "Renewable energy alternatives for remote communities in northern Ontario, Canada," *IEEE Transactions on Sustainable Energy*, vol. 4, no. 3, pp. 661–670, July 2013.

[51] A. O. Converse, "Seasonal energy storage in a renewable energy system," *Proceedings of the IEEE*, vol. 100, no. 2, pp. 401–409, Feb 2012.

[52] NRCan. (2018) Towards renewable energy integration in remote communities. a summary of electric reliability considerations. [Accessed on 2019-06-11]. [Online]. Available: http://publications.gc.ca/site/eng/9.860462/publication.html

[53] R. Diao, S. Lu, M. Elizondo, E. Mayhorn, Y. Zhang, and N. Samaan, "Electric water heater modeling and control strategies for demand response," in *2012 IEEE Power and Energy Society General Meeting*, July 2012, pp. 1–8.

[54] B. V. Solanki, A. Raghurajan, K. Bhattacharya, and C. A. Cañizares, "Including smart loads for optimal demand response in integrated energy management systems for isolated microgrids," *IEEE Transactions on Smart Grid*, vol. 8, no. 4, pp. 1739–1748, July 2017.

[55] D.Vu and C. Agee, "WECC tutorial on speed governors," 2002, [Accessed on 2019-06-11]. [Online]. Available: https://www.wecc.org/Reliability/Governor%20Tutorial.pdf

[56] D. Chassin, J. Malard, C. Posse, A. Gangopadhyaya, N. Lu, S. Katipamula, and J. V. Mallow, "Modeling power systems as complex adaptive systems," Jan 2004.

[57] R. Gran, *Numerical Computing with Simulink, Vol. 1.* Society for Industrial Applied Mathematics,U.S., 2007.

[58] Y. Cengel, *Heat Transfer: A Practical Approach.* McGraw-Hill, 2002.

[59] E. Pita, *Air conditioning principles and systems.* American Society of Heating, Refrigerating and Air-Conditioning Engineers, Inc. (ASHRAE), 2014.

[60] *2007 ASHRAE Handbook - Heating, Ventilating, and Air-Conditioning Applications (I-P Edition).* American Society of Heating, Refrigerating and Air-Conditioning Engineers, Inc. (ASHRAE), 2007.

[61] Condair. (2019) The Sterling chart - relative humidity chart. [Accessed on 2019-06-11]. [Online]. Available: https://www.condair.com/why-humidify-importance-of-humidification/the-sterling-chart

[62] S. Kavanaugh and K. Rafferty, *Ground-Source Heat Pumps: Design of Ground Source Heat Pump Systems.* American Society of Heating, Refrigerating and Air-Conditioning Engineers, Inc. (ASHRAE), 2014.

[63] D. Parker, "Estimating daily domestic hot-water use in north american homes," *ASHRAE Transactions*, vol. 121, no. 2, pp. p258+, 2015.

[64] R. Ian and T. Murray, "CREST domestic electricity demand model." [Online]. Available: https://dspace.lboro.ac.uk/dspace-jspui/handle/2134/5786

[65] U.S Department of Energy, "DHW event schedule generator." [Online]. Available: https://www.energy.gov/eere/buildings/building-america-analysis-spreadsheets

[66] E. N. Azadani, C. Canizares, and K. Bhattacharya, "Modeling and stability analysis of distributed generation," in *2012 IEEE Power and Energy Society General Meeting*, July 2012, pp. 1–8.

[67] C. Lin, C. Wu, J. Yang, and C. Liao, "Parameters identification of reduced governor system model for diesel-engine generator by using hybrid particle swarm optimisation," *IET Electric Power Applications*, vol. 12, no. 9, pp. 1265–1271, 2018.

[68] R. Tonkoski, L. A. C. Lopes, and D. Turcotte, "Active power curtailment of PV inverters in diesel hybrid mini-grids," in *2009 IEEE Electrical Power Energy Conference (EPEC)*, Oct 2009, pp. 1–6.

[69] M. C. Argyrou, P. Christodoulides, C. C. Marouchos, and S. A. Kalogirou, "A grid-connected photovoltaic system: Mathematical modeling using MATLAB/Simulink," in *2017 52nd International Universities Power Engineering Conference (UPEC)*, Aug 2017, pp. 1–6.

[70] Solar Nexus. (2019) PV modules. [Accessed on 2019-06-10]. [Online]. Available: http://www.solarhub.com/product-catalog/pv-modules/218-Day4-48MC-180-Day4-Energy

[71] University of Victoria. (2019) School-based weather station network. [Accessed on 2019-06-10]. [Online]. Available: http://www.victoriaweather.ca/

[72] B. Johnson, "Patterns of residential occupancy," 1981. [Online]. Available: http://web.mit.edu/parmstr/Public/NRCan/ir464.pdf

[73] C. Tang, "Modeling packaged heat pumps in a quasy-steady state energy simulator program," Master's thesis, Oklahoma State University, U.S., 2003.

[74] R. Stull, "Wet-bulb temperature from relative humidity and air temperature," *Journal of Applied Meteorology and Climatology*, vol. 50, no. 11, pp. 2267–2269, 2011. [Online]. Available: https://doi.org/10.1175/JAMC-D-11-0143.1

[75] TRANE. (2019) Split system cooling product and performance data. [Accessed on 2019-06-10]. [Online]. Available: https://www.trane.com/commercial/uploads/pdf/1111/2ttb3.pdf

[76] A. Shenoy, "Simulation, modeling and analysis of a water to air heat pump," Master's thesis, Oklahoma State University, U.S., 2004.

[77] F. Ruiz-Calvo, M. D. Rosa, J. Acuña, J. Corberán, and C. Montagud, "Experimental validation of a short-term borehole-to-ground (B2G) dynamic model," *Applied Energy*, vol. 140, pp. 210–223, 2015.

[78] M. D. Rosa, F. Ruiz-Calvo, J. M. Corberán, C. Montagud, and L. A. Tagliafico, "A novel TRNSYS type for short-term borehole heat exchanger simulation: B2G model," *Energy Conversion and Management*, vol. 100, pp. 347–357, 2015.

[79] S. Chapra and R. Canale, *Numerical Methods for Engineers*. McGraw Hill, 2015.

[80] BOSH. (2019) Residential Geothermal Heat Pumps. [Accessed on 2019-06-10]. [Online]. Available: https://www.bosch-climate.us/files/Greensource_BP_engineering_submittal_sheet_11.2018_US.pdf

[81] National Research Energy Laboratory NREL. (2019) Domestic hot water (DHW) draw profile generation. [Accessed on 2019-06-10]. [Online]. Available: https://buildingsfieldtest.nrel.gov/domestic_hot_water_dhw_draw_profile_generation

[82] S. Pelland, D. Turcotte, G. Colgate, and A. Swingler, "Nemiah Valley photovoltaic-diesel mini-grid: system performance and fuel saving based on one year of monitored data," *IEEE Transactions on Sustainable Energy*, vol. 3, no. 1, pp. 167–175, Jan 2012.

[83] D. Zhang, S. Li, P. Zeng, and C. Zang, "Optimal microgrid control and power-flow study with different bidding policies by using powerworld simulator," *IEEE Transactions on Sustainable Energy*, vol. 5, no. 1, pp. 282–292, Jan 2014.

[84] Wei-Tzer Huang and Wen-Chih Yang, "System steady-state analysis of a low-voltage microgrid with various distributed energy resources," in *2010 IEEE Conference on Cybernetics and Intelligent Systems*, June 2010, pp. 237–242.

[85] Hydro One, "Distributed generation technical interconnection requirements - Interconnections at voltages 50kV and below," Hydro One, Toronto, Canada, Tech. Rep., 2013.